Copyright Warning & Restrictions

The copyright law of the United States (Title 17, United States Code) governs the making of photocopies or other reproductions of copyrighted material.

Under certain conditions specified in the law, libraries and archives are authorized to furnish a photocopy or other reproduction. One of these specified conditions is that the photocopy or reproduction is not to be "used for any purpose other than private study, scholarship, or research." If a, user makes a request for, or later uses, a photocopy or reproduction for purposes in excess of "fair use" that user may be liable for copyright infringement,

This institution reserves the right to refuse to accept a copying order if, in its judgment, fulfillment of the order would involve violation of copyright law.

Please Note: The author retains the copyright while the New Jersey Institute of Technology reserves the right to distribute this thesis or dissertation

Printing note: If you do not wish to print this page, then select "Pages from: first page # to: last page #" on the print dialog screen

NJIT
New Jersey's Science & Technology University

The Van Houten library has removed some of the personal information and all signatures from the approval page and biographical sketches of theses and dissertations in order to protect the identity of NJIT graduates and faculty.

ABSTRACT

LOW PRESSURE CHEMICAL VAPOR DEPOSITION OF SILICON NITRIDE FILMS FROM TRIDIMETHYLAMINOSILANE

by
Xin Lin

In this study amorphous stoichiometric silicon nitride films were synthesized by low pressure chemical vapor deposition (LPCVD) using tri(dimethylamino) silane (TDMAS) and ammonia (NH_3). The growth kinetics were determined as a function of temperature in the range of 650 - 900 °C, total pressure in the range of 0.15 - 0.60 Torr, and NH_3/TDMAS flow ratio in the range of 0 - 10. At constant condition of pressure (0.5 Torr), TDMSA flow rate (10 sccm) and NH_3 flow rate (100 sccm), the deposition rate of as-deposited silicon nitride films was found to follow an Arrehnius behavior in the temperature range of 650 - 800 °C with an activation energy of 41 $\pm$ 3 kcal mol^{-1}. The film characterizations including compositional, structural, physical, optical and mechanical properties were determined by using XPS, RBS, X-ray diffraction, Nanospec interferometry, Ellipsometer, FTIR, UV Visible, as well as other techniques. The results demonstrated the feasibility of using TDMAS in the synthesis of high quality silicon nitride films by LPCVD.

LOW PRESSURE CHEMICAL VAPOR DEPOSITION OF SILICON NITRIDE FILMS FROM TRIDIMETHYLAMINOSILANE

by
Xin Lin

A Thesis
Submitted to the Faculty of
New Jersey Institute of Technology
in Partial Fulfillment of the Requirements for the Degree of
Master of Science in Engineering Science

Committee for the Interdisciplinary Program in Materials Science and Engineering

January 1995

APPROVAL PAGE

LOW PRESSURE CHEMICAL VAPOR DEPOSITION OF SILICON NITRIDE FILMS FROM TRIDIMETHYLAMINOSILANE

Xin Lin

Dr. Roland A. Levy, Thesis Advisor — Date
Professor of Physics,
Director of Materials Science and Engineering Program, NJIT

Dr. James M. Grow, Thesis Advisor — Date
Professor of Chemical Engineering, Chemistry, and
Environmental Science, NJIT

Dr. David Kristol — Date
Professor of Chemistry,
Director of Biomedical Engineering Program, NJIT

BIOGRAPHICAL SKETCH

Author: Xin Lin

Degree: Master of Science in Engineering Science

Date: January 1995

Undergraduate and Graduate Education:

- Master of Science in Engineering Science,
  New Jersey Institute of Technology,
  Newark, New Jersey, January 1995

- Bachelor of Science in Inorganic Nonmetallic Materials,
  Tsinghua University
  Beijing, P.R.China, 1992

Major: Materials Science and Engineering

Professional Background

Research Staff,
Beijing Founder High Technology Ceramics, Inc.
Beijing, P.R.China, 1992
August 1992 - July 1993

This thesis is dedicated to
my parents, Xiru Lin & Jinzhu Fu

ACKNOWLEDGMENT

The author wishes to express her sincere gratitude to her advisors, Professor Roland A. Levy and James M. Grow, for their guidance, friendship, moral and financial support throughout this thesis work, without which it would not have been completed.

Special thanks to Professor David Kristol for serving as member of the committee.

The author appreciates the timely help and suggestions from the CVD Laboratory members, including: Vitaly Sigal, Roumiana Petrova, Xiangqun Fan, Wei-shang King, Chenna Ravindranath, Mahalingam Bhaskaran, Venkat Paturi, Jan Opyrchal, and Abhijit Datta, Emmanuel Ramos.

TABLE OF CONTENTS

Chapter **Page**

1 INTRODUCTION TO CVD 1

1.1 Some Basic Aspects of CVD 2

1.2 Principles of CVD 5

1.2.1 Thermodynamics of CVD 5

1.2.2 Dynamics of CVD 5

1.2.2.1 Boundary Layer Theory 7

1.2.2.2 Diffusion 9

1.2.2.3 Application of Dynamics Principles to CVD 11

1.2.3 Kinetics of CVD 14

1.2.3.1 Unimolecular Surface Reactions 16

1.2.3.2 Bimolecular Surface Reactions 21

1.3 Types of CVD Processes 24

1.3.1 Thermally Activated Atmospheric Pressure Processes (APCVD) 25

1.3.2 Thermally Activated Low Pressure Processes (LPCVD) 25

1.3.3 Plasma-enhanced Deposition Process (PECVD) 26

1.3.4 Photo-enhanced Chemical Vapor Deposition (PHCVD) 27

1.3.5 Lase-induced Chemical Vapor Deposition (LDCVD) 30

2 LITERATURE REVIEW 32

2.1 History of CVD Silicon Nitride 33

TABLE OF CONTENTS
(Continued)

Chapter **Page**

2.2 Comparison of Properties of Silicon Nitride Films Deposited by LPCVD and PECVD 41

2.3 Application of Silicon Nitride Films 41

3 EXPERIMAENTAL PROCEDURE 45

3.1 Properties of the Precursor 45

3.2 Set-up of LPCVD System 45

3.2.1 Source Section 45

3.2.2 Flow Control Section 47

3.2.2.1 Flow Controller 47

3.2.2.2.1 MKS Mass Flow Controller 47

3.2.2.1.2 1150B Mass Flow Controller 49

3.2.2.2 The Switches of Flow Lines 50

3.2.3 Vacuum Stations 50

3.2.3.1 Mechnical Pump 51

3.2.3.2 Booster Pump 52

3.2.4 Reaction Chamber 53

3.2.5 Wafer and Wafer Holder 53

3.3 Deposition Procedure 54

3.3.1 Pre-deposition Procedure 54

TABLE OF CONTENTS
(Continued)

Chapter **Page**

3.3.1.1 Temperature Calibration of the Reaction Chamber 54

3.3.1.2 Leak Check 55

3.3.1.3 Flow Rate Calibration 56

3.3.2 Experimental Procedure 57

3.3.2.1 Wafer Loading 57

3.3.2.2 Heating and Deposition Condition Setting 59

3.3.2.3 Film Deposition 59

3.3.2.4 Taking the Wafers out of the Chamber 60

3.3.3 The Experimental Parameters 60

3.4 Film Chacterization Technique 60

3.4.1 Structure Studies 60

3.4.1.1 X-ray Diffraction 61

3.4.1.2 SEM 62

3.4.1.3 Optical Microscopy 64

3.4.2 Composition 65

3.4.2.1 XPS 66

3.4.2.2 RBS 67

3.4.3 Properties 69

TABLE OF CONTENTS
(Continued)

Chapter **Page**

3.4.3.1 Physical Properties 69

3.4.3.1.1 Thickness Measurement 69

3.4.3.1.2 Density Measurement 71

3.4.2.1.3 Etching 71

3.4.3.2 Optical Properties 72

3.4.3.2.1 Refractive Index 72

3.4.3.2.2 Transmission Spectra 74

3.4.3.3 Stress 74

4 RESULTS AND DISCUSSIONS 77

4.1 The Effects of Deposition variables on Film Growth Rate 77

4.1.1 Temperature Dependent Study of Si_3N_4 Thin Films 77

4.1.2 Pressure Dependent Study of Si_3N_4 Thin Films 79

4.1.3 NH_3/TDMAS Flowrate Ratio Study of Si_3N_4 Thin Films 82

4.2 Structure study 83

4.3 The Effects of Deposition Variables on Composition 85

4.3.1 Temperature Dependent Study of Si_3N_4 Thin Films 85

4.3.2 NH_3/TDMAS Flowrate Ratio Study of Si_3N_4 Thin Films 88

4.4 The Effects of Deposition Variables on Film Density 88

TABLE OF CONTENTS
(Continued)

Chapter **Page**

4.4.1 Temperature Dependent Study of Si_3N_4 Thin Films 89

4.4.2 Pressure Dependent Study of Si_3N_4 Thin Films 92

4.4.3 NH_3/TDMAS Flowrate Ratio Study of Si_3N_4 Thin Films 93

4.5 Optical Properties Study 94

4.5.1 the Effects of Deposition Variables on Film refractive Index 94

4.5.1.1 Temperature Dependent Study of Si_3N_4 Thin Films 95

4.5.1.2 Pressure Dependent Study of Si_3N_4 Thin Films 96

4.5.1.3 NH_3/TDMAS Flowrate Ratio Study of Si_3N_4 Thin Films 97

4.5.2 FTIR Analysis 98

4.5.2.1 Temperature Dependent Study of Si_3N_4 Thin Films 98

4.5.2.2 Pressure Dependent Study of Si_3N_4 Thin Films 101

4.5.2.3 NH_3/TDMAS Flowrate Ratio Study of Si_3N_4 Thin Films 102

4.5.3 UV-visible Analysis 103

4.5.3.1 Temperature Dependent Study of Si_3N_4 Thin Films 104

4.5.3.2 Pressure Dependent Study of Si_3N_4 Thin Films 107

4.5.3.3 NH_3/TDMAS Flowrate Ratio Study of Si_3N_4 Thin Films 108

4.6 Stress Study 108

4.6.1 Temperature Dependent Study of Si_3N_4 Thin Films 110

TABLE OF CONTENTS
(Continued)

Chapter **Page**

4.4.2 Pressure Dependent Study of Si_3N_4 Thin Films 113

4.4.3 NH_3/TDMAS Flowrate Ratio Study of Si_3N_4 Thin Films 113

5. CONCLUSIONS 114

REFERENCE 116

LIST OF TABLES

Table Page

1.1 Some Basic Aspects of CVD Reaction 4

1.2 Thermodynamic Calculations 6

1.3 Sequential Kinetics Steps in Heterogeneous CVD Processes 14

1.4 Plasma and Plasma CVD 28

2.1 Properties of LPCVD and PECVD Deposited Silicon Nitride Films 42

3.1 Indentification of TDMAS 46

3.2 Physical Properties of TDMAS 46

3.3 Reactivity Information of TDMAS 47

LIST OF FIGURES

Figure	Page
1.1 Laminar Gas Flow Patterns	8
1.2 Reactants and Products Diffuse across Boundary Layer	10
1.3 Horizontal Slab CVD Reactor	11
1.4 Radiantly Heated Cylinder Reactor	12
1.5 Gas Flow for Mid-temperature, Hot Wall, Low Pressure	13
1.6 Deposition Rate of Silicon from Various Source Gases as a Function of Substrate Temperature Exemplifying Diffusion Controlled and Reaction Controlled Regimes	15
1.7 Variation of Rate with Concentration for Various Type of Surface Reaction	18
1.8 Energy Diagram for a Unimolecular Surface Reaction	20
3.1 Schematic of LPCVD Reactor Used to Synthesize Silicon Nitride Films	48
3.2 Schematic of a Switch of the Flow Pipes of Reactant Gases	50
3.3 Installation Arrangement for a Vaccum System	51
3.4 Schematic of a Rotary Piston Pump	52
3.5 Schematic of the Booster Pump	53
3.6 Temperature Profile of LPCVD Reactor	55
3.7 Wafers Arrangement on Silica Boat	58
3.8 Geometrical Arrangement of Source, Sample, and Detecor in the "θ-2θ" X-ray Diffractometer	62
3.9 Schematic of the Scanning Electron Microscope	63

LIST OF FIGURES
(Continued)

Figure | Page

3.10 Diagram of the Differencial Interference Contrast Equipment for Transmitted Light 65

3.11 Schematic of Spectrometer with Compared AES and XPS Capabilities 67

3.12 Schematic of the 1.7-MeV Tandem Accelaťor, RBS facility at AT&T Bell Laboratories, Murray Hill, NJ 68

3.13 Calculated Variation of Reflectance (on Air Side) with Normalized Thickness ($n_1 d/\lambda$) for Films of Various Refractive Indices on a Glass Substrate of Index 1.5 69

3.14 Schematic of Interferometer 70

3.15 Experimental Arrangement in Ellipsometry 73

3.16 Schematic of Optical System for Stress Measurement Setup 75

4.1 Variation of Growth Rate of Silicon Nitride Films as a Function of DepositionTemperature 78

4.2 Variation of TDMAS flowrate as a function of the chamber pressure with a set flowrate of 10 sccm in MFC 80

4.3 Variation of Growth Rate of Silicon Nitride Films as a Function of Deposition Pressure 81

4.4 Variation of Growth Rate of Silicon Nitride Films as a Function of NH_3/TDMAS Flowrate Ratio 83

4.5 X-ray Diffraction Prattern for a Silicon Nitride Film on Silicon Deposited at a temperature of 900 °C, Pressure of 0.5 Torr, TDMAS Flowrate of 10sccm, and NH_3 Flowrate of 100 sccm 85

4.6 Atomic Concentration of Silicon Nitride Films as a Function of Deposition Temperature by RBS 86

LIST OF FIGURES
(Continued)

Figure | Page

3.10 Diagram of the Differencial Interference Contrast Equipment for Transmitted Light 65

3.11 Schematic of Spectrometer with Compared AES and XPS Capabilities 67

3.12 Schematic of the 1.7-MeV Tandem Accelaíor, RBS facility at AT&T Bell Laboratories, Murray Hill, NJ 68

3.13 Calculated Variation of Reflectance (on Air Side) with Normalized Thickness ($n_1 d/\lambda$) for Films of Various Refractive Indices on a Glass Substrate of Index 1.5 69

3.14 Schematic of Interferometer 70

3.15 Experimental Arrangement in Ellipsometry 73

3.16 Schematic of Optical System for Stress Measurement Setup 75

4.1 Variation of Growth Rate of Silicon Nitride Films as a Function of DepositionTemperature 78

4.2 Variation of TDMAS flowrate as a function of the chamber pressure with a set flowrate of 10 sccm in MFC 80

4.3 Variation of Growth Rate of Silicon Nitride Films as a Function of Deposition Pressure 81

4.4 Variation of Growth Rate of Silicon Nitride Films as a Function of NH_3/TDMAS Flowrate Ratio 83

4.5 X-ray Diffraction Prattern for a Silicon Nitride Film on Silicon Deposited at a temperature of 900 °C, Pressure of 0.5 Torr, TDMAS Flowrate of 10sccm, and NH_3 Flowrate of 100 sccm 85

4.6 Atomic Concentration of Silicon Nitride Films as a Function of Deposition Temperature by RBS 86

LIST OF FIGURES
(Continued)

Figure **Page**

4.19 Variation of Si-N Absorption Peak in FTIR Spectra for Silicon Nitride Films as a Function of NH_3/TDMAS Flowrate Ratio 103

4.20 UV Spectrum for a Silicon Nitride Film on Silicon Deposited at a Temperature of 800 °C, Pressure of 0.5 Torr, SiN-1000™ Flowrate of 10sccm, and NH_3 Flowrate of 100 sccm 104

4.21 Variation of Index of Absorption of Silicon Nitride Films as a Function of Deposition Temperature 106

4.22 Variation of Index of Absorption of Silicon Nitride Films as a Function of Deposition Pressure 108

4.23 Variation of Index of Absorption of Silicon Nitride Films as a Function of NH_3/TDMAS Flowrate Ratio 109

4.24 Spring-dashpot Model for Stress Relaxation 111

4.25 Variation of Stress in Silicon Nitride Films as a Function of Deposition Temperature 111

4.26 Variation of Stress in Silicon Nitride Films as a Function of Deposition Pressure 112

4.27 Variation of Stress in Silicon Nitride Films as a Function of NH_3/TDMAS Flowrate Ratio 113

CHAPTER 1

INTRODUCTION TO CVD

Chemical vapor deposition (CVD) is defined as a process whereby constituents of a gas react chemically near or on a substrate surface to form a solid product. The occurrence of a chemical reaction distinguishes CVD from physical vapor deposition processes such as evaporation and sputtering. The product of CVD can be in the form of a thin film, a thick coating, or, if allowed to grow, a massive bulk. It can have a single crystal, polycrystalline, or amorphous structure.

CVD is an important method of synthesizing the films used in the fabrication of integrated circuits, as well as other microelectronic devices. A large variety of materials, practically all those needed in microelectronic device technology, can be created by CVD. These materials include dielectrics, elemental and compound semiconductors, metals, and superconductors. A survey of materials that have been created by CVD for applications in solid state electronics exemplify the extent and versatility of this powerful method of deposition.

In addition to its unique versatility, this materials synthesis and vapor phase growth method can take place at relatively low temperatures. For example, refractory oxide glasses and metals can be deposited at temperatures in the range

of 300 to 500 °C. This feature is very important in semiconductor technology, particularly for advanced ultra large scale integration (ULSI) devices with short channel lengths and shallow junctions where lateral and vertical diffusion of dopants must be minimized. Low fabrication temperatures are generally desirable to minimize process-induced crystallographic damage, wafer warpage, and contamination by diffusion impurities.

Another important feature of CVD processing is the ease of creating films of both homogeneous and graded structures as well as of controllable composition. Unusual solid solutions and alloys can be prepared, as well as materials that cannot be readily obtained by other methods. Both composition and structure of the deposits can be tailored by control of the reaction chemistry and processing conditions [1]. However, one current drawback of CVD stems from the use of precursors that tend to be toxic, explosive, and corrosive.

1.1 Some Basic Aspects of CVD

Chemical reaction types characteristic of CVD include pyrolysis (thermal decomposition), oxidation, reduction, hydrolysis, nitride and carbide formation, synthesis reactions, and disproportionation. A sequence of several reaction types may be involved to create a particular end product. Deposition variables such as temperature, pressure, input concentrations, gas flow rates, reactor geometry, and reactor operating principle determine the deposition rate and the properties of the film deposit. Instrumental analysis, such as mass spectrometry of the vapor phase

during CVD, can yield important information on the reaction chemistry of a particular process.

Some important basic aspects of CVD reactions are summarized in Table 1.1. Volatility requirements dictate that the vapor pressure of liquid reactants is sufficiently high (usually when heated) to produce an adequate quantity of vapor that can be transported by a carrier gas to the reaction chamber. Gaseous reactants, if available, are preferred since they can be readily metered and introduced into the CVD reactor. Both inorganic, organometallic, and organic reactants are used as starting materials. The vapor pressure of side products must be high to facilitate their elimination from the reactor, whereas the resulting coating product must have a low volatility to remain on the substrate. The reaction energy to activate and drive the chemical processes can be thermal, supplied by an electric glow discharge (plasma), or attained by electromagnetic radiation (usually ultraviolet or laser radiation). CVD reactions are classified as homogeneous, heterogeneous, or a combination of both. Homogeneous reactions nucleate in the gas phase and lead to particle formation, a serious problem in CVD technology. Most CVD processes are chosen to be heterogeneous reactions. That is, they take place at the substrate surface rather than in the gas phase and form the desirable film deposit. In general, increasing temperature leads to increased film deposition rate, greater density, improved structural perfection, and crystallinity of the deposits. In exothermic chemical transport reactions, however, the substrate is kept below that of the reactants to attain high deposition rates.

Table 1.1 Some basic aspects of CVD reaction [2]

A. VAPOR PRESSURE OR VOLATILITY REQUIREMENTS 1. High for reactants to be transported to reactor 2. High for side products to be eliminated 3. low for product to remain
B. TYPES OF REACTION ENERGY 1. Thermal 2. Plasma glow discharge 3. Electromagnetic radiation such as ultraviolet
C. NUCLEATION AND FILM GROWTH 1. Homogeneous reactions (uniform on gas phase) lead to gas phase nucleation: the major problem in all CVD to avoid 2. Heterogeneous reactions proceed selectively on substrate surface: the desirable type of CVD reaction
D. EFFECTS OF TEMPERATURE INCREASE 1. Higher growth rate if reaction is endothermic 2. Greater density of deposit 3. Improved crystallinity 4. Generally improved film properties 5. Greater interdiffusion of dopants and impurities

1.2 Principles of CVD

1.2.1 Thermodynamics of CVD

The theoretical feasibility and efficiency of the reaction under specified temperature and pressure conditions can be predicted by thermodynamic calculations, which can serve as a valuable guide for establishing process conditions [3-5]. However, reliable thermochemical data are equired, specially the ree energy (ΔG_f^0) and enthalpy (ΔH_f^0) of formation values for all vapor species and condensed constitutes of the system. A second limitation is the assumption that thermodynamic equilibrium exists in the reactor, which is a prerequisite for valid calculations; this is rarely the case under practical conditions. Nevertheless, thermodynamic calculations based on either the optimization technique or the non-linear equation method are useful for basic considerations. A simplified summary of basic thermodynamic calculations is outlined in Table 1.2.

1.2.2. Dynamics of CVD

It is important to understand dynamics of CVD for the following reasons:

1. The deposited film or coating thickness uniformity depends on the delivery of equal amounts of reactants to all substrate surfaces.
2. High deposition growth rate depends on optimizing the flow of reactants through the system and to substrates.
3. More efficient utilization of process gases can be achieved as a result.

4. The computer modeling of CVD processes can be facilitated, enabling improved reactor design and better predicitive capability with regard to performance.

Table 1.2 Thermodynamic calculations [6]

- Important for establishing theoretical feasibility for reaction
- Free energy of formation (ΔG_f^0) of chemical species needed as startingpoint, both for vapor species and condensed constituents of system
- Free energy of reaction (ΔG_f^0) can be calculated if ΔG_f^0 values are know: (G_f^0 sum of products) minus (G_f^0 sum of reactants)
- Equilibrium constant (K_p) of reaction is related to partial pressure in system:

$$K_p \cong \frac{(\text{product of pressure of substances produced})^a}{(\text{product of reactant pressures})^b}$$

where a and b are the coefficients of each substance in the chemical reaction equation

- Free energy of reaction (ΔG_r^0) and equilibrium constant (K_p) are related:

$$-\Delta G_r^0 = 2.3\ RT \log K_p$$

Table 1.2 (Continued) Thermodynamic calculations [6]

- A general CVD reaction can be represented by

$$A_{(g)} + B_{(g)} + \ldots \Leftrightarrow M_{(s)} + N_{(g)} + \ldots$$

where only one component is solid

- The Van't Hoff expression relates K_p, T, and ΔH:

$$d\ln K_p/dT = \Delta H/RT$$

where K_p = equilibrium constant

T = absolute temperature

ΔH = enthalpy of reaction (positive or negative)

$= \Delta G_f^0 + \Delta (TS)$

S = entropy of formation

- A positive value of ΔH indicates an endothermic reaction type
- A negative value of ΔH indicates an exothermic reaction type
- Thermodynamic calculation assume a reaction equilibrium and reliable thermodynamic data (either equilibrium constant or free energy of formation of chemical species)

1.2.2.1 Boundary Layer Theory

Boundary Layer Theory (BLT) provides the key to understanding the dynamics of the CVD process. As shown in Figure 1.1 when a viscous fluid (gas) flows in a

laminar fashion through a pipe or over a body, viscous flow theory [7-9] states that the velocity of gas is zero at the surface and rises exponentially to a uniform flow velocity v_0 some distance away from the surface. For simplification, the BLT assumes that the velocity of the gas near the surface is zero for some distance away from the surface and then rises instantly to a uniform flow velocity v_0. The area where the gas velocity was assumed to be zero is called the boundary layer.

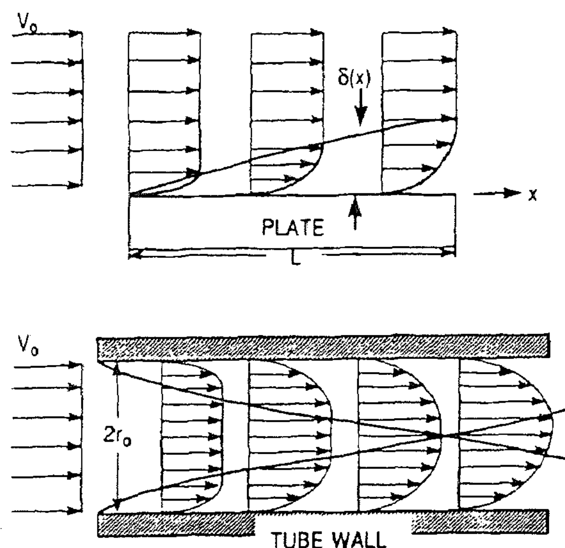

Figure 1.1 Laminar gas flow patterns: (top) flow across flat plane; (bottom) flow through circular pipe.

In BLT for CVD, the effect of the reactor vessel walls are ignored and only with the boundary layer developed above the deposition surface is considered. When a laminar gas with uniform flow velocity v_0 flows across flat plate of length L, the average boundary-layer thickness over the plate is

$$\bar{\delta} = \frac{10}{3} \frac{L}{\sqrt{\mathrm{Re}_L}} \quad (1.1)$$

where Re_L is Reynolds number, which is a dimensionless parameter that characterizes that flow of a fluid, defined as $Re_L = \rho v_0 L/\eta$. The quantities η and ρ are gas viscosity and density, respectively. The kinetic theory of gases predicts that η varies with temperature as $T^{1/2}$ but is independent of pressure. Experimental data bear out the lack of a pressure dependent at least to several atmospheres, but indicate that η varies as T^n, with n having values between 0.6 and 1.0.

Because both gaseous reactants and products must pass through the boundary layer separating the laminar stream and film deposit, low values of $\bar{\delta}$ are desirable in enhancing mass-transport rates. This can be practically achieved by increasing the gas flow (v_0), which raises the value of Re. Typical value of Re in CVD reactors range up to a few hundred. If, however, Re exceeds approximately 2100, a transition from laminar to turbulent flow occurs. The resulting erratic gas eddies and swirls are not conductive to uniform defect-free film growth and are to be avoided [10].

1.2.2.2 Diffusion

The phenomenon of diffusion occurs in gases and liquids as well as in solids. If two different gases are initially separated and then allowed to mix, each will move

from regions of higher to lower concentration, thus increasing the entropy of the system. The process by which this occurs is known as diffusion.

Figure 1.2 illustrates how reactants moving through the fluid must diffuse across the boundary layer to react at the surface, and how the gaseous products must diffuse up from the surface to be removed by the main gas flow.

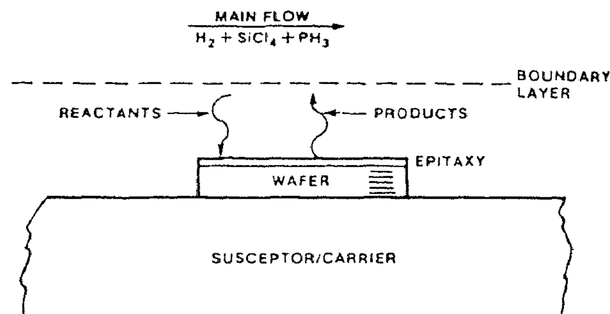

Figure 1.2 Reactants and products diffuse across boundary layer.

The rates at which the reactants and gaseous products diffuse across the imaginary boundary layer vary with temperature and pressure as follows:

1. Directly proportional to temperature to the 3/2 power ($T^{3/2}$).
2. Inversely proportional to total pressure ($1/p_T$).
3. Directly proportional to the partial pressure of ingredients (p_n).

Since diffusion rate (D) varies inversely with pressure, gas mass-transfer rates can be enhanced by reducing the pressure in the reactor. Advantage of this fact is taken in low-pressure CVD (LPCVD) systems, which are now employed in semiconductor processing.

The D is also controlled by many other parameters associated with the gases being used and the nature of the thermal gradients on the system.

1.2.2.3 Application of Dynamics Principles to CVD System

CVD technology was practiced in reactors of many different geometries: however, all these different technologies can be understood by examining the simplest of the epitaxy reactors, namely, the horizontal slab reactor depicted in Figure 1.3.

In the horizontal slab system, the gases enter at one end, pass over the heated surface, and exit. A boundary layer is established above the susceptor due to the viscosity of the flowing gases as they flow over the heated surface. Reactants diffuse across the boundary layer and react to form a solid film; gaseous products diffuse out of the boundary layer to be swept away by the mainstream.

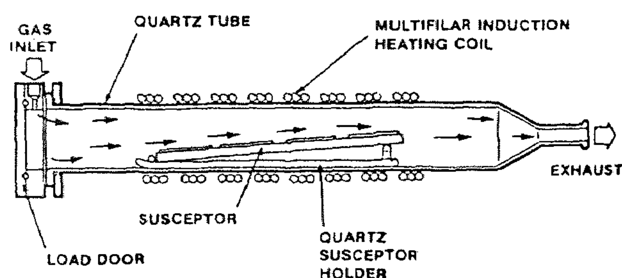

Figure 1.3 Horizontal slab CVD reactor.

Some depletion of reactants occurs as the gas sweep past the heated surface. Other complications occurs such as convection currents due to the strong temperature gradients and chemical reactions take place while the reactants heat up

as they diffuse toward the heated surface. These complex chemical reactions could result in gas phase reactions, creating solid particles above the heated surface.

In light of the information presented above, one can deduce some important adjustment parameters for the horizontal reactor. These are:

1. Tilting the wafer carrier makes its surface more nearly parallel to the $X^{1/2}$ boundary layer shape.
2. Increasing in the main gas velocity will make the boundary layer thinner especially toward the downstream area of the wafer carrier.
3. Increasing the temperature at the rear of the wafer carrier will help compensate for the lower partial pressure or the depletion of the reactants.

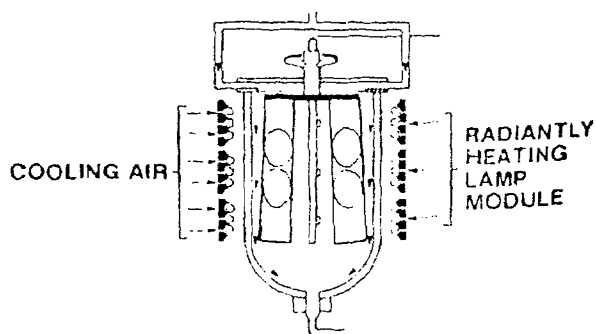

Figure 1.4 Radiantly heated cylinder reactor.

In the case of a radiantly heated cylinder, illustrated in Figure 1.4, the gases enter at the top of an inverted bell jar, flow down the tilted wafer carriers and exit at the bottom of the bell jar. Gas velocities, which determine boundary layer

thickness, are controlled by nozzles which direct the gas down over the wafers. Tilting the susceptors out at the bottom serves two purposes: supporting the wafers in pockets and providing the tilt angle necessary to minimize variations on the boundary layer thickness from top to bottom. Rotation of the wafer carrier serves to average out thickness variations around the wafer carriers.

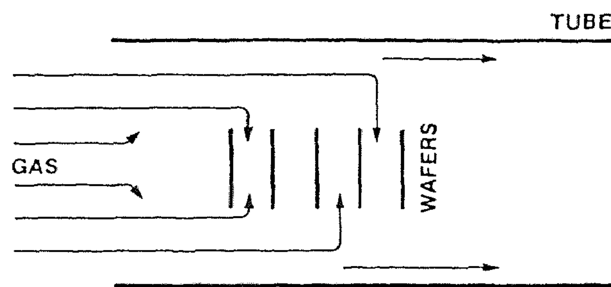

Figure 1.5 Gas flow for mid-temperature, hot wall, low pressure.

For mid-temperature, hot wall, low pressure CVD, the flow situation is complicated by the fact that the wafers are placed perpendicular to the main gas flow direction as illustrated in Figure 1.5. In this case, the total pressure in the system is approximately 1/700 of one atmosphere; therefore, the gaseous diffusion rates are very high. Compensating effects of velocity, density, and mobility cause the boundary layer thickness to be about the same as that for atmospheric pressure processes; however, the high diffusion rate allows reactants to pass between the layers and reacts uniformly over the surface, provided the wafer spacing is large enough. Variable wafer spacing could be one solution to compensating for depletion toward the rear of the deposition area; however, slightly increased

temperature at the rear is a more practical solution. Increasing the total gas flow rate increases the thickness at the rear while increasing the total pressure in the system increases the thickness at the front of the deposition area [6].

1.2.3. Kinetics of CVD

Chemical kinetics determines the available rate of product deposition, which is dependent primarily on temperature [3, 11-13]. The rate of deposition can be strongly affected by the chemical nature and crystallographic orientation of the substrate; the chemical composition, density and geometry of surface sites; and the physical surface features of the substrate.

Table 1.3 Sequential kinetic steps in heterogeneous CVD processes

1. Mass transport of reactant(s) to substrate
2. Adsorption of reactant(s) on substrate surface
3. Chemical reaction (including surface diffusion) on surface
4. Desorption of product gas(es) from surface
5. Mass transport of product gas(es) away substrate
Exception: epitaxial films (nucleation-controlled)

The sequential kinetic steps involved in heterogeneous CVD reactions are listed in Table 1.3. The slowest step determines the overall rate of the reaction. The nature of the rate-controlling step changes with temperature. The lower temperature range of a particular CVD reaction is often surface-process controlled characterized by an exponential temperature dependence of the deposition rate.

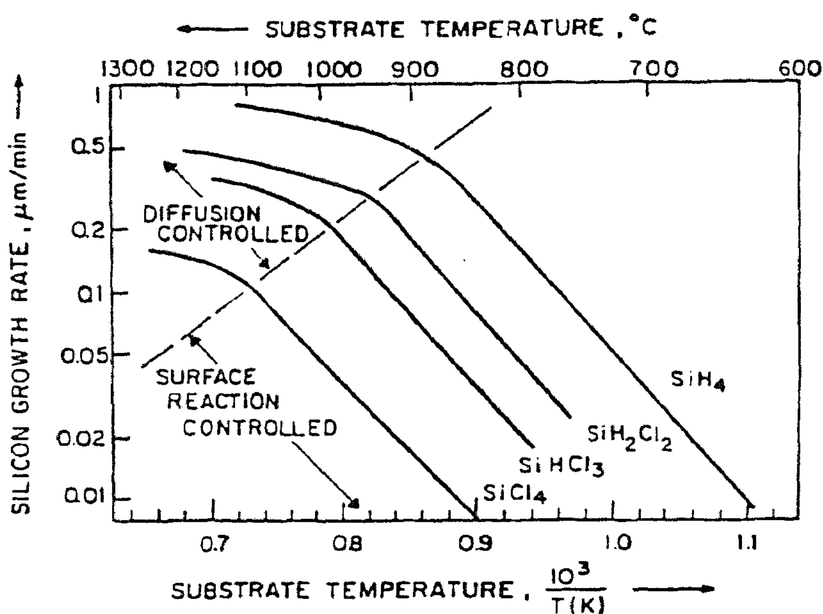

Figure 1.6 Deposition rate of silicon from various source gases as a function of substrate temperature exemplifying diffusion controlled and reaction controlled regimes.

The most likely rate-controlling step is a weak adsorption of reactants on the substrate surface. The higher temperature range is often controlled by diffusion processes where the temperature dependence of the deposition rate is usually mild and follows a less steep slope. The most probable rate-controlling step is the diffusion of reactants and products through a boundary layer to and from the

substrate surface. A typical example that illustrates these effects is presented in Figure 1.6 for the deposition of silicon films from various source gases.

1.2.3.1 Unimolecular Surface Reactions

Surface reactions involving single adsorbed molecules are classified as unimolecular reaction. The simplest situation is when the gas atoms or molecules occupy single sites on the surface and are not dissociated. Langmuir's kinetic derivation of the isotherm is essentially as follows. Let θ be the fraction of surface that is covered; $1-\theta$ is the fraction bare. The rate of adsorption is then $k_a[A](1-\theta)$, where [A] is the gas concentration and k_a is a constant. The rate of desorption is $k_{-a}\theta$. At equilibrium the rates are equal so that

$$k_a[A](1 - \theta) = k_{-a}\theta \qquad (1.2)$$

or

$$\frac{\theta}{1-\theta} = \frac{k_a}{k_{-a}}[A] \qquad (1.3)$$

$$= K_a[A] \qquad (1.4)$$

where K_a, equal to k_a/k_{-a}, is an equilibrium constant for the adsorption process. This equation can be written as

$$\theta = \frac{K_a[A]}{1 + K_a[A]} \tag{1.5}$$

The surface reaction rate is proportional to the fraction θ of surface that is covered and is thus

$$r = k\theta = \frac{kK_a[A]}{1 + K_a[A]} \tag{1.6}$$

The dependence of rate on [A] is shown in Figure 1.7a. At sufficiently high concentrations of A the rate is independent of the concentration, which means that the kinetics are zero order. At low concentrations, when K[A] << 1, the kinetics are first order.

The rate constant k appearing in Equation (1.6) is expected to obey the Arrhenius equation to a good approximation

$$\frac{d \ln k}{dT} = \frac{E_2}{RT^2} \tag{1.7}$$

where E_2 is the activation energy corresponding to the reaction of the absorbed species, that is, to the reaction

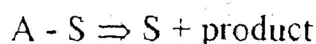

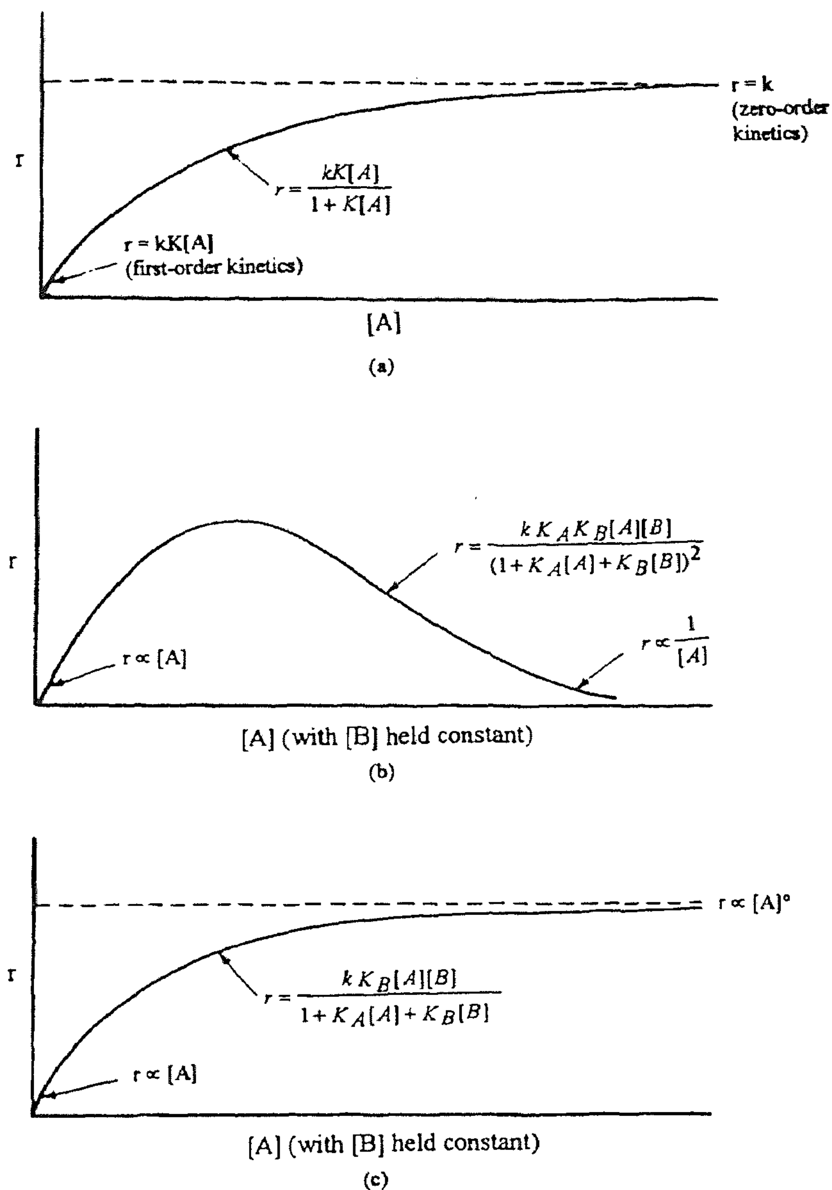

Figure 1.7 Variation of rate with concentration for various types of surface reaction: (a) simple unimolecular process; (b) bimolecular process occurring by a Langmuir-Hinshelwood mechanism: and (c) bimolecular process occurring by a Langmuir-Rideal mechanism.

The temperature dependence of the equilibrium constant K, if it is expressed as a concentration equilibrium constant, will follow the analogous van't Hoff relationship

$$\frac{d\ln k}{dT} = \frac{\Delta U^0}{RT^2} \tag{1.8}$$

where ΔU^0 is the standard molar internal energy change in the adsorption process.

If the reactant pressure is low, ($K[A] \ll 1$), the rate expression [Equation (1.6)] reduces to

$$v = kK[A] \tag{1.9}$$

and the first-order rate coefficient k' is given by

$$k' = kK \tag{1.10}$$

From Equations (1.7) and (1.8) it follows that

$$\frac{d\ln v}{dT} = \frac{d\ln k'}{dT} = \frac{d\ln k}{dT} + \frac{d\ln K}{dT} \tag{1.11}$$

$$= \frac{E_2 + \Delta U^0}{RT^2} \tag{1.12}$$

The apparent activation energy E_a is thus $E_2 + \Delta U^0$.

If the pressure is high the rate equation is simply

$$v = k[A] \tag{1.13}$$

The observed activation energy is then E_2.

The relationships are illustrated by potential-energy diagram shown in Figure 1.8. Reaction first involves the passage of the system over an initial energy barrier to give the adsorbed state, the energy of which is always lower than that of the initial state; that is, ΔU^0 is always negative. The system then passes over a second barrier of height E_2. If the pressure is low, most of the reactant molecules are not adsorbed, and to pass to the second activated state they have to acquire the energy $E_2 + \Delta U^0$, which is less than E_2. At high pressures, however, the equilibrium favors the adsorbs state, and the activation energy is E_2.

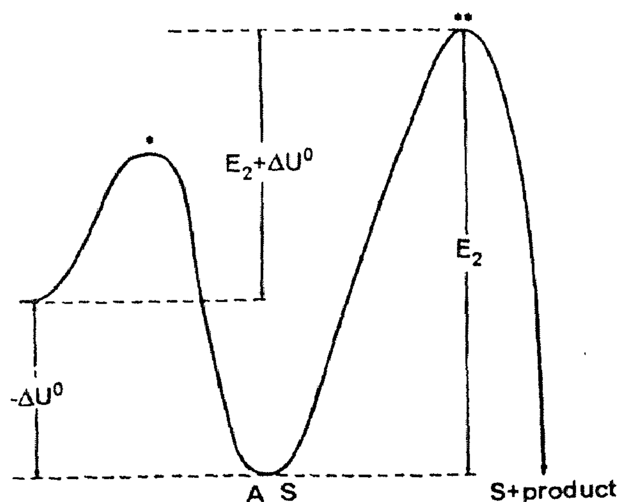

Figure 1.8 Energy diagram for a unimolecular surface reaction. The different ΔU^0 between the energy of A-S and that of A+S is always negative (adsorption is exothermic).

1.2.3.2 Bimolecular Surface Reactions

As already noted, there are two distinctly different mechanisms for a surface reaction between two reactants A and B. In the Langmuir-Hinshelwood mechanism, reaction occurs between A and B molecules when both are adsorbed on the surface. Alternatively, in the Langmuir-Rideal mechanism, the reaction occurs between an adsorbed molecule and a molecule in the gas phase. These mechanisms may be distinguished on the basis of the different kinetic equations to which they give rise.

Suppose that two substances adsorb on the same surface and that the fraction of surface covered by molecules of type A is θ_A and the fraction covered by B is θ_B. The bare fraction is $1 - \theta_A - \theta_B$. If both substances are adsorbed without dissociation, the rates of adsorption of A and B are

$$v_a^A = k_a^A[A](1-\theta_A-\theta_B) \quad (1.14)$$

and

$$v_a^B = k_a^B[B](1-\theta_A-\theta_B) \quad (1.15)$$

The rates of desorption are

$$v_{-a}^A = k_{-a}^A\theta_A \quad (1.16)$$

$$v_{-a}^B = k_{-a}^B\theta_B \quad (1.17)$$

Equating Equations (1.14) and (1.16) leads to

$$\frac{\theta_A}{1-\theta_A-\theta_B}=K_A[A] \qquad (1.18)$$

where $K_A = k_a^A/k_{-a}^A$. From Equations (1.15) and (1.17) it follows that

$$\frac{\theta_B}{1-\theta_A-\theta_B}=K_B[B] \qquad (1.19)$$

where $K_B = k_a^B/k_{-a}^B$. Equations (1.18) and (1.19) are two simultaneous equations that can be solved to give, for the fractions covered by A and B, respectively,

$$\theta_A=\frac{K_A[A]}{1+K_A[A]+K_B[B]} \qquad (1.20)$$

$$\theta_B=\frac{K_B[A]}{1+K_A[A]+K_B[B]} \qquad (1.21)$$

In a Langmuir-Hinshelwood mechanism the rate is proportional to the fractions of the molecules A and B that are adsorbed.

$$v = k\theta_A\theta_B \qquad (1.22)$$

$$=\frac{k\,K_A\,K_B[A][B]}{(1+K_A[A]+K_B[B])^2} \qquad (1.23)$$

If [B] is held constant and [A] is varied, the rate varies in accordance with Figure 1.7b. The rate first increases, then passes through a maximum, and finally decrease. The explanation of the fall off in the rate at high concentrations is that one reactant displaces the other as its concentration is increased. The maximum rate corresponds to the existence of the maximum number of neighboring A-B pairs on the surface.

Suppose that the mechanism is of the Langmuir-Rideal type, and that the reaction occurs between an adsorbed B molecule and a molecule of A in the gas phase. The fraction of surface covered by B is given by Equation (1.21), and the rate is now proportional to this fraction and to the concentration of A:

$$v = k\theta_B[A] \tag{1.24}$$

$$= \frac{k K_B[A][B]}{1+K_A[A]+K_B[B]} \tag{1.25}$$

In this mechanism it is not assumed that A is not at all adsorbed, and the term $K_A[A]$ in the denominator corresponds to the adsorption of A. Adsorbed A molecules do not enter directly into reaction, but they reduce the rate by occupying surface that might otherwise be occupied by B molecules.

If [B] is held constant and [A] is varied, there is now no maximum as [A] increases; instead, the rate varies with the concentration of the reactant in the manner shown in Figure 1.7c. A decision between the two mechanisms may be

made by seeing if the rate decreases at higher concentrations of reactants [14]. In all cases

$$k = k_0 e^{-\frac{E_a}{RT}} \quad (1.26)$$

where k_0 is a constant.

1.3 Types of CVD Processes

CVD systems are divided into two primary types: cold-wall systems and hot-wall systems. Cold-wall systems use induction or radiant heating to directly heat the wafer holder or wafers through a quartz reaction chamber. Hot-wall types supply the reaction energy by a method that heats the wafers, the wafer holder, and the chamber walls.

CVD processes can also be classified according to the type of energy supplied to initiate and sustain the reaction: (1) Thermally activated reactions at various pressure ranges, which comprise the vast majority of CVD processes; heat is applied by resistance heating, rf induction heating, or infrared radiation heating techniques. (2) Plasma promoted reactions, where an rf (or dc)-induced glow discharge is the source for most of the energy that initiates and enhances the rate of reaction. (3) Photon induced reactions, where a specific wavelength radiation triggers and sustains the reaction by direct photolysis or by an energy tranfer agent, such as uv-activated mercury.

1.3.1 Thermally Activated Atmospheric Pressure Processes (APCVD)

The simplest CVD process type is conventional atmospheric or normal pressure CVD (APCVD or NPCVD) [15, 16]. Reactant vapors or gases are introduced in the reactor at normal atmospheric pressure. The pressure in the reactor system is slightly above atmospheric due to the impedance of gas flow at the exit part of the system. Control of the pressure is often necessary to achieve good uniformity of the film deposit. Energy is supplied by resistance heating, by rf induction techniques, or by infrared radiation to heat the substrate to an appropriate temperature to initiate and maintain the chemical reaction. The temperature and reactant flow rate determine the rate of film deposition. The advantage of APCVD is its simplicity, no vacuum pumps are needed. The disadvantage is the tendency for homogeneous gas phase nucleation that leads to particle contamination, unless special optimized gas injection techniques are used. Currently, APCVD are used only for low temperature oxide (LTO) deposition and epitaxy.

1.3.2 Thermally Activated Low Pressure Processes (LPCVD)

Most low pressure CVD process are conducted by resistance heating or, less frequently, by infrared radiation heating techniques to attain isothermal conditions so that the substrate and the reactor walls are of similar temperature.

Lowering the gas pressure enhances the mass transfer rate relative to the surface reaction rate, this makes it possible to deposit films uniformly in a highly economical close spaced positioning of the substrate wafers in a standup fashion.

Furthermore, unexpectedly high deposition rates are attainable with LPCVD despite the fact that the operating total pressure is usually two to four orders of magnitude less than that used in APCVD. The reason for the relatively high rate is the large mole fraction of reactive gases in LPCVD, since no or little diluent gas is required. And the thickness uniformity of the films and the step coverage are substantially improved over those obtainable in conventional atmospheric pressure CVD reactors. The films have fewer defects, such as particulate contaminants and pinholes, because of the inherently cleaner hot wall operations and the vertical wafer positioning that minimize the formation and codeposition of homogeneously gas phase nucleated particulates. Further, stoichiometric compositions of the films can be achieved by optimizing LPCVD. But some disadvantanges of LPCVD exist, such as using toxic, explosive or corrosive gaseous reactants, comparatively high deposition temperature.

Low pressure CVD is widely used in the extremely cost competitive semiconductor industry for depositing films of insulators, amorphous and polycrystalline silicon, refractory metals, and silicides. Epitaxial growth of silicon at reduced pressure minimizes autodoping (contamination of the substrate by its dopant), a major problem in atmospheric pressure epitaxy[17].

1.3.3 Plasma-enhanced Deposition Process (PECVD)

Plasma deposition [18-24] is a combination of a glow discharge process and low pressure chemical vapor deposition highly reactive chemical species are generated

from gaseous reactants by a glow discharge and interact to form a thin solid film product on the substrate and electrode surfaces. Since the plasma assists or enhances the chemical vapor deposition reaction, the process is denoted as PACVD or PECVD. Salient features of plasmas and PECVD are summarized in Table 1.4.

By utilizing plasma enhancement techniques, many high temperature chemical reaction can be made to take place on temperature sensitive materials at low temperatures and in a much more energy efficient fashion than can be produced by other techniques. Other advantages of PECVD are that film deposition rates are substantially higher than in thermally activated LPCVD, and step coverage is more conformal.

Concerning disadvantages of PECVD, the complexity of reactions makes the synthesis of stoichiometric compositions difficult. A consequence of the low temperature of film formation, gases are trapped in the kilns, which frequently causes thermal instability due to outgassing. In the case of plasma nitride films, hydrogen given off may cause deleterious changes in the electronic properties of certain devices. Sensitive MOS devices may be damaged by the radiation by a thermal anneal by the deposition temperature.

1.3.4 Photo-enhanced Chemical Vapor Deposition (PHCVD)

This type of process is based on activation of the reactants in the gas or vapor phase by electromagnetic (usually short wave ultraviolet) radiation [25]. Selective

Table 1.4 Plasma and plasma CVD

A. PLASMA

- Partially ionized gas composed of ions, electrons, neutral species
- species, generated by high temperature or strong electric or magnetic fields

B. PLASMA CVD

- Chemical vapor deposition reactions in plasmas produced by gaseous electric discharges
- Free electrons gain energy from imposed electric fields, then transfer it by collisions to reactant molecules, leading to free radicals, ions, atoms, metastable species, excited molecules, photons
- Chemical interactions create new products, often of unique properties, strongly condition-dependent, usually non-stoichiometric

C. LOW-PRESSURE GLOW DISCHARGE PLASMA

- Concentrations of positive and negative charge carriers approximately equal
- Condition satisfied if discharged gas volumes are larger than Debye length λ_D, the distance over which charge imbalanced can exist

Table 1.4 (Continued) Plasma and plasma CVD

• Electron energies ≅ 1-12 eV at 10^{-3}-10 Torr; electron densities ≅ 10^{9}-10^{12} /cm^3
• Electron temp./gas temp. ≅ 10-1000. The high electron temperature is the key to plasma reactions. The free electrons have energies equivalent to 10^4 - 10^5 °K.
D. MOST IMPORTANT FILM PRODUCTS
• Silicon nitrides, silicon oxynitrides
• Silicon oxides, phosphorous silica glass
• Amorphous silicon, polycrystalline silicon

absorption of photonic energy by the reactant molecules or atoms initiates the process by forming very reactive free radical species that interact to form a desired film product. Typically, mercury vapor is added to the reactant gas mixture as a photosensitizer and is being activated by the radiation from a high intensity quartz mercury resonance lamp (253.7 nm wavelength). The excited mercury atoms transfer their energy kinetically by collision to the reactants to generate free radicals. The advantages of this versatile and very promising CVD process is the low temperature (typically 150 °C) needed to form film such as SiO_2, Si_3N_4, and

silicon, and the greatly reduced radiation damage (compared to PECVD) that results. The limitations at present are the unavailability of effective production equipment and the need (in most cases) for photoactivation with mercury to achieve acceptable rates of film deposition. Direct photolysis without the need for mercury can be accomplished in some cases if very intense high energy ultraviolet is used.

1.3.5 Lase-induced Chemical Vapor Deposition (LDCVD)

Chemical vapor deposition involving the use of lasers [26, 27] can be categorized in three types of processes: (1) pyrolysis, (2) evaporation, and (3) photolysis. Pyrolysis utilizes a laser beam for highly localized heating of the substrate that Induces film deposition by CVD surface reactions, and can be exploited for the direct writing of patterns on a substrate. In evaporation applications the laser simply acts an energy source to vaporize atom from a target to the substrate. Photolysis utilizes laser (or electron radiation) to activate gaseous reactant atoms or molecules by their absorption of the specific wavelength of the photonic energy supplied. The resulting chemical gas phase reactions are very specific, leading to highly pure film deposition. On the other hand, the activation matching of the spectral properties with the reactant species limits the choice of reactions and hence restricts the film deposits that can be obtained.

Among several advantages of these techniques are the spatial resolution that can be achieved and the ability to interface with laser annealing, diffusion, and

localized heat treatments. Focused light from a low power ultraviolet laser, such as a frequency-doubled Ar laser, can be utilized for gas phase photodecomposition to produce localized metal films deposits from metal alkyl vapors. This technique has been used for repairing localized transparent metal defects (open areas) on photomasks.

CHAPTER 2

LITERATURE REVIEW

Silicon nitride has been known as a refractory material for over a century. Crystalline silicon nitride ceramics, obtained by reaction-sintering or hot-pressing, are noted for its chemical inertness, high temperature strength, high electrical resistivity, good thermal shock resistance, and extreme hardness. They have been used for many high temperature applications, including container for molten metals and glasses, radiation heat shields, rocket-nozzle inserts, and stator blades for gas turbines.

More recently, silicon nitride has been used as a dielectric in electronic devices, utilizing it imperviousness to supplement the more commonly used silicon dioxide. The disadvantages of silicon dioxide, such as the high permeability toward moisture and other impurities, associated with its inherent structural porosity are well known. To be useful in devices, however, silicon nitride must be prepared in the form of amorphous and adherent films on semiconductor surfaces; the amorphous films possess more uniform properties than polycrystalline films.

Si_3N_4 films can be synthesized by numerous techniques including CVD, chemical transport, direct nitridation of silicon, r.f. glow discharge, r.f. sputtering, vacuum evaporation, ion implantation and ion planting. CVD is the preferred method in semiconductor applications because uniform and adherent layers

without defects and impurities are produced with hig throughout using comparatively simple and inexpensive equipment.

2.1 History of CVD Silicon Nitride

The first reported attempt to prepare silicon nitride films was the work of Sterling and Swern in 1965 [28]. They synthesized silicon nitride films from the mixture of silane and anhydrous ammonia using r.f. discharge assisted CVD.

Before the advent of LPCVD, silicon nitride films were synthesized by CVD at atmospheric pressure around 900 °C from a variety of reactants. Doo et al., successfully synthesized silicon nitride films in the temperature range of 750 °C - 1100 °C by pyrolitic dissociation of the SiH_4-NH_3-H_2 precursor systems in 1966 [29]. The following year, Bean et al., synthesized silicon nitride films from same precursor system and studied the effect of process variables on the growth rate and properties of the resulting films [30]. They pointed out that the growth rate dependence on 1/T had a break at 900 °C, coincident with an observed amorphous-polycrystalline transition. Hardness, growth rate, and refractive index were found to move toward values appropriate for silicon as the per cent ammonia was reduced. The thermal expansion coefficient could be varied from approximately that of silicon to that of silicon nitride by increasing the per cent ammonia. At the same time, the use of hydrazine in place of ammonia to reduce the deposition temperature was reported [31]. The growth rate in this case reached a saturation value above 750 °C, and the films produced from this process were

transparent, smooth, and highly adherent, but had large etch rates in hydrofluoric acid than those from the ammonia process.

Amorphous silicon nitride films deposited in a gas flow system by the ammonolysis of silicon tetrachloride and the nitridation of silane with ammonia on heated substrate surfaces was reported in 1967. The dependence of the deposition rate on the substrate temperature, the reactant composition, and flow rate were discussed [32]. The films deposited from this process had been shown by chemical analysis and electron beam induced crystallization to have the composition Si_3N_4. In that paper, the density, refractive index, infrared absorption, and dissolution rate of deposited silicon nitride films were determined too. The substrate temperature during the deposition process appeared to have the most significant influence on these properties, particularly density and dissolution rate. Consequently, the synthesis of silicon nitride films on silicon substrates from the $SiCl_4$-NH_3 precursor system over the range of 550 °C to 1250 °C was reported by Grieco et al., in 1968 [33]. In their work effects of deposition temperature, and of $SiCl_4$ and NH_3 concentrations on the deposition rate were investigasted. The etch rate of the deposits was shown to be a function of deposition temperature. Electrical evaluation revealed the dielectric strength to be independent of thickness, and the dielectric constant to be in the range from seven to eight. Surface charge ranged from 7 to 18 x 10^{11} /cm^2. Nonlinear I-V characteristics of the films were observed. These films were extremely effective diffusion masks for sodium. In 1972, another paper was published that discussed the operating

characteristics of a production system for the deposition of silicon nitride by the ammonolysis of silicon tetrachloride in a hot wall furnace, and the characteristics of the resulting films [34].

With the advent of LPCVD techniques in 1973, Tanikawa et al., first reported the low pressure deposition of silicon nitride films using $SiCl_4$-NH_3 precursors, but no details on the effects of varying the deposition parameters on film properties were given [35]. In 1977, Rosler reported the synthesis of amorphous silicon nitride films by LPCVD from the SiH_2Cl_2-NH_3 precursor system and the effects of processing variables on thickness uniformity, growth rate and load size [36]. Following this discovery, a number of LPCVD silicon nitride films synthesized from the SiH_4-NH_3-H_2 (N_2) or SiH_2Cl_2-NH_3 precursor systems were reported including articles by Pan and Berry in 1985 [37], Roenigk and Jensen in 1987 [38], Gregory et al., in 1991 [39], Zhang et al., in 1992 [40], as well as Wang et al., in 1993 [41].

Paihung et al., synthesized silicon nitride films at 770 °C with different NH_3/SiH_2Cl_2 reactant gas ratios (R) ranging from 2 to 20 [37]. Auger electron spectroscopy (AES) showed that the Si/N ratio was about 0.75, and the compositional uniformity was good for all samples. No excess Si clusters were detected by TEM for the samples annealed at 1000 °C in N_2 for 5h. Only N-H bonds were observed by infrared (IR) analysis; the amount of N-H bonds in the as-deposited samples was estimated to be about 5×10^{16} cm^{-2}; the normalized N-H absorption peak area was found to increase with increasing R values, while the

amount of N-H bonds was found to decrease after annealing at 1000 °C in N_2 for 30 min. The plasma etch rates were found to increase by increasing R values and showed a good correspondence to the trend of increasing N-H bonds. The film stress for all samples was tensile and had a level of 1×10^{10} dyn/cm^2. No difference was observed in the film's ability to act as oxidation barrier for samples deposited with different R values.

In a paper written by Roenigk and Jensen [38], a model of the hot wall tubular reactor for LPCVD was applied to the study of silicon nitride film growth from dichlorosilane and ammonia. The model predicted the effects of process conditions and reactor configuration on distributed wafer rate profiles. The formulation included contributions from convection, multicomponent diffusion, and gas surface reaction of several chemical species. Rival chemical mechanisms were compared to experimental data obtained in a conventional LPCVD reactor over widely varying conditions. Results indicated that the in-wafer film thickness nonuniformities may be explained by the effect of diffusion-limited film growth from highly reactive gas-phase intermediates, with simultaneous uniform deposition from less reactive dichlorosilane. Model predictions agreed well with experimental data over the composition, pressure, and temperature ranges considered. The model was also used in the design of optimal operating conditions for 100 and 150 mm wafer processes.

The conditions employed in the study done by Gregory et al. [39], were dictated by a full factorial matrix of the independent variables over 20 deposition

runs, then the effect of the variables, the flow rates of NH_3 and SiH_2Cl_2, the temperature, and the time of deposition, and their interactions on the electrical, physical, and chemical properties of the Si_3N_4 were determined. Thus deposition condition can be judiciously chosen to optimize film properties.

Zhang et al. [40], experimentally studied the growth of stoichiometric and non-stoichiometric silicon nitride on 100 mm silicon wafers by batch deposition from the dichlorosilane-ammonia system in a hot horizontal LPCVD reactor. The growth kinetics were discussed in terms of the Langmuir adsorption isotherm: the kinetic parameters were determined by comparing the experimental data with a one-dimensional simulation model. The decomposition of NH_3 at high temperature was included on the simulation procedure. When the SiH_2Cl_2 : NH_3 ratio were greater than 1.5, a quantity higher than critical values above which Si-rich nitride films began to deposit, various SiN_x films with $x < 4/3$ were obtained. The composition of the SiN_x films was found to vary to along the LPCVD reactor. The film stiochiometry was examined by Rutherford backscattering and ellipsometry measurements. According to kinetic and thermodynamic studies, the pyrolysis of dichlorosilane at elevated temperature (> 700 °C) caused deposition of Si-rich nitride films.

Wang et al. [41], distinguished reactions in deposition of Si_3N_4 by LPCVD from SiH_2Cl_2+NH_3 systems into two overall reactions: (1) the chemical reaction between SiH_2Cl_2 and NH_3, (2) the pyrolysis of NH_3. The kinetics equations corresponding to the chemical reactions above as follows:

$$r_1 = \frac{K_s p_{SiH_2Cl_2} p_{NH_3}}{1 + K_1 p_{SiH_2Cl_2} + K_2 p_{NH_3}} \quad (2.1)$$

$$r_2 = K_d \cdot p_{NH_3} \quad (2.2)$$

According to that model, the pyrolysis of NH_3 did not play an important role at low temperatures (such as at 700 °C). Therefore, the dilution of SiH_2Cl_2 by increasing the NH_3 concentration reduced the deposition rates at low temperature. At high temperatures (above 800 °C), the pyrolysis of NH_3 played a main role. This was because a large amount of NH_3 was already decomposed in the upstream or in the pre-wafer deposition region. So increasing NH_3 flow rate was benefitial in overcoming an insufficient amount of NH_3 and to increase the deposition rate. At medium temperatures (about 750 °C), the pyrolysis of SiH_2Cl_2 became considerable, but it did not completely dominate the process. The competition between pyrolysis of NH_3 and dilution of in the upstream region was obvious.

Currently, more and more inorganic precursor systems were investigated to deposit silicon nitride films by LPCVD. For example, Scheid et al., tested Si_2H_6-NH_3 systems [42]. They concluded that the films were Si rich, with only the lowest Si_2H_6/NH_3 ratio giving stoichiometric Si_3N_4, and that the deposition rate can reach adequate values (20 Å min^{-1} or more) for high values of R (according to what can be obtained in the case of Si deposition from Si_2H_6) but with a high Si content in the resulting film. The buffer HF etching rate was low, with a minimum

when the Si content was at a maximum, despite the fact that the density of Si-bonds can be quite high (about 5%). The I-V characteristics of the different films showed that the stoichiometric films presented a breakdown field of about 7 mV cm^{-1} and that the Si-rich films had a semi-resistive behavior.

PECVD became another important method to deposit silicon nitride films in order to passivate and encapsulate completely fabricated microelectronic devices. Work on PECVD silicon nitride was reported by van de Ven in 1981 [43], as well as Katoh et al. [44], in 1983. Excellent silicon nitride films which could be used as gate insulator on an a Si FET, were fabricated by RF glow-discharge of SiH_4 - N_2 -H_2 gas mixture. Resistivity values larger than 1×10^{16} Ω·cm and breakdown strength of 6×10^6 V/cm were realized. Finally the optimum deposition conditions were evaluated and briefly discussed in connection with mechanisms of the plasma-enhanced deposition. Blaauw reported his work on preparation and characterization of plasma silicon nitride films deposited on Si substrates from SiH_4, NH_3 and Ar [45]. In his work several parameters were systematically varied, including the deposition temperature (20 °C - 500 °C), RF power (10 - 300 W), chamber pressure (0.5 - 1.4 Torr), and gas flow rates. Relationships between deposition parameters and film characteristics such as deposition rate, etch rate, and index of refraction were discussed in terms of current understanding of the deposition process. The author concluded that pinhole densities were reduced by increase of the film thickness. At 500 °C specular films were grown with the

following characteristics: refractive index 1.9 -2.1, pinhole density 5 cm^{-2} at 1.0 μm thickness, 100 Å/min etch rate in buffered HF, and good stability to annealing.

In the synthesis of silicon nitride by CVD, SiH_4, SiH_2Cl_2 or $SiCl_4$ were typically used as a silicon source. While SiH_4 is known to be toxic, pyrophoric and explosive, the products of the SiH_2Cl_2 are corrosive and represented a reliability threat when incorporated in the deposits, and $SiCl_4$ is corrosive. Furthermore, their use requires gas cabinets and cross purging supply systems to insure safety and prevent corrosion of vacuum pumps. The use of organosilanes can resolve the safety issue. Now more and more organosilane systems have been tested for deposition silicon nitride films. As to technical feasibility, ditertiarybutylsilane (DTBS) and tri (dimethylamino) silane (TDMAS) have been used in hot wall horizontal LPCVD to deposit chemically stable silicon nitride films [46]. The results indicated that for silicon nitride formation by DTBS, the typical growth rates were on the order of 30 - 300 Å/min, with the optimum being from about 75 to 250 Å/min at a pressure range of 0.6 -2.0 Torr and at temperature range of 600 °C to 700 °C [46]. Preliminary results for LPCVD silicon nitride films using TDMAS indicated that the deposition rate followed an Arrhenius behavior in range of 600 °C to 825 °C which yielded an activation energy of 48 kcal/mole. The deposits had a refractive index of 2.00, bulk resistivity of 1×10^{16} Ω·cm, Si/N ratio of 0.77, N-H content of 4 at%, and Si-H content of 0.06 at%. The etch rate of the deposits was 32 Å/min in 49 % HF.

2.2 Comparison of Properties of Silicon Nitride Films Deposited by LPCVD and PECVD

Currently, LPCVD and PECVD are two most importantly and widely used CVD processes to obtain silicon nitride film. The properties of LPCVD and PECVD silicon nitride films are compared in Table 2.1 [47]. From this data we can conclude that when silicon nitride is used as a mask for selective oxidation or as a gate dielectric material, the film is generally deposited by high-temperature LPCVD technique for reasons of film uniformity and lower processing cost [48]; when it is used as a passivation layer, the deposition process must be compatible with such low melting-point metals as aluminum and must, therefore, be produced at temperatures of < 400 °C [49,50]. PECVD silicon nitride films are generally nonstoichiometric and contain high quantities of hydrogen (10 - 30 %). The narrow range for the refractive index values in the above table indicates that LPCVD tends to produce stoichiometric films while the broader values for the refractive index of PECVD silicon nitride reflects formation of non-stoichiometric films.

2.3 Application of Silicon Nitride Films

Deposits of Si_3N_4 thin film are widely used in semiconductors and in integrated circuit technology. Other applications include Si_3N_4 as a target with low energy nucleate reactions, Si_3N_4 films on silicon for optical waveguides, and Si_3N_4 for forming glass-to-metal seals.

Table 2.1 Properties of LPCVD and PECVD deposited silicon nitride films

Property	LPCVD	PECVD
Deposition temperature	550 - 850 °C	200 - 400 °C
Composition	Si_3N_4	$Si_XN_YH_Z$
Si/N ratio	0.75	0.8 - 1.0
Refractive index	2.0 - 2.1	1.8 - 2.5
Dielectric constant	6 - 7	6 - 9
Dielectric strength	1×10^7 V/cm	6×10^6 V/cm
Stress (dyne/cm^2)	1.2 - 1.8 x 10^{10} (tensile)	1 - 8 x 10^9 (compressive)
H_2O permeability	Zero	Low - None
Thermal stability	Excellent	Variable > 400 °C
Density (g/cm^3)	2.8 - 3.1	2.5 - 2.8
Step coverage	Conformal	Good
Si-N major	870 cm^{-1}	830 cm^{-1}
Si-H minor	None	2180 cm^{-1}

Some of the many important applications of films are the following:

1. As electrical insulators which have a comparatively high dielectric constant.
2. As chemically and electrically stable passivation layers for semiconductor surfaces hich withstand the corrosive action of most reagents and which prevent ion diffusion.

3. As masks for semiconductors to protect against donor and acceptor impurity diffusion (aluminum, boron, gallium, indium, arsenic, phosphorus, antimony, zinc etc.), as they are impermeable to these impurities under the normal diffusion conditions of p-n junctions.
4. As masks for semiconductors to protect against oxidation.
5. As masks for selective epitaxial deposition of silicon.
6. The storage of electric charges (memory effect).
7. The elimination of the effects of electric charges in SiO_2 to obtain devices with stable characteristics.
8 Decreasing the threshold voltage in insulated gate field effect transistors (FETS).
9 Improving the high frequency performances of transistors.

Si_3N_4 is highly suitable as a passivation layer because of its following properties:

- It behaves as a nearly impervious barrier to diffusion (in particular, moisture and sodium find it very difficult to diffuse through the nitride film).
- It can be prepared by PECVD to have a low compressive stress, which allows it to be subjected to severe environmental stress with less likelihood of delamination or cracking.
- Its coverage of underlying metal is conformal.
- It is deposited with acceptably low pinhole densities.

Si_3N_4 is useful as masking for selective oxidation as itself oxidizes very slowly, but it is not penetrated by oxygen; as etching masks in multi-level resist structure [51]; as supporting membranes for x-ray lithography masks [52].

CHAPTER 3

EXPERIMENTAL PROCEDURES

3.1 Properties of the Precursor

In this thesis, tris (dimethylamino) silane (TDMAS) was used in the presence of ammonia (NH_3) to produce silicon nitride films by LPCVD. The physical properties and reactivity information of TDMAS are listed in Table 3.1, Table 3.2 and Table 3.3 [86].

3.2 Set-up of LPCVD System

The LPCVD reactor shown in Figure 3.1 was used to deposit the silicon nitride films of this study. It could be divided into five sections: source section, flow control section, vacuum stations, reaction chamber and wafer holder.

3.2.1 Source Section

The source chemicals were housed in a source section. The TDMAS used as Si precursor to deposit Si_3N_4 was obtained from pressurized liquid source bubbler. Ammonia, another precursor to deposit Si_3N_4, and nitrogen used as "work" gas to open the cap of the LPCVD reactor were in pressured gas cylinders.

Table 3.1 Identification of TDMAS

Chemical name	Tris (Dimethylamino) silane (TDMAS)
Synonyms	Silanetriamine, N, N, N', N', N'', N'' -hexamethyl-
Chemical family	Silane
Formula	$C_6H_{19}N_3Si$

Table 3.2 Physical properties of TDMAS

Appearance	Liquid
Boiling point	145 °C
Specific gravity	0.8
Solubility in water	Reacts with water
Volatiles, percent by volume	100 %
Molecular weight	125
Odor	Amine odor
Flash point	25 °C (77 °F)

Table 3.3 Reactivity information of TDMAS

Explosive	No
Oxidizer	No
Pyrophoric	No
Organic peroxide	No
Water reactive	Yes

3.2.2 Flow Control Section

3.2.2.1 Flow Controller

An MKS mass flow controller Model 8240 and an MKS 200 sccm vapor phase flow rate controller Model 1150B-162M were used to measure and control the flow rate of ammonia and TDMAS respectively.

3.2.2.1.1 MKS Mass Flow Controller

The MKS mass flow controller is a laminar flow device whose precise indication of mass flow is achieved through the use of a range controlling changeable bypass and a paralleling sensor tube. Upon entering the MKS, the gas stream is divided into two parallel paths; the first being directed through the sensor tube, the second through the changeable bypass. The two paths are then rejoined to pass through the control valve before exiting the instrument. The two paths possess in L/D ratio

of greater than 100:1, assuring laminar flow.

The amount of energy required to maintain a fixed temperature profile along a tube through which laminar flow is occurring is a function of mass-flow rate. In the MKS mass flow meter, resistance heaters are wound on the sensor tube and form the active legs of bridge circuits. Their temperatures are established such that a voltage change on the sensor winding is a linear function of a flow change. This signal was then amplified to provide a 0-5 VDC output.

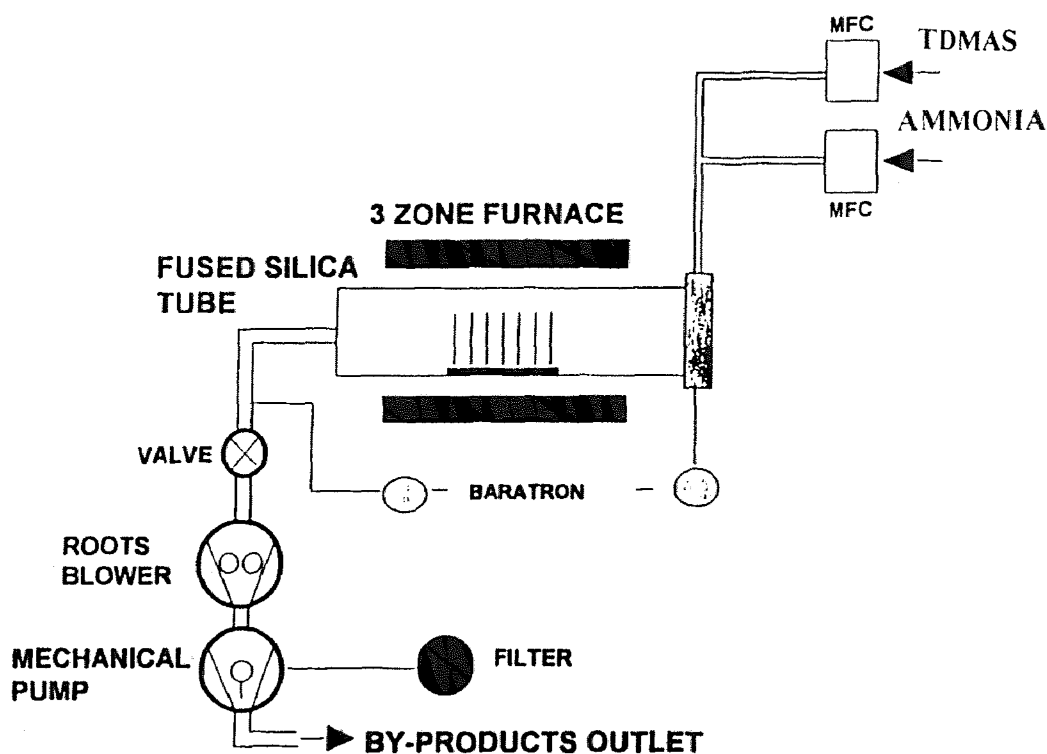

Figure 3.1 Schematic of LPCVD reactor used to synthesize silicon nitride films.

Control circuitry provides drive current for the proportioning control valve. The flow controller accepts a 0-5 VDC setpoint signal, compares it to its own flow

signal, and generates an error voltage. This error signal is then conditioned and amplified so that it may reposition the controlling valve, thus reducing this error to within the accuracy specification of the instrument.

3.2.2.1.2 1150B Mass Flow Controller

The 1150B Mass Flow Controller (MFC) is designed for precise and repeatable mass flow control of most low vapor pressure liquid or solid materials. It utilizes all-metal seals to eliminate permeation normally found with the use of elastomeric sealing materials. Mass flow measurement and control is accomplished without the need of bubbler systems or thermal mass flow sensors. The 1150B MFC uses a pressure sensor and an integral proportional-integral-differential (PID) controller to control the pressure above a choked orifice.

The operation of 1150B MFC is based on the linear relationship between the total pressure upstream of a sonic nozzle and the mass flow through it, given choked flow, inlet to outlet pressure ratio of approximately 2:1. If this ratio drops below approximately 2:1 the flow through the sonic nozzle would not be choked and the flow may become non-linear. A Baratron pressure sensor of appropriate range measures this pressure and generates an output voltage which is appropriately scaled to give a 0 to 5 VDC output equal to 0 to 100% full scale flowrate of the specified material. The output signal and the setpoint signal are compared in an integral PID control circuit. An error signal is generated, and after

further signal conditioning, a drive current for the proportioning flow control valve is generated which opens the valve to the correct position for the desired flowrate.

3.2.2.2 The Switches of Flow Pipes

The switches of the flow pipes consists of the pneumatic valves and the relay switches (shown in Figure 3.2). The pneumatic valves are used as doors of the flow pipes which are controlled by compressive air. Electrical circuitry controls the relay switches which decided whether the compressive air flows or not.

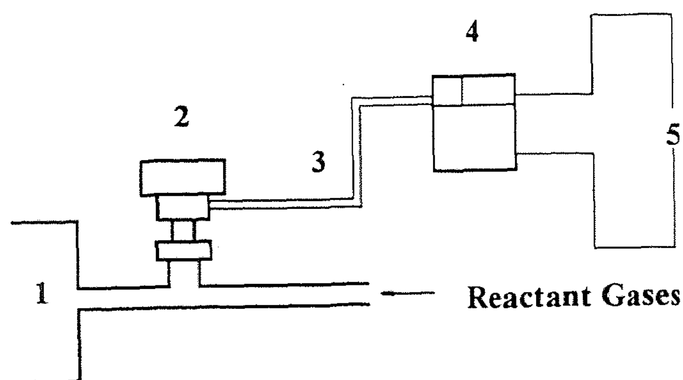

Figure 3.2 Schematic of a switch of the flow pipes of reactant gases: 1. chamber; 2. pneumatic valve; 3. compressive air flow tube; 4. relay switch; 5. electrical circuitry.

3.2.3. Vacuum Stations

An Edwards two-stage vacuum station (shown in Figure 3.3) consisted of a mechanical pump Model E2M40 and a booster pump Model EH250 is used to establish the required vacuum.

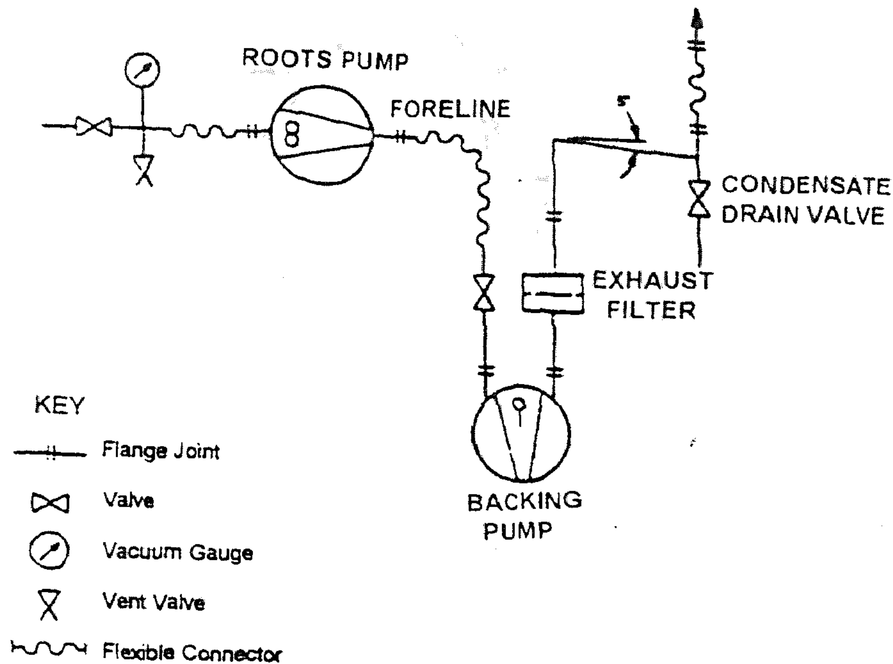

Figure 3.3 Installation arrangement for a vacuum system.

3.2.3.1 Mechnical Pump

The mechanical pump system shown in Figure 3.4 contains eccentrically mounted rotor with spring-loaded vanes. During rotation the vanes slide in and out within the cylindrical interior of the pump, enabling a quantity of gas to be confined, compressed, and discharged through an exhaust valve into the atmosphere. Compression ratios of up to 10^6 can be achieved in this way. Oil is employed as a sealant as well as a lubricant between components moving within tight clearances. N_2 is added in the oil to dilute the exhaust gases. Oil filter system is used to filter unnecessary particles from the pump oil and thereby increases the lifetime of the pumping system.

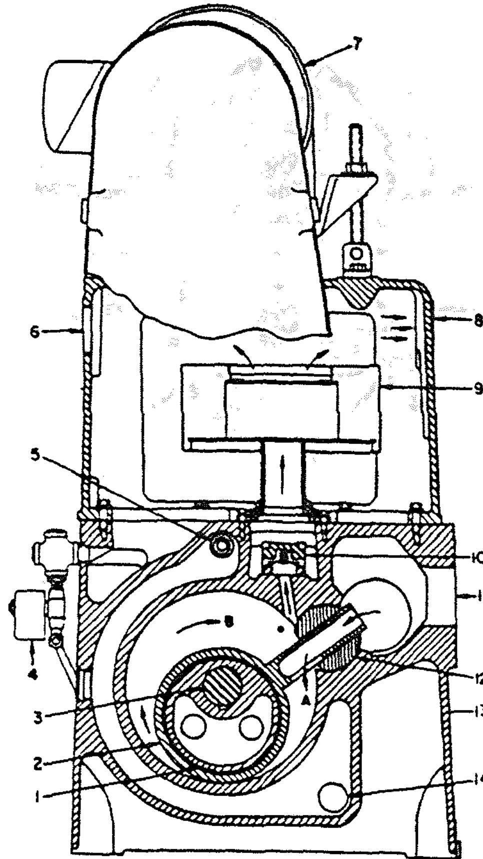

Figure 3.4 Schematic of a rotary piston pump: 1. eccentric; 2. piston; 3. shaft; 4. gas ballast; 5. colling water; 6. optional exhaust; 7. motor; 8. exhaust; 9. oil mist separator; 10. poppet valve; 11. inlet; 12. hing bar; 13 casing 14; cooling water.

3.2.3.2 Booster Pump

The booster pump (shown in Figure 3.5) was used in the combination with the mechanical pump for the applications requiring high pumping speeds, where two figure-right shaped lobes rotated in opposite directions against each other. The extremely close tolerances eliminate the need to seal with oil. These pumps have very high pumping speeds, and even though they can attain ultimate pressures below 10^{-5} torr.

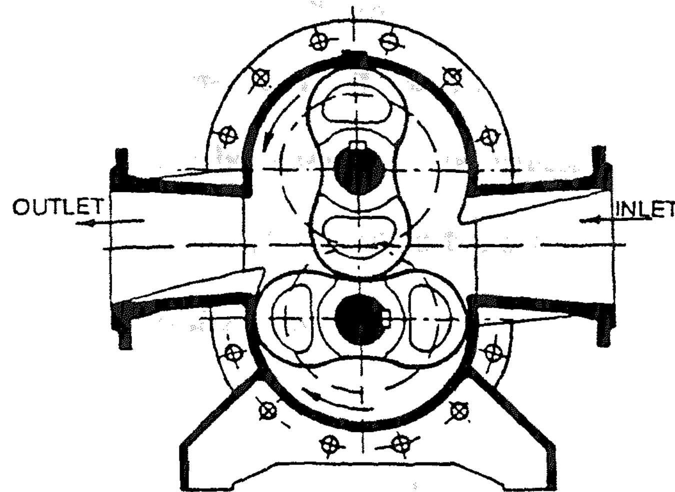

Figure 3.5 Schematic of the booster pump.

3.2.4 Reaction Chamber

The reaction chamber consists of a fused silica tube, having an inner diameter of 12.5 cm and a length of 120 cm. It is mounted horizontally within a three zone Lindberg furnace capable of operating at a maximum temperature of 1200 °C. The fused silica tube which is sealed on both ends by water cooled O-ring caps separated from coils by a ceramic enclosure. A type K (nickel-aluminum vs. nickel-chromium) thermocouple was used to measure temperature. The pressure in the reactor was monitored by an MKS Baratron pressure gauge.

3.2.5 Wafer and Wafer Holder

The wafers used in the deposition were <100> silicon wafers with the diameter of 10 mm, the thickness in the range from 525-50 μm to 525+50 μm and resistivity of 1-25 Ω·cm.

The wafer holder in the deposition experiments was a fused silica boat with 12 single wafer slots on which only one wafer can be inserted and 11 double wafer slots on which two wafers can be inserted. The spacing between the adjacent single and double wafer slots is 1.25 cm while the spacing between the adjacent single wafer slots (or double wafer slots) is 2.5 cm.

3.3 Deposition Procedure

Several pre-deposition experiments were done before deposition procedure to insure accurate experiment conditions of temperature, pressure and flow ratio series.

3.3.1 Pre-deposition Procedure

3.3.1.1 Temperature Calibration of the Reaction Chamber

In order to obtain temperature profile of LPCVD reaction chamber, temperature calibration were done before the experiments on deposition. During temperature calibration procedure, a calibrated type K thermocouple was introduced into the reaction chamber from a inlet in the front end-cap. Reading was taken every 5 cm along a 35 cm length of the central zone beginning from the position which was 50 cm far away the front end of the reaction chamber. A 20 minute wait took place between reading to insure temperature equilibrium. This work had been finished by Xiangqun Fan for 650 °C, 700 °C, 750 °C, 800 °C, 850 °C set temperatures. From the temperature profile shown in the Figure 3.6, the conclusion can be drawn

that actual temperatures approximately equal to the set temperatures in the center range of the reaction chamber.

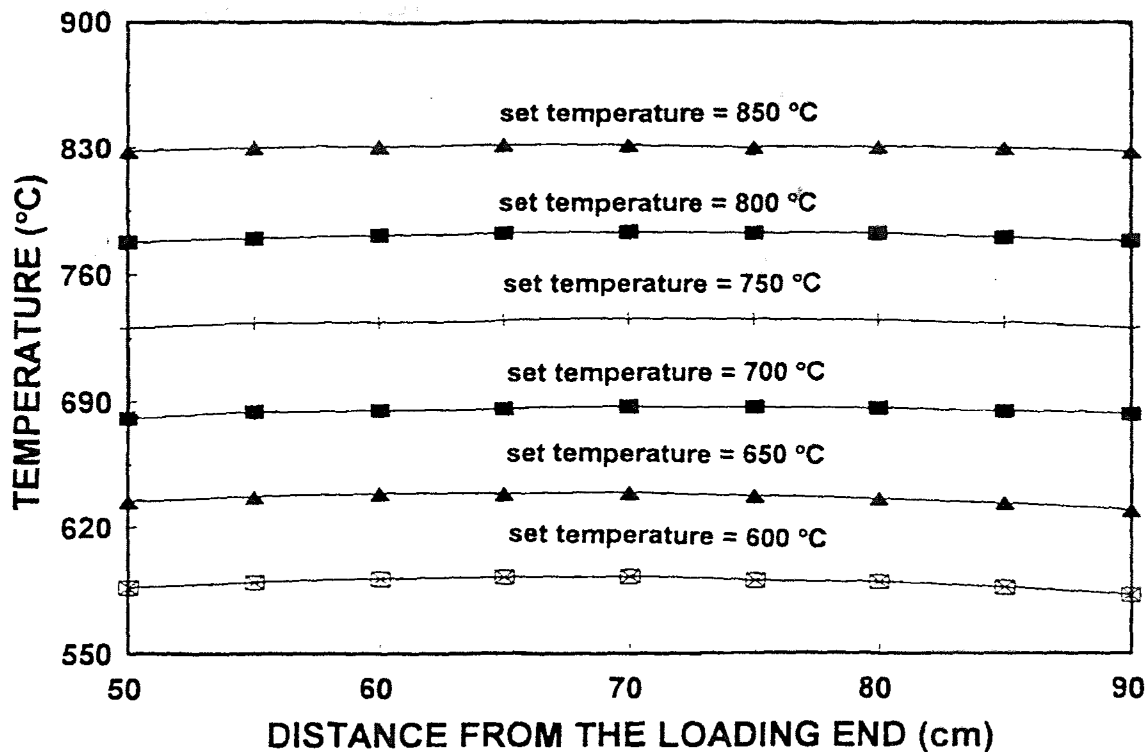

Figure 3.6 Temperature profile of LPCVD reactor.

3.3.1.2 Leak Check

A leak check was conducted before flow rate calibration and experimental run to avoid oxygen and insure formation of films with desirable and reproducible quality. During this leak check procedure, all pneumatic valves, mass flow controllers and gas regulators were fully close. After sealing the outlet of the reaction chamber, the pressure rise in the reactor was measured and the leak rate

was calculated. Typical leak rates were on the order of 5 mTorr/min which was deemed acceptable.

3.3.1.3 Flow Rate Calibration

In order to obtain exact flow rates of the precursors, flow rate calibration was done before every run.

Flow rate is defined as the volume change per unit time, (sccm/min - standard cubic centimeter/minute), that is

$$\text{Flow Rate} = \frac{\partial V}{\partial t} \tag{3.1}$$

where V = volume

t = time

With aid of the Ideal Gas Law:

$$PV = nRT \tag{3.2}$$

at standard condition (temperature is fixed at 273°K, pressure at 760 Torr)

$$\text{Flow Rate} = \frac{\partial V}{\partial t} = \frac{RT}{P} * \frac{\partial n}{\partial t} = R * \frac{273}{760} * \frac{\partial n}{\partial t} \tag{3.3}$$

In this experiments, flow rate, in unit of sccm, was calibrated at room temperature T_r (absolute temperature scale), changing pressure (expressed by Torr/sec), and the volume of the LPCVD reactor chamber is 16700 ccm, according to (3.2)

$$\frac{\partial n}{\partial t} = 60 * 16700 * \frac{273}{T_r} * \frac{1}{760} * \frac{\partial P}{\partial t} \tag{3.4}$$

Thus flow rate can be calculated from Epuation (3.5)

$$\text{Flow Rate} = \frac{273}{T_r} * \frac{16700}{760} * 60 * \frac{\partial P}{\partial t} \tag{3.5}$$

During the calibration chamber was kept at room temperature and pumped down for about 30 minutes. After the flow rate was set, the gas line was opened to induce the gas into the reaction chamber, and the outlet valve was closed, then the reactant gas flow rate can be obtained by measuring the pressure variation rate.

3.3.2 Experimental Procedure

3.3.2.1 Wafer Loading

Three virgin silicon wafers, one virgin quartz wafer, five "dummy" wafers as well as a small piece of silicon step coverage, with trench structure, for step coverage

evalution were positioned standup in a standup position on a fused silica boat. As shown in Figure 3.7, the first "dummy" wafer was placed on the third single wafer slot which was 9 cm from the end of the boat. The first virgin wafer was located on the sixth single wafer slot right after first three "dummy" wafers. The virgin quartz wafer was put after two virgin silicon wafers for optical transmission measurement and a small piece of trenched wafer material for step coverage evaluation for uniformity measurement was on the subsequent double wafer slot. The third virgin silicon wafer was placed back to back on the next double wafer slot with a fourth "dummy" wafer. The fifth "dummy" wafer was used on the tenth single wafer slot.

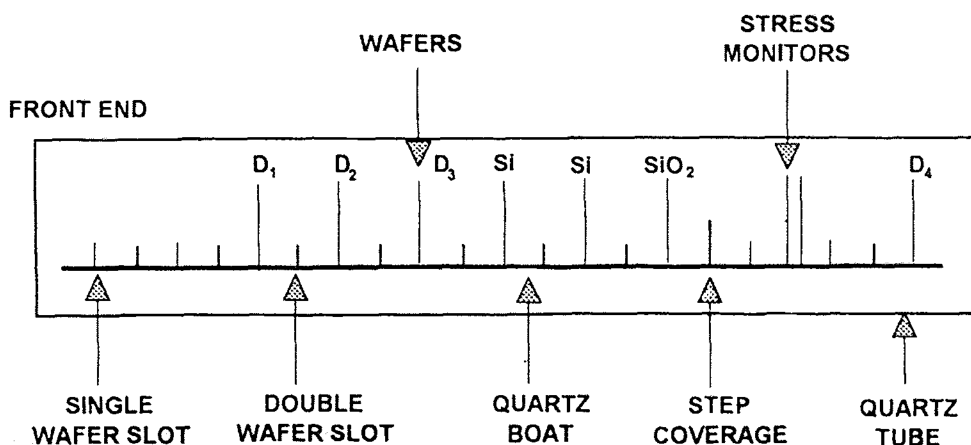

Figure 3.7 Wafers arrangement on silica boat.

All wafers were weighted accurately to 0.1 mg before and after deposition to obtain the weight gain needed to calculate the density of the thin film and evaluate the degree of depletion in each run. The radius of curvature was

measured on the stress monitor before and after each deposition to determine stress values.

3.3.2.2 Heating and Deposition Condition Setting

After loading the wafers, the chamber was evacuated for about one hour. Cooling water and running fans were used to cool O-ring and plastic parts of the chamber. Because of the non-equal heating speed of the three resistance heating zones, the beginning temperature was first set was much lower than that desirable, Three steps were usually used in the heating process to obtain the deposition temperature. When the deposition temperature was reached, ten more minutes were needed to stabilize the furnace. Meanwhile, the flow rates of TDMAS and ammonia were set and the vapor mass flow controller was warmed up to make ready for TDMAS flow.

3.3.2.3 Film Deposition

Ammonia was first introduced into the reaction chamber for 2 minutes prior to introduction of TDMAS. As soon as TDMAS was introduced, the desired total pressure of the reaction chamber was adjusted to the desired value using type 252A exhaust valve controller and maintaining it constant throughout the entire deposition process. At the end of deposition, the samples were cooled overnight before removing them from the chamber.

3.3.2.4 Taking the Wafers out of the Chamber

After closing the exhaust valve and loosening the screws connecting the cap of the tube with the tube, nitrogen was introduced into the chamber until the pressure in the chamber equaled to an atmosphere, then the wafers can be taken out.

3.3.3 The Experimental Parameters

The kinetics and the properties of Si_3N_4 film deposition onto silicon wafers, and the dependence of deposition rate on the deposition temperature, on total pressure in the chamber, and on the flow ratio of NH_3 to TDMAS was investigated..

3.4 Film Characterization Technique

Because of the correlation which existed between structure and properties, there were studies of the Si_3N_4 film structure. Three methods of analysis for the Si_3N_4 film composition were exploited, this data are of importance, since composition of the thin film has a great effect on the its properties. Finally physical properties, optical properties, and mechanical properties of the Si_3N_4 thin film were studied

3.4.1 Structure Studies

There are many methods applied to the study of the structures of thin films, the main structural investigation methods in the thesis work were X-ray diffraction to identify any long range structure of the thin films, scanning electron microscopy

(SEM) to obtain the images of the film surface as well as optical microscopy to study morphology of the thin film.

3.4.1.1 X-ray Diffraction

The structural configuration of the thin films were established by X-ray diffraction conducted with Cu target on Rigaku DMAX II system operating at 30 kV and 20 mÅ.

As shown in Figure 3.8, X-ray are incident on the sample at an angle θ from the sample surface, and a detector is located at an angle θ from the sample surface at the other side. As the angle θ of the sample is varied with respect to the fixed incident beam, the detector is simultaneously moved to a new position at an angle 2θ from the incident beam. The X-ray are diffracted from crystal planes with a spacing d when Bragg's law

$$m\lambda = 2d_{h,k,l}\sin\theta \quad (3.6)$$

is satisfied, where h, k, l are the miller indices. By varying the angle θ, a series of peaks in the X-ray signal appear as grains with different crystal planes parallel to their surface satisfied Bragg's law. Thus, the relative intensities of the various peaks give a quantitative indication of the prevalence of crystals with different orientations within the polycrystalline film. When the structure of the thin film is amorphous which does not exist long-range order, X-ray diffraction patterns

generally do not exhibit peaks in which strong peaks are seen in the diffraction patterns of the corresponding crystals.

X-ray diffraction is a highly accurate method of structural investigation and it offers many benefits over other methods because they are nondestrustive and do not require elaborate sample preparation or film removal from the substrate.

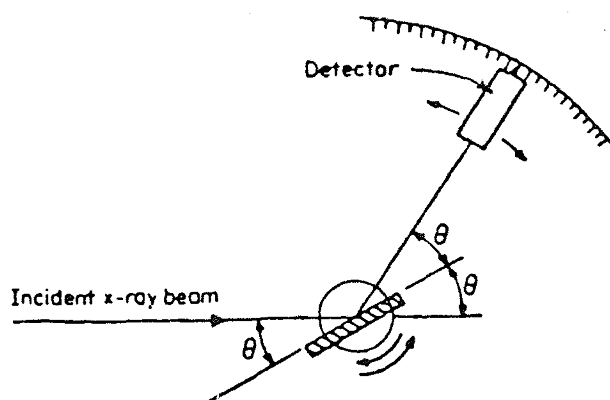

Figure 3.8 Geometrical arrangement of source, sample, and detector in the "θ-2θ" X-ray diffractometer.

3.4.1.2 SEM

The step coverages of 1 μm deep and 1.25 μm wide were used to measure the uniformity of the thin films. Images of the surface of the step coverages were produced by SEM.

A schematic of the typical SEM was shown in Figure 3.9. Electrons thermionically emitted from a tungsten or LaB_6 cathode filament are drawn to an anode, focused by two successive condenser lenses into a beam with a very fine spot size (~ 50 Å). Pairs of scanning coils located at the objective lens deflect the

beam either linearly or in raster fashion over a rectangular area of the specimen surface. Electron beams having energies ranging from a few thousand to 50 keV, with 30 keV a common value, are utilized. Upon impinging on the specimen, the primary electrons decelerate and losing energy transfers it inelastically to other atomic electrons and to the lattice. Secondary electrons, Auger electrons, elastic back scattered electrons as well as X-ray are emitted from the surface of the specimen. In SEM analysis, secondary electron detectors are used to detect secondary electrons. And the whole film surface is scanned by an electron beam, the image of the sample is obtained.

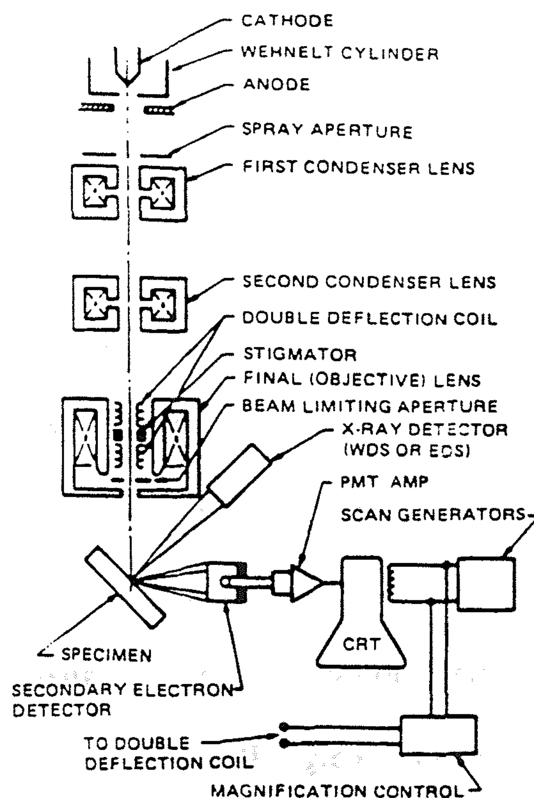

Figure 3.9 Schematic of the scanning electron microscope.

This technique has some important advantages - the surface of a comparatively bulky sample can be directly investigated; a wide field of investigation is available; a comparatively high resolution power is available.

3.4.1.3 Optical Microscopy

Large polarization microscope "ZETOPAN - POL" was used in the thesis work to obtain data on the morphology and structure of thin film.

The polarization microscopy is based on interference of the two coherent light. The two coherent light waves are obtained by splitting of rays with suitable devices, such as polarization optical means, after the specimen. Both partial waves in this design are slightly displaced against each other so that the one partial waves always interfer with the neighboring second partial waves. Interference fringes of equal path difference are produced as results of the wave fronts following each other at a distance of a half wave length each.

The schematic of the differencial interference contrast equipment for transmitted light is shown in Figure 3.10 in which the microscope objective (O) depicts the specimen (P), that is illuminated through the condenser (K) and through the slit diaphragm (S) at the entrance pupil of the condenser, at (P'). If a polarizer (F_1) is in the path of rays, a Wollaston prism (W_1) supplies two waves, the normals of which formes the small angle ε (shown greatly enlarged in Figure 3.10) and which projects two interfering images at P' if an analyzer (F_2) is in the light path. The two images at P' are displaced by the small amount Δ. If the

directions of polarization of analyzer and polarizer are perpendicular to each other and inclined at 45°, against the plane of the sketch, then both partial waves possess equal amplitude which results in maximal contrast.

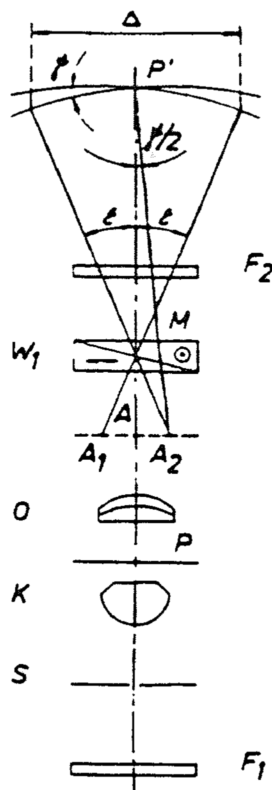

Figure 3.10 Diagram of the differencial interference contrast equipment for transmitted light.

3.4.2 Composition

The elemental composition and chemical states were studied by X-ray photoelectron spectroscopy (XPS) and Rutherford backscattering spectroscopy (RBS).

3.4.2.1 XPS

In the analyses of as-deposited silicon nitride films, XPS was used and the atomic concentration data were collected from individual peak spectra after etching 200 Å from the surface by Ar ion with 242.1 eV.

In the measurement, Al K_{α} X-ray (1486.6 eV, 250 W) is employed to bombard the sample which causes the ejection of an electron from one of the core electronic levels. The kinetic energy KE of the photoemitted core electron is:

$$KE = h\gamma - BE + \Phi \qquad (3.7)$$

where $h\gamma$ is the energy of the exciting radiation, BE is the binding energy of the emitted electron in the thin film and Φ is the spectrometer work function. So it defines the type of the atom, and the number of electrons at this energy is related to the density of the atom present. A schematic of spectrometer of XPS capabilities is shown in Figure 3.11.

Aside from providing information about the chemical bonding of the elements and about several top monolayers of thin film, XPS has an important advantage that is less probability to damage the surface. The limitation of the XPS is that it cannot detect hydrogen and helium since the XPS measurement processes involving the excitation and emission of at least 3 electrons.

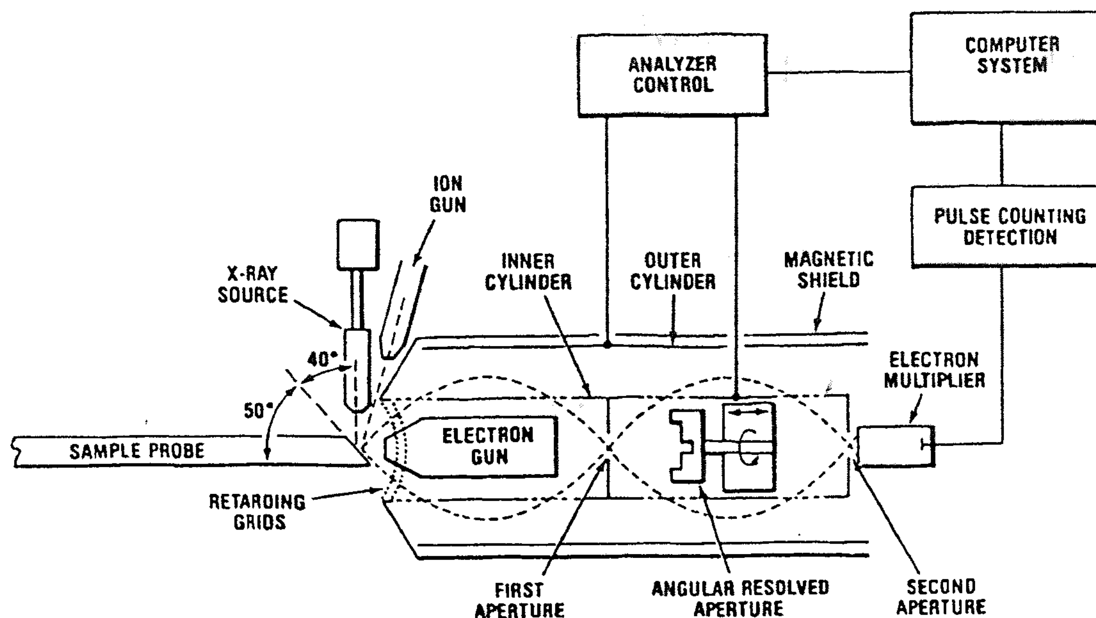

Figure 3.11 Schematic of spectrometer with compared AES and XPS capabilities.

3.4.2.2 RBS

RBS were taken using a high engineering AK accelerator with He^+ ions at an energy of 1.7 meV to corroborate the XPS data.

Elastic collision occurs between the high energy incident ions (atomic mass m and energy E_0) and the outer surface and subsurface atoms of the sample (atomic mass M_2). Upon colliding, some of the incident ions are backscattered with a scattering angle θ and experienced an energy loss (energy E_1). A scattering kinematic factor (K) that is defined as the ratio of E_1 to E_0 can be derived from conservation of energy and conservation of momentum along a longitudinal direction and an incident direction for cases before and after scattering:

$$K \equiv \frac{E_1}{E_0} = \left[\frac{(M_2^2 - m^2 \sin^2\theta)^{1/2} + m\cos\theta}{M_2 + m}\right]^2 \quad (3.8)$$

Thus, the energy scale for a given backscattering spectrum can be translated into a mass scale, and elemental analysis can be determined. A scematic of the 1.7-Mev tandem accelerater, RBS facility at AT&T Bell Laboratories is shown in Figure 3.12.

All elements and their isotopes including Li and those above it in the perodic table are, in principle, dectable with He^+ ions. High-Z elements produce a stronger backscattered signal than low-Z elments. RBS can be of wide use in composition quantification, thin film thickness determination within 5% as well as stress in the thin film. Besides those advantages, specimen is less nondestructive by RBS comparing with other analysis method.

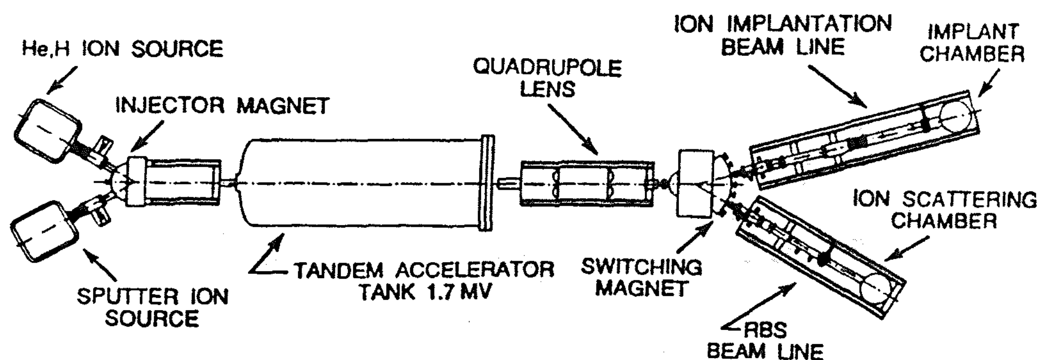

Figure 3.12 Schematic of the 1.7-MeV tandem accelerator, RBS facility at AT&T Bell Laboratories, Murray Hill, NJ.

3.4.3 Properties

The properties of Si_3N_4 films which were most concerned in the thesis work can be divided into physical, optical and mechanical properties.

3.4.3.1 Physical Properties

3.4.3.1.1 Thickness Measurement

Film thickness was measured by Nanospec interferometry which is based on the interference of light naturally between beams reflected from the two film surfaces which involve the air-film surface and film-substrate surface. The relevant Figure 3.13 summarizes what happens when monochromatic light of wavelength λ is normally incident on a transparent film-substrate combination. If n_1 and n_2 are the

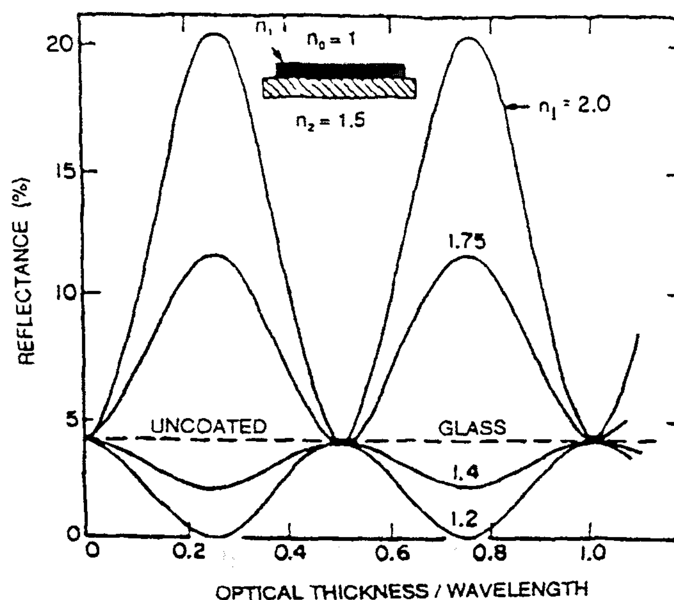

Figure 3.13 Calculated variation of reflectance (on air side) with normalized thickness ($n_1 d/\lambda$) for films of various refractive indices on a glass substrate of index 1.5.

respective film and substrate indices of refraction, the intensity of the reflected light undergoes oscillations as a function of the optical film thickness, or $n_1 d$. When $n_1 > n_2$, then maxima occur at film thickness equal to

$$d = \frac{\lambda}{4n_1}, \frac{3\lambda}{4n_1} \frac{5\lambda}{4n_1} \quad (3.9)$$

For values of d halfway between these, the reflected intensity is minimum. When $n_1 < n_2$, a reversal in intensity occurs at the same optical film thickness. In Fig. 3.13 these results are shown for the case of a glass substrate ($n_2 = 1.5$).

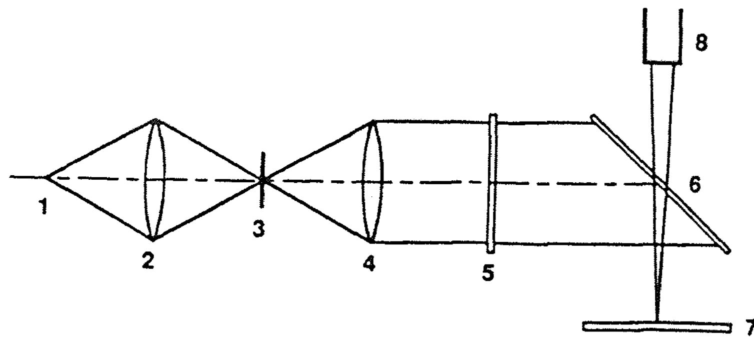

Figure 3.14 Schematic of interferometer: 1. light source; 2. condenser; 3. diaphragm; 4. collimator; 5. filter; 6. semitransparent mirror; 7. sample; 8. microscope.

The interference pattern, which is seen with the help of a low power microscope, is also shown in Figure 3.14. Light passes from the monochromatic source (namely, a sodium vapor lamp with $\lambda/2$ = 2946 Å), through the condenser, the diaphragm, the collimator and filter, and falls on the semi-transparent mirror.

Then it is partially reflected to the substrate covered by a thin reflecting layer, interference of light occurs as the light are reflected from the two film surfaces.

In all cases, a minimum of five points, one in the middle of the wafer and four near circumference of the wafer, were measured and average thickness can be calculated as the true thickness of the wafer.

3.4.3.1.2 Density Measurement

Density is defined as

$$D = \frac{\Delta W}{A * h} \tag{3.10}$$

where ΔW is the weight gain due to deposition on the silicon wafer, A is the wafer surface area and h is the thickness of the film. As A in the experiments is constant, after measuring ΔW and h, density of the thin film is easily calculated as Equation (3.11).

3.4.3.1.3 Etching

Etching experiments were done at room temperature in which 49% hydrofluoric acid (HF) was employed as etching solution. Thickness of the thin film before and after etching was measured, then etching rate can be calculated as

$$\text{Etching Rate} = \frac{\Delta h}{t} \tag{3.11}$$

where Δh is the thickness decrement after etching (Å), and t is the etching duration (second). At least a film was etched for four times, then the figure of the thickness change of the thin film versus etching time was plotted. Regression analysis was applied to calculate the slpoe of the plot, thus the etching rate was obtained.

From the etch rate of the thin films, the density calculated from Equation 3.10 can be certified. The film of high density has low etch rate.

3.4.3.2 Optical Properties

3.4.3.2.1 Refractive Index

The refractive index values were measured with a Rudolph Research/AutoEL ellipsometer (shown in Figure 3.15). In the ellipsometric method modification state of a light wave, which are produced as a result of the wave with examined sample, are analyzed. The polarization state is characterized by the phase and amplitude relations between the two plane waves which are components of the electric field vector in which the polarized oscillation can be solved. One wave p is in the incidence plane; the other wave s is normal to the incidence plane. The modification of the relative phases of the p and s waves is made by reflection. Reflection also modifies the amplitude ratio. The ellipsometric magnitudes characteristic of the wave reflection on the sample surface are defined as follows: the angle Δ represents the phase modification and the angle ψ represents the factor by which the amplitude ratio is modified.

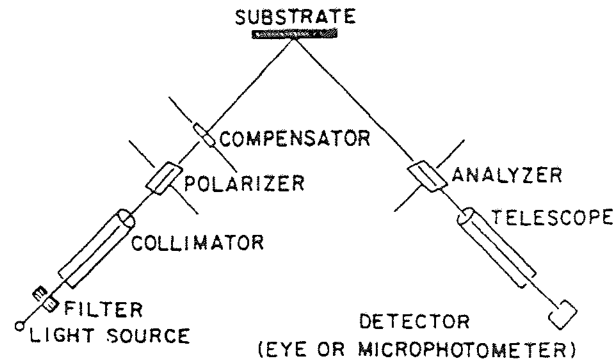

Figure 3.15 Experimental arrangement in ellipsometry.

The data (the values Δ and ψ are determined experimentally) yield the refractive index when the fundamental relation of ellipsometry is applied:

$$\tan\psi\exp(i\Delta) = \frac{r_{1p} + r_{2p}\exp(-2i\delta) + r_{1s}r_{2s}\exp(-2i\delta)}{1 + r_{1p}r_{2p}\exp(-2i\delta) + r_{1s}r_{2s}\exp(-2i\delta)} \qquad (3.12)$$

$$d = C_{n1}\delta \qquad (3.13)$$

$$C_{n1} = (\lambda/2\pi)(n_1^2 - n_0^2\sin^2\phi_0)^{-1/2} \qquad (3.14)$$

$$d = (m\pi + x)C_{n1} \qquad (3.15)$$

where d is the film thickness, δ is the phase difference, n_0 is the refractive index of silicon, Φ_0 is the angle of incidence (70 °), and r_1 and r_2 are the Fresnel reflection coefficients at the ambient-film and film-substrate interfaces respectively.[2]

3.4.3.2.2 Transmission Spectra

The Infrared spectra were taken using a Perkin Elmer 1600 series FTIR spectrophotometer while the optical transmission was calculated from the Ultraviolet/Visible transmission spectra measured with a PERKIN-ELMER Lambda 3B UV/VIS spectrophotometer.

Electronic processes such as valence-to-conduction band transitions are responsible for the high energy absorption cut-off observed in the ultraviolet section. In the infrared region, the low energy cut-off is produced by the strong molecular and atomic vibrations of the glass. Optical absorption in the visible is typically a composite of the tails of the electronic and vibrational edges of the glass plus the contributions from impurities.

In the thin film the ions are closed together and interact to form bands of allowed states, consequently the transitions observed also correspond to a range of energies so that more or less broad absorption bands are observed rather than discrete spectral lines.

3.4.3.3 Stress

In the thesis work, film stress was determined with a home built system that measured changes in the radius of curvature of a wafer resulting from deposition on a single side. Figure 3.16 shows an optical imaging system for setup. The distance between two points generated by light from two fixed and parallel He-Ne lasers is determined by reflection from the surface of a wafer before and after

deposition. An angled mirror is used to project the reflection of the two points onto a wall where their separation could be accurately measured.

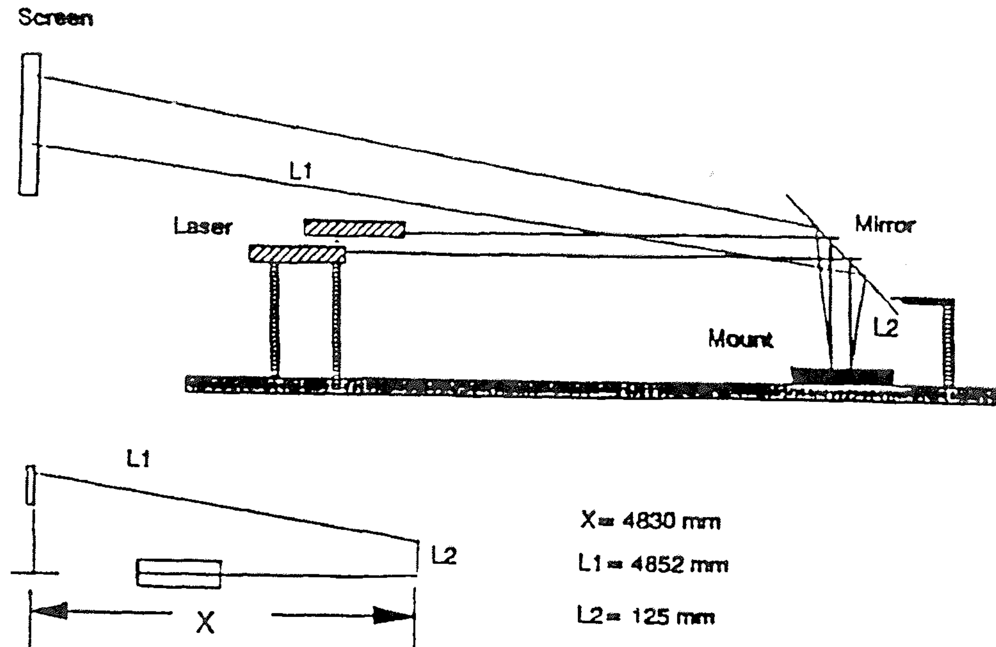

Figure 3.16 Schematic of optical system for stress measurement setup.

The stress is calculated using Stoney's equation: [10]

$$\sigma = \frac{Et_s^2}{6(1-\nu)Rt} \tag{3.16}$$

where E is Young's modulus for the substrate, t_s is the substrate thickness, ν is Poisson's ratio for the substrate, t is the film thickness. And the net radius of curvature R is

$$R = 1/(1/R_2 - 1/R_1) \tag{3.17}$$

where R_1 and R_2 are the radii of curvature of wafer before and after deposition respectively. For Si <100> wafers, $E = 1.8*10^{11}$ Pa and $t_s = 525$ µm. This simple and inexpensive apparatus yields stress values which are within 5% of those obtained from the Flexus Model 2-300 system.

CHAPTER 4

RESULTS AND DISCUSSIONS

In this thesis work, the reaction of tri (dimethylamino) silane (TDMAS) and ammonia (NH_3) was studied as a function of deposition temperature, deposition pressure, and NH_3/TDMAS flowrate ratio. In the temperature dependency study, the growth rate, composition, structure as well as the properties of silicon nitride films were determined as a function of deposition temperatures between 650 °C and 900 °C while maintaining a constant pressure of 0.5 Torr, a TDMAS flowrate of 10 sccm, and a flowrate ratio (NH_3/TDMAS) of 10/1. The pressure dependent behaviors of Si_3N_4 thin films were investigated from 0.15 Torr to 0.60 Torr at constant temperature of 750 °C, a TDMAS flowrate of 10 sccm, and a flowrate ratio (NH_3/TDMAS) of 10/1. In the experiments of flowrate ratio series, NH_3/TDMAS flowrate ratio was varies from 0 to 10 for constant conditions of temperature (750 °C), TDMAS flowrate (10 sccm), and total pressure (0.5 Torr).

4.1 The Effects of Deposition Variables on Film Growth Rate

4.1.1 Temperature Dependent Study of Si_3N_4 Thin Films

As seen in Figure 4.1, which shows the temperature-dependent behavior of deposition, the growth rates increased rapidly with increasing temperature between 650 °C and 800 °C following an Arrhenius type behavior and yielding an apparent

activation energy of 41 ± 3 kcal/mole. The depletion across the reaction chamber is negligible in this temperature range. However, the growth rates decreased with a further increase in temperature above 800 °C, and the depletion became more noticeable.

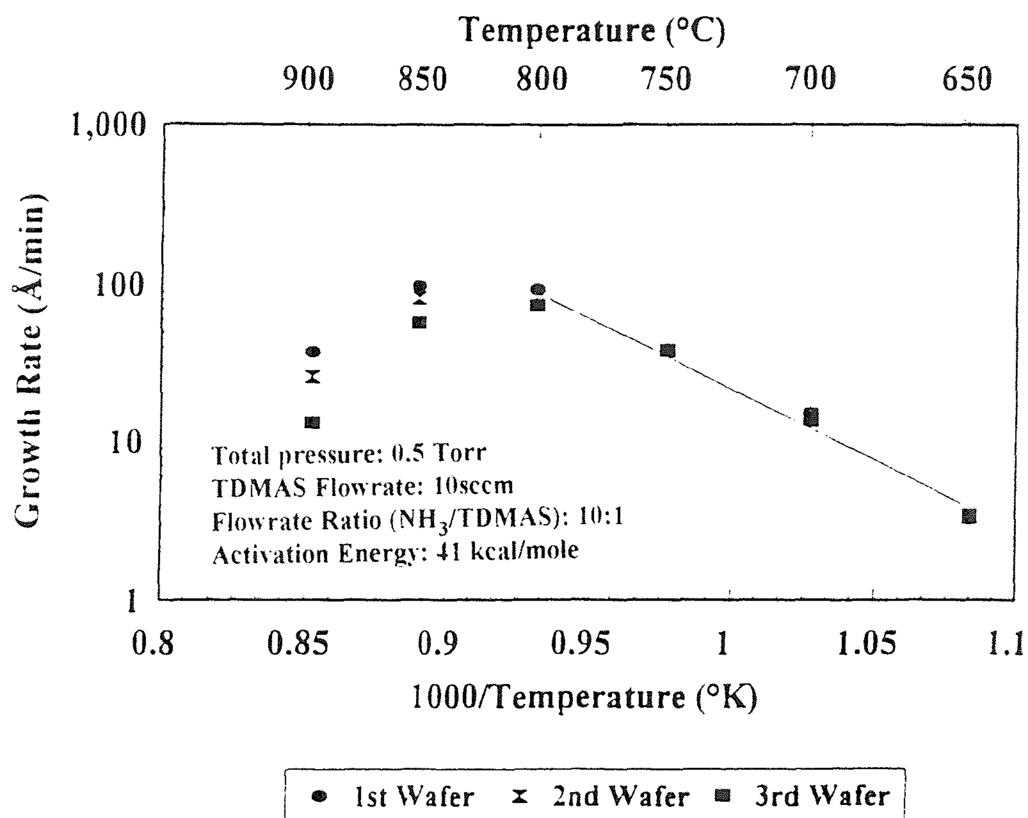

Figure 4.1 Variation of growth rate of silicon nitride films as a function of deposition temperature.

Above this temperature the growth rate leveled out and even decreased because of a combination of factors including increased desorption rates, depletion of reactants on reactor walls, and the emergence of an alternative reaction pathways. The apparent activation energy can be calculated from the slope of a semilog plot

for the growth rates versus 1000/T [53, 54]. The slope obtained from Figure 4.1 was 20.85 ± 1.43, thus E_a = 1.987 kcal/mole * 20.85 = 41 kcal/mole. This value approaches the 48 kcal/mole value obtained by Olin Hunt Co.

Deposition of Si_3N_4 at upstream is responsible to the depletion across the chamber. Furthermore, this tendency increasing with the temperature makes larger depletion at higher temperature. Another reason for depletion across the chamber is that depletion of TDMAS causes the decrement of its concentration giving rise to lower growth rate at the back of the chamber.

4.1.2 Pressure Dependent Study of Si_3N_4 Thin Films

1150B mass flow controller was used to measure and control the flow rates of TDMAS as it is low vapor pressure liquid. The operation of the 1150B MFC is based on the linear relationship between the total pressure upstream of a sonic nozzle and the mass flow through it, given choked flow, inlet to outlet pressure ratio of approximately 2:1. If this ratio drops below approximately 2:1 the flow through the sonic nozzle will not be choked and the flow may become non-linear. Experimental calibration results shown in Figure 4.2 where the flowrate of TDMAS was set to 10 sccm indicated that the 1150B MFC can accurately control the flowrate of TDMAS when the chamber pressure is below 0.60 Torr. Beyond this value, the flowrate of TDMAS begins to drop below the set value, indicating that the 1150B mass flow controller could not been used to study the pressure dependent behavior above 0.6 Torr.

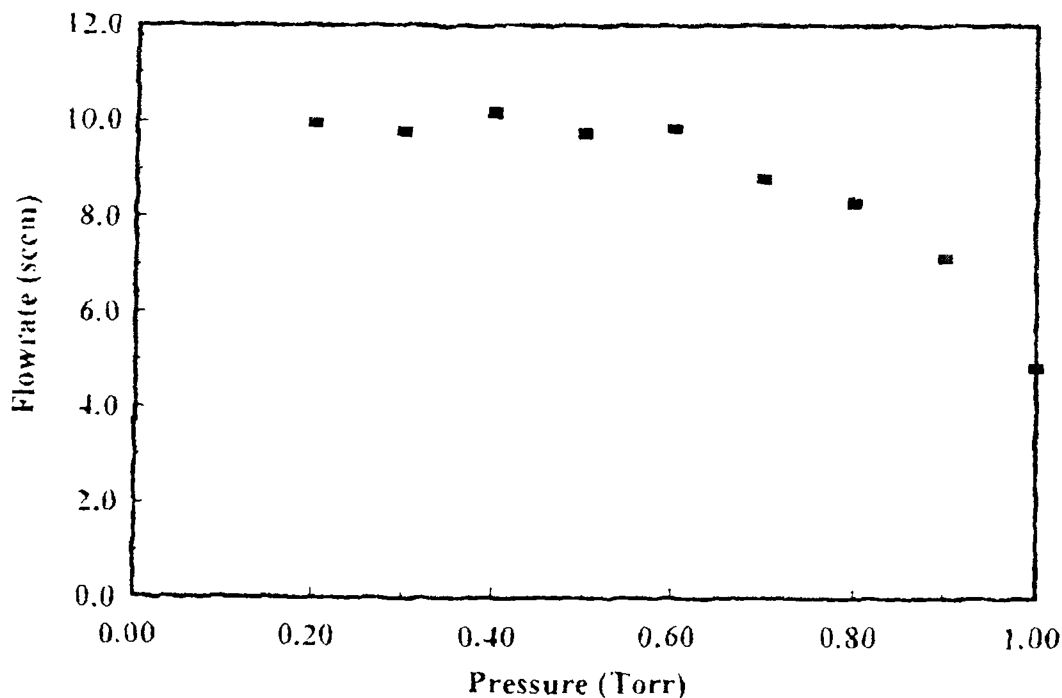

Figure 4.2 Variation of TDMAS flowrate as a function of the chamber pressure with a set flow rate of 10 sccm in MFC.

Because of equipment limitations, the pressure dependent study was done in the low pressure regime (shown in Figure 4.3). In the range of 0.15 Torr to 0.60 Torr, the growth rates increased linearly with deposition pressure. This behavior is consistent with unimolecular surface reaction mechanism described in the Chapter 1. The surface reactions involve single adsorbed of both TDMAS and NH_3. However, only the surface concentration of TDMAS control the reaction rate while the NH_3 adsorbed inhibits the adsorption of TDMAS, reducing the effective surface area availble, and, therefore, the rate of deposition. Hence the growth rate can be expressed as

$$v = \frac{kK_{TDMAS}p_{TDMAS}}{1 + K_{TDMAS}p_{TDMAS} + K_{NH_3}p_{NH_3}} \quad (4.2)$$

In the pressure dependent study, P_{TDMAS} and P_{NH_3} are low enough that both $K_{TDMAS}p_{TDMAS}$, $K_{NH_3}p_{NH_3}$ << 1, therefore, Equation 4.2 becomes:

$$v = kK_{TDMAS}p_{TDMAS} \quad (4.3)$$

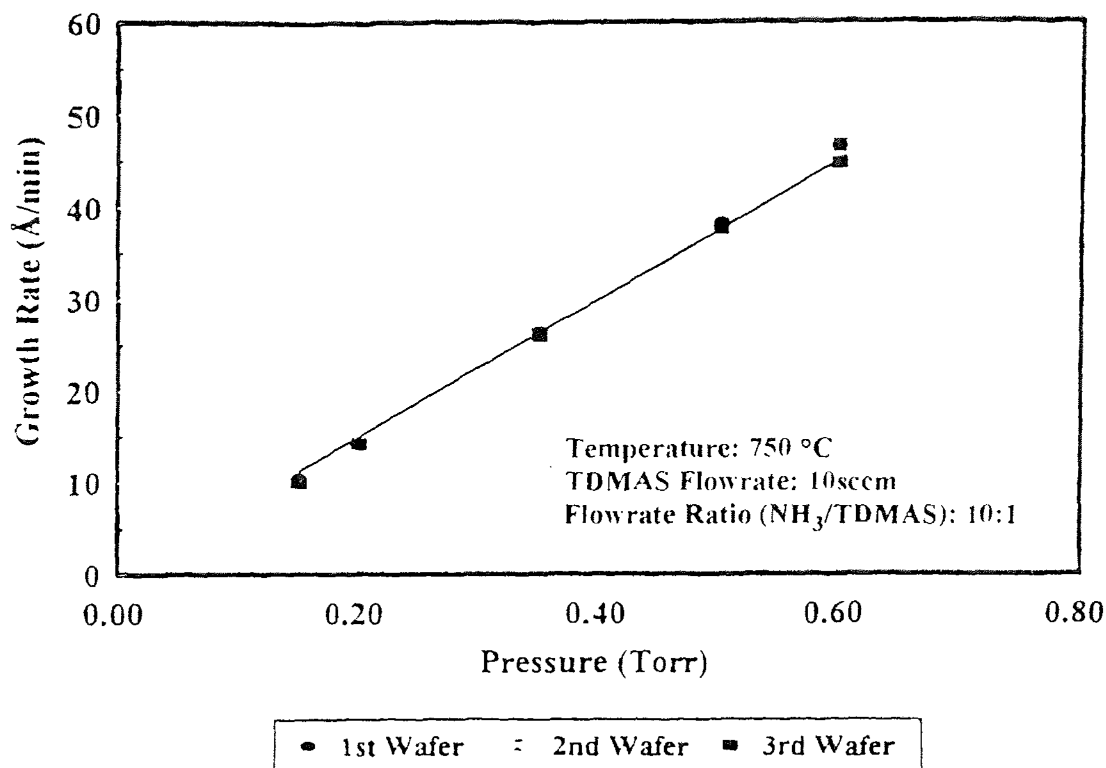

Figure 4.3 Variation of growth rate of silicon nitride films as a function total reactor pressure.

Because the flowrates of TDMAS and NH_3 were not changed during the deposition processes, the relationship between p_{TDMAS} and total pressure in the chamber p_T can be considered to be proportional.

4.1.3 NH_3/TDMAS Flowrate Ratio Dependent Study of Si_3N_4 Thin Films

The growth rates of the thin films as a function of the NH_3/TDMAS flowrate ratios are plotted in Figure 4.4. A non-linear decrease in the growth rate as this ratio was increased was observed. The growth rate increases rapidly in low ratio region and slow at higher ratio. On the other hand, depletion across the chamber decreased as NH_3/TDMAS flowrate ratio increased.

This phenomena can be explained as a combination of two effects, the diluting effect of NH_3 and the occupation of surface sites by NH_3. As NH_3/TDMAS flowrate ratio increased, the pumping rate in this region must be increased accordingly in order to maintain the desired constant pressure. Since more NH_3 flowed as the ratio was increased, a TDMAS dilution resulted. On the other hand, more and more surface were occupied by NH_3 molecules. Adsorbed NH_3 molecules do not enter directly into reaction, but they reduce the reaction rate by occupying surface that might otherwise be occupied by TDMAS molecules. The fraction of surface that is covered by TDMAS molecules, which enter directly into reaction, became less and less, so the growth rate decreases.

As the gases flow down the tube, TDMAS become gradually depleted as Si_3N_4 is deposited. Increasing the flowrate of NH_3, has the effect of lowering the

amount of TDMAS adsorbed on each wafer leaving more TDMAS for down stream reactions.

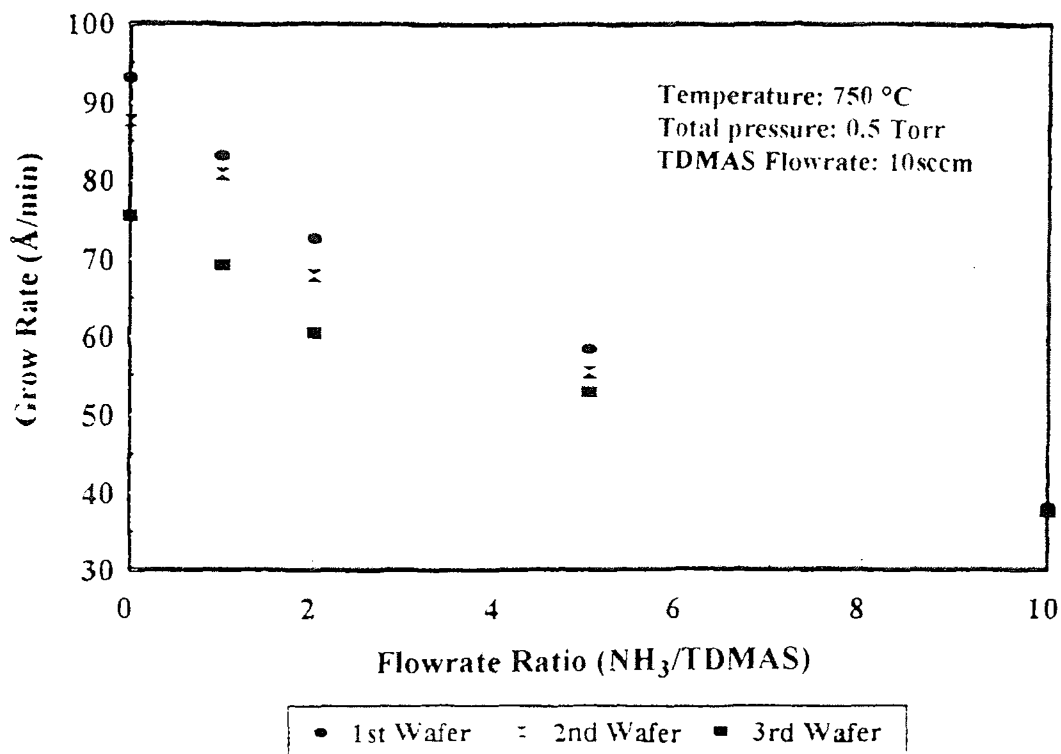

Figure 4.4 Variation of growth rate of silicon nitride films as a function of NH_3/TDMAS flowrate ratio.

4.2 Structure Study

In the case of the synthesizing Si_3N_4 thin films, heterogeneous a reaction must occurred in order to obtain good films. However, some portions of the overall reaction may occur in the gas phase. Si_3N_4 molecules adsorbed on the Si wafer surface diffused randomly and had a greater opportunity to re-evaporate (desorb) because they were less firmly bound to the surface. As the adsorbed molecules

diffused on the surface, they may encounter other diffusing molecules and form a pair. This molecule pair would be more stable than an isolated molecule and would less likely to desorb. As the pairs diffused on the surface, they may join other molecules, forming a larger and more stable cluster, until the cluster had a low probability of desorbing, and a critical cluster or stable nucleus was formed. Because the probability of diffusing molecules encountering each other depended strongly on the number of adsorbed molecules on the surface, it is a strong function of their arrival rate (through the pressures of the precursors) and their desorption rate (through the temperature of substrate and the binding energy of the diffusing molecules to exposed surface). After stable deposited nuclei formed, additional adsorbed molecules diffusing on the surface can either initiate additional nuclei or join existing nuclei. When the existing nuclei were close enough together, additional molecules were more likely to join an existing nucleus, and the number of nuclei saturated and remained constant as the size of each nuclei grows. The saturation number of nuclei depended on the substrate, the arrival rate of molecules, and the temperature. Thus, a continuous film formed as the nuclei impinged on each other. Ever after a continuous film formed, the structure was strongly influenced by the thermal energy available for surface migration. At very low temperatures, the adsorbed Si_3N_4 molecules had little thermal energy and cannot diffuse significantly on the substrate surface before they were covered by subsequently arriving molecules. Once they were covered, their random arrangement was locked into place, and an amorphous structure with

no long-range order formed. At higher temperatures, adequate surface diffusion was possible to allow a crystalline structure to form [55].

The X-ray diffraction pattern of Si_3N_4 films deposited on silicon at the highest deposition temperature of 900 °C (shown in Figure 4.5) only exhibits the peak of Si (100) at about 69 °, the peaks of Si_3N_4 are not present. Therefore, the films are amorphous at all temperatures which were studied.

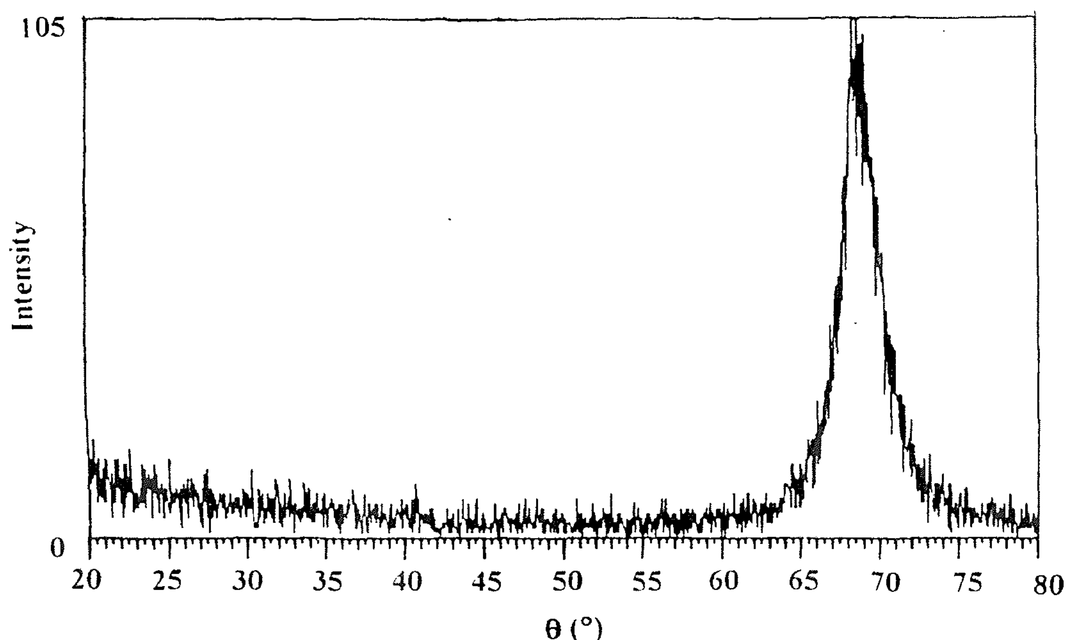

Figure 4.5 X-ray diffraction pattern for a silicon nitride film on silicon deposited at a temperature of 900 °C, pressure of 0.5 Torr, TDMAS flowrate of 10 sccm, and NH_3 flowrate of 100 sccm.

4.3 The Effects of Deposition Variables on Film Composition

4.3.1 The Temperature Dependent Study of Si_3N_4 Thin Films

RBS analysis results (shown in Figure 4.6) indicate stiochiometric silicon nitride

film can be obtained over the entire temperature range of 650-900 °C. Furthermore, the fact that all thin films obtained were predominantly Si_3N_4 was determined using XPS, which is a more sensitive techique to composition.

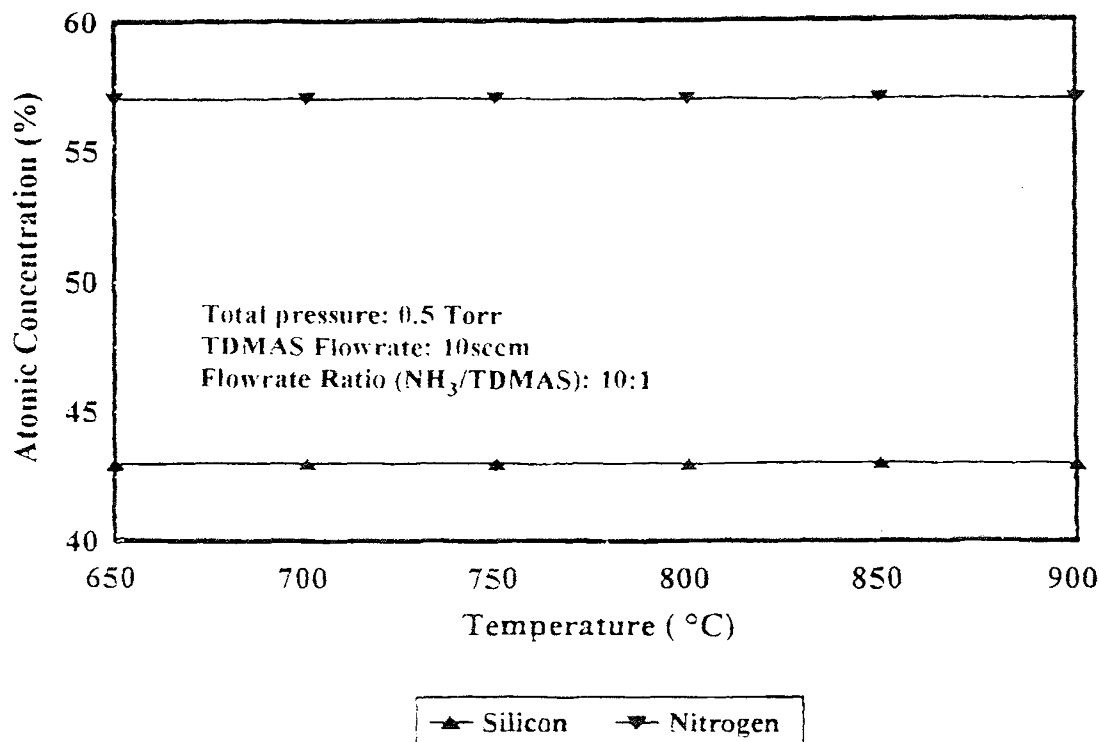

Figure 4.6 Atomic concentration of silicon nitride films as a function of deposition temperature by RBS.

The silicon and nitrogen lines in the XPS spectra were narrow and symmetric showing a uniform composition. The observed binding energy of silicon, 101.6 eV, was higher than that of SiC (100.2 eV), lower than that of SiO_2 (103.3 eV); and close to that of Si_3N_4 (101.8 eV). The observed binding energy of nitrogen, 398.0 eV, is a bit higher than 397.6 eV for the plain nitride (less charge

on the nitrogen) which reflects the effects of the carbon and oxygen impurities present. The oxygen line observed can reflect many structures including silicon oxides. While the carbon spectra has a primary peak reflecting a carbide type carbon with two secondary peaks (each about 10 %) which are neutrally charged, and positively charged. The third peak would reflect C-O or C-N bonding.

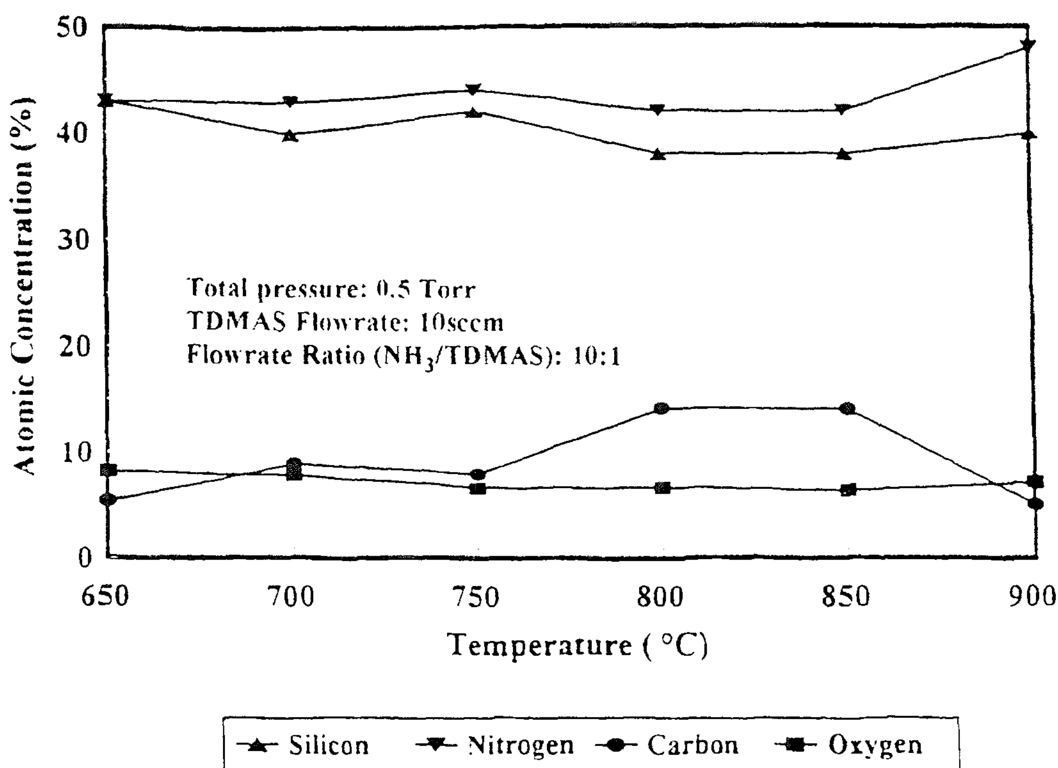

Figure 4.7 Atomic concentration of silicon nitride films as a function of deposition temperature by XPS.

As seen in Figure 4.7, the N to Si ratio increased with increasing temperature. At low temperature (650 °C and 700 °C) a some what higher (7.7 %) oxygen concentration was observed due to oxidization of the porous thin films in

the air. Moderate carbon and oxygen contamination is detected at the intermediate temperature (750 °C). When the temperature was increased to 800 °C, a non-carbide carbon is present in the thin films as a result of the decomposition of TDMAS to $N(CH_3)_2$ at higher temperatures. Carbide begins to be formed at higher temperature (850 °C). When the temperature reaches 900 °C, the tendency of decomposition of NH_3 to N_2 and H_2 becomes obvious and an alternative reaction pathway lead to the lowest carbon content and the highest nitrogen content observed in this study.

In the light of above illustration about the composition of the thin films, we can draw a conclusion that perfect Si_3N_4 film can be synthesized in narrow temperature range from NH_3 + TDMAS precursor system.

4.3.2 NH_3/TDMAS Flowrate Ratio Study of Si_3N_4 Thin Films

XPS analysis indicates that Si-C-N film was synthesized when NH_3 was absent. As shown in Figure 4.8, when the NH_3/TDMAS flowrate ratio increases, content of carbide or graphite carbon became lower. At the same time, rapid increment of Si concentration and slow addition of N content makes the silicon nitride thin film more stiochiometric.

4.4 The Effects of Deposition Variables on Film Density

A reduced film density relative to the bulk density is not an unexpected outcome of the zone structure of films and its associated porosity. Because of the causal

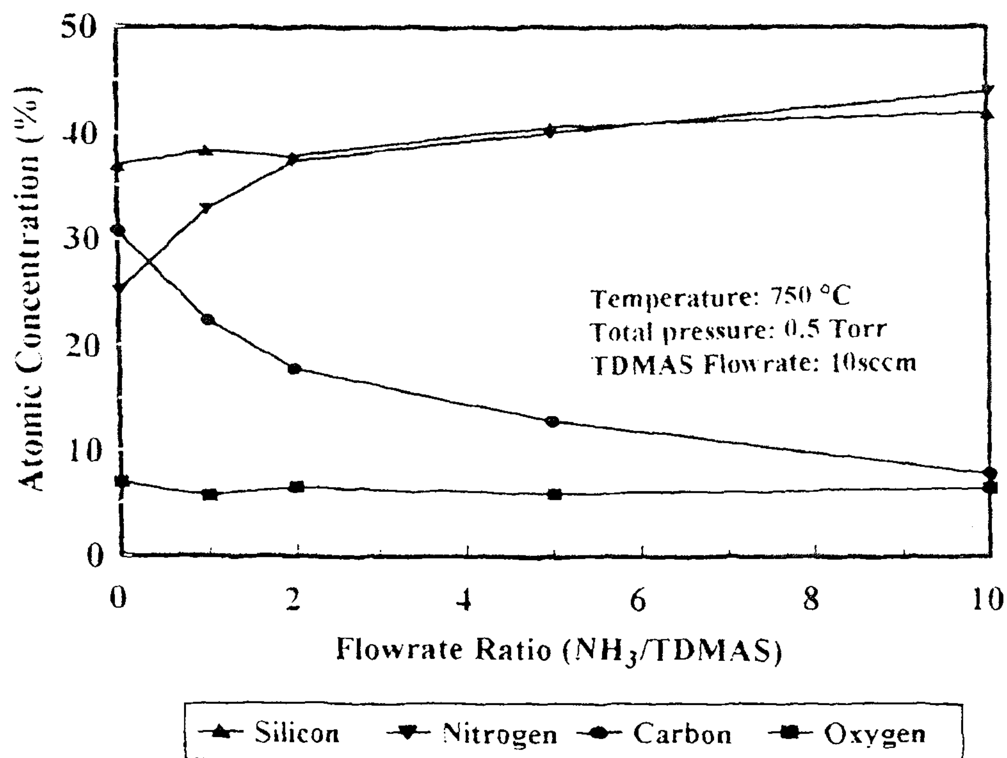

Figure 4.8 Atomic concentration of silicon nitride films as a function of NH_3/TDMAS flowrate ratio by XPS.

tructure-density and structure-property relationships, density is expected to strongly influence film properties, such as the deleterious effect of lowered overall film densities on optical and mechanical properties, similar degradation of film adhesion and chemical stability can occur.

4.4.1 Temperature Dependent Study of Si_3N_4 Thin Films

Figure 4.9 illustrates the dependency of the density of deposited silicon nitride films on deposition temperature. Comparing with theoretical density (3.1 g/cm^3), it is low for films deposited over the entire temperature range. The density of the

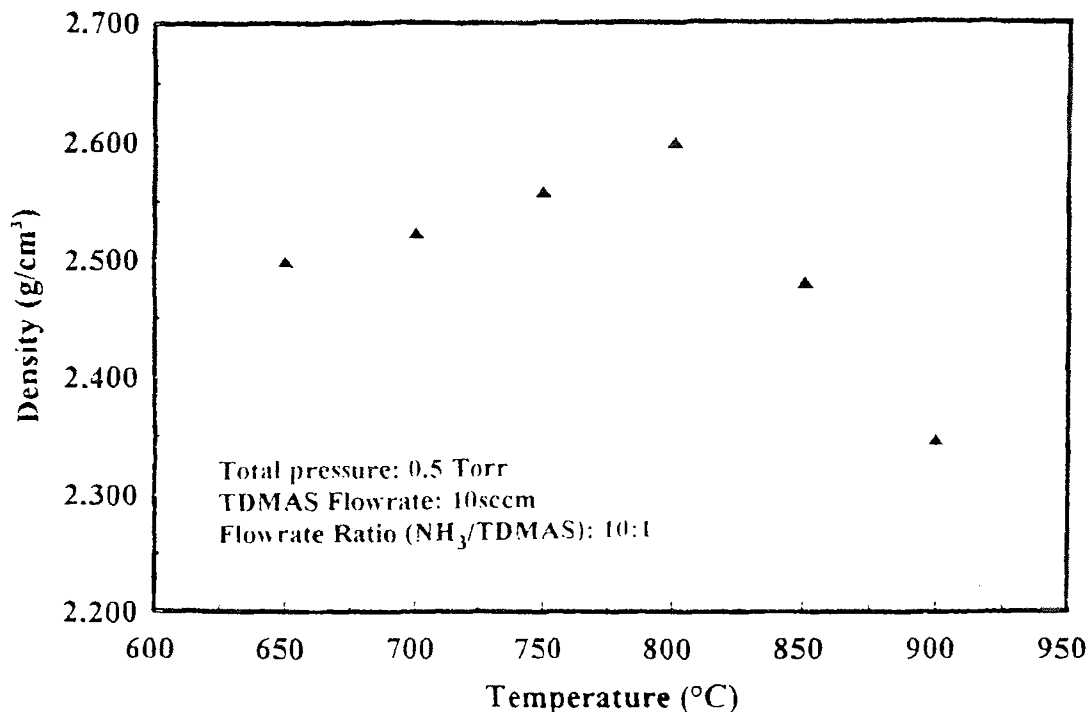

Figure 4.9 Variation of density of silicon nitride films as a function of deposition temperature.

films increases with increasing temperature in the range of 650 °C to 800 °C. This phenomenon can be explained by consideration of the processes occurring on the surface during and after nucleation and how these processes influence the structure of the films. As mentioned above, nucleation is the process that adsorbed Si_3N_4 molecules diffuse on the surface and join other diffusing Si_3N_4 molecules to form stable nucleus. After stable nuclei form, additional adsorbed molecule can either initiate additional nuclei or join existing nuclei [55]. At higher temperatures, adsorbed molecules, can diffuse greater distances to join an already formed nucleus rather than initiating a new nucleus, so fewer, but larger, nuclei form. Thus, more Si_3N_4 molecules must be deposited before a continuous film forms as

the nuclei impinge on each other. To be brief, the Si_3N_4 molecules have more thermal energy to arrange themselves and a film which is more dense.

As the temperature increases continually, the density of the films decreases because of the incorporation of large nonequilibrium concentrations of vacancies and micropores. Presence of different reaction pathway at high temperature is responsible for the decrement of the density as the temperature was increased above 800 °C.

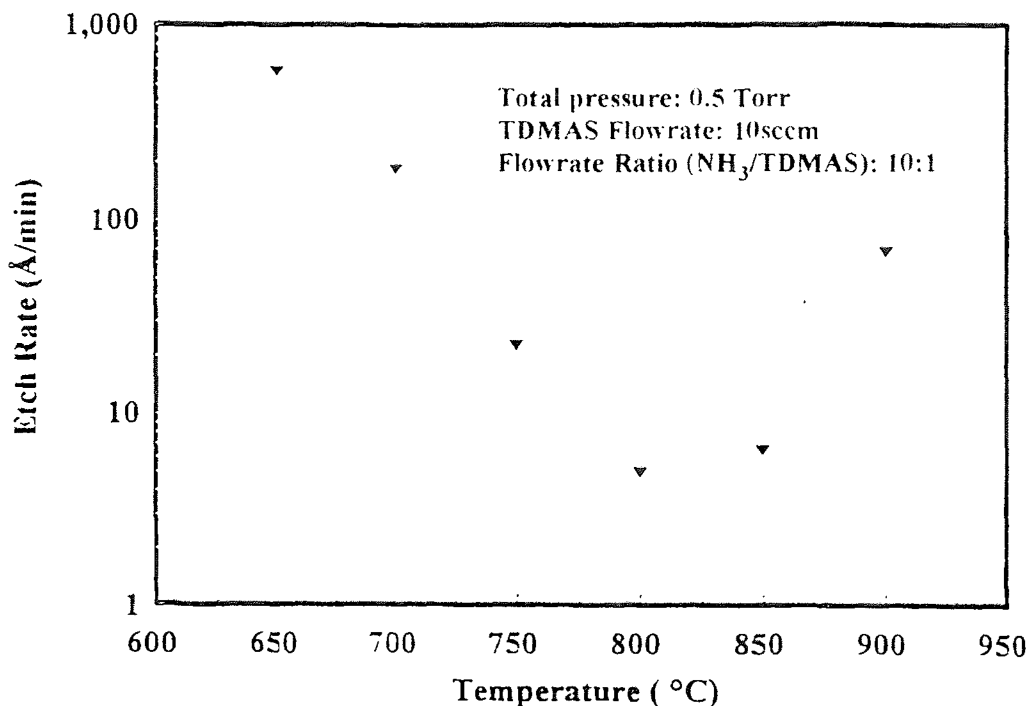

Figure 4.10 Variation of etch rate of silicon nitride films in 49 % HF as a function of deposition temperature.

It can be seen in Figure 4.10 that the lowest etch rate observed were for films deposited at the higher temperatures800 °C and 850 °C. A typical etch rate

of 30 Å/min of Si_3N_4 film in 49 % HF was observed for films synthesized at 750 ° C. At higher temperatures the organosilanes tend to decompose incresing the carbon and nitrogen content of the films while decreasing its density.

4.4.2 Pressure Dependent Study of Si_3N_4 Thin Films

Figure 4.11 represents the variation of density as a function of deposition pressure. There appears to be an increase in the density values as the deposition pressure was raised to 0.35 Torr, then a decrease of the density was observed with higher pressure.

Increasing pressure produces two effects on the film formation process. As mentioned in this thesis, during the nucleation process the probability of diffusing Si_3N_4 molecules encounting each other depends strongly on the number of adsorbed Si_3N_4 molecules on the surface which is a strong function of their arrival rate. A pressure increment leads to higher arrival rate of Si_3N_4 molecules [55]. On one hand, high arrival rate causes more Si_3N_4 molecules form larger nuclei which result in compact structure. On the other hand, it leads to the trend that the adsorbed Si_3N_4 molecules can not diffuse significantly on the substrate surface before they are covered subsequently arriving molecules, then a large number of micropores form. These two aspects compete each other. In the low pressure range the former is dominant, so the density increases with increasing deposition pressure. The latter becomes notable with higher pressure, this results in density decrement.

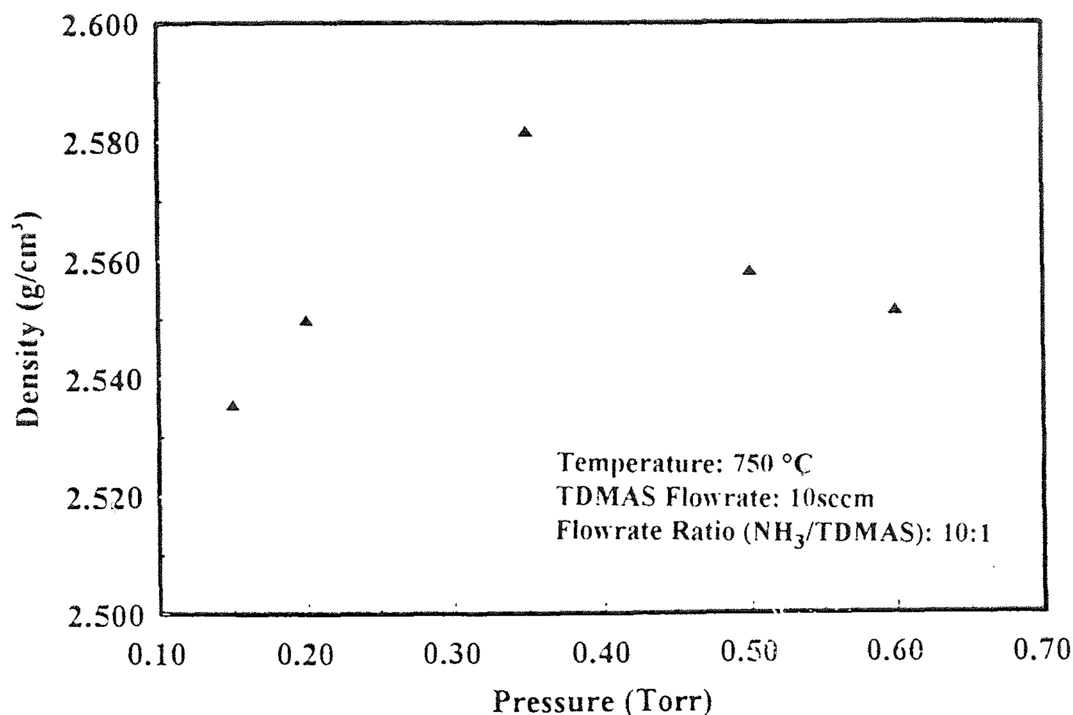

Figure 4.11 Variation of density of silicon nitride films as a function of deposition pressure.

4.4.3 NH_3/TDMAS Flowrate Ratio Study of Si_3N_4 Thin Films

It can be seen in Figure 4.12 that the density increased when the NH_3/TDMAS flowrate ratio increased from 1 to 10. This relationship is opposite to that of growth rate. Higher NH_3/TDMAS flowrate ratio causes slower arrival rate of Si_3N_4 molecules to the surface and more adequate surface diffusion which results in less porosity. When TDMAS was used as a sole precursor, silicon carbo-nitride was formed with a density of 2.35 g/cm^3 which is lower than that most of the Si_3N_4 thin films synthesized in this thesis work.

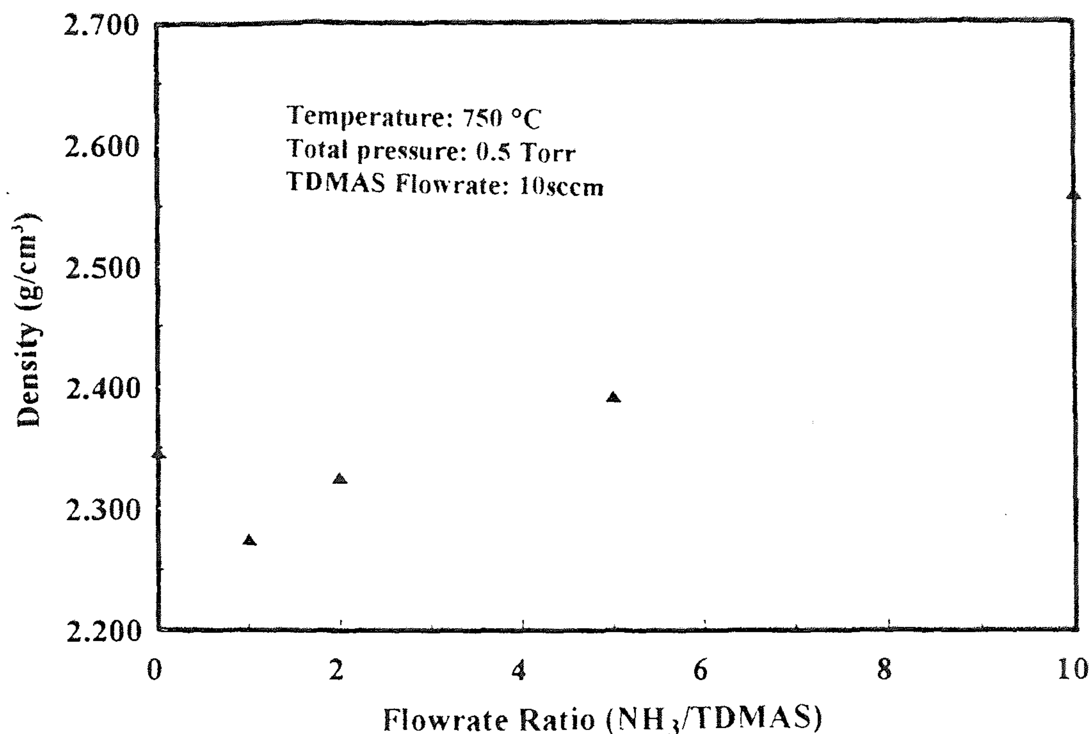

Figure 4.12 Variation of density of silicon nitride films as a function of NH_3/TDMAS flowrate ratio.

4.5 Optical Properties Study

4.5.1 The Effects of Deposition Variables on Film Refractive Index

Electromagnetic radiation propagates differently in materials than in free space because of the presence of charge. As a result, there is a change in the wave velocity and intensity of the radiation described by the complex index of refraction

$$N = n - ik \tag{4.4}$$

The quantity n is the real index of refraction, and k is the index of absorption, which is also known as the extinction coefficient. The Si_3N_4 films used for

optical purposes are highly transparent and k is vanishingly small compared with n, so the refractive index n is basically the only optical constant of interest insofar as optical design is concerned.

4.5.1.1 Temperature Dependent Study of Si_3N_4 Thin Films

The dependency of refractive index of the thin films on the deposition temperature (as shown in Figure 4.13) is determined mainly by the variation of the film composition. In addition, this is a high correlation between the index of refractive index and density of the films.

The presence of silicon oxide in the thin films, which has the refractive index of 1.46 leads to lowing the index values of the films synthesized at 650 °C and 700 °C from 2.0 to about 1.9. The low density of these films is also a factor.The refractive index of the films deposited at 850 °C and 800 °C increases to 2.1 and above which arises from high carbon concentration existing as carbide and graphite carbon. When the deposition temperature increases to 900 °C, the deposition reaction occurs according to different mechanism contrasting to that of reaction taking place at 750 °C. But in both cases, moderate C and O content brings about favorable index values which much close to 2.0, the theoretical refractive index of Si_3N_4.

Refractive index is also related to the microstructure of the thin films which can be represented quantitatively as the packing density P. The simplest relationship proposed is a linear law of mixing

$$n = n_S P + n_V(1 - p) \quad (4.6)$$

where n_S and n_V are the refractive indices associated with the solid film and voids (or pores).

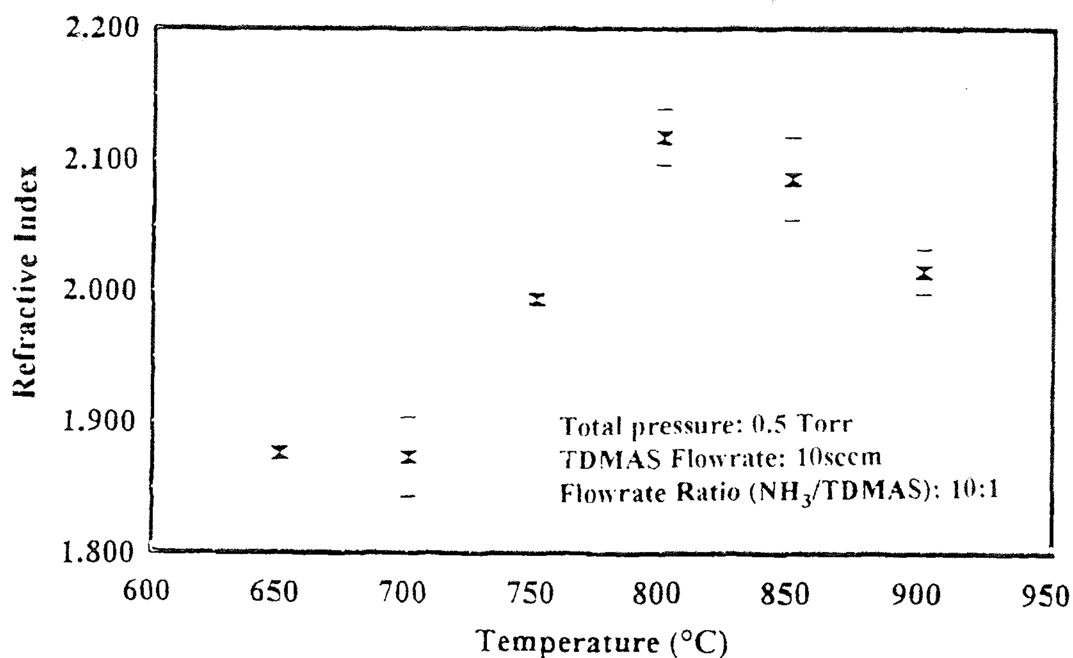

Figure 4.13 Variation of refractive index of silicon nitride films as a function of deposition temperature.

4.5.1.2 Pressure Dependent Study of Si_3N_4 Thin Films

No significant variation in the refractive index of deposited silicon nitride films was noted when the deposition pressure was varies from 0.15 to 0.60 Torr shown in Figure 4.14. Furthermore, it can be deduced that stoichiometric Si_3N_4 can be obtained over entire investigated pressure range.

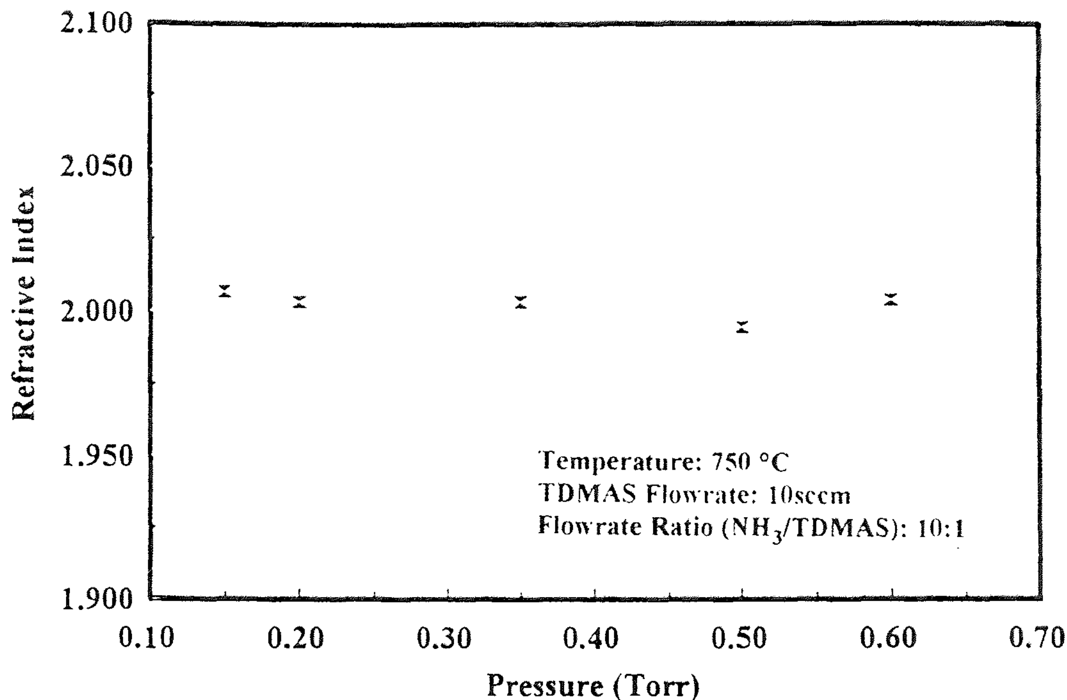

Figure 4.14 Variation of refractive index of silicon nitride films as a function of deposition pressure.

4.5.1.3 NH_3/TDMAS Flowrate Ratio Study of Si_3N_4 Thin Films

In Figure 4.15 the refractive index versus NH_3/TDMAS flowrate ratio is shown for 10 sccm TDMAS. Over most of compositional range studied, it varies from 1.992 to 2.007. But as NH_3/TDMAS flowrate ratio decreases to 1 an increase in the index of refraction is noted. It can be observed that the index increases to the range of 2.359- 2.395 corresponding to the formation of Si-C-N as the ammonia flowrate is decreased to zero.

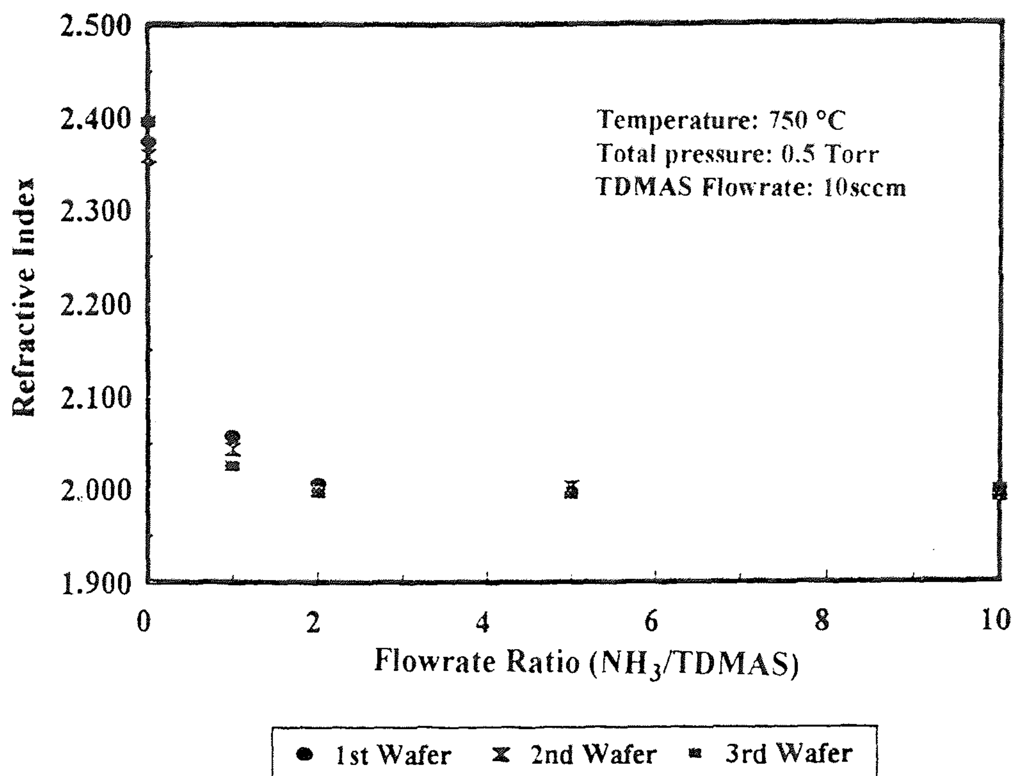

Figure 4.15 Variation of refractive index of silicon nitride films as a function of NH_3/TDMAS flowrate ratio.

4.5.2 FTIR Analysis

4.5.2.1 Temperature Dependent Study of Si_3N_4 Thin Films

Figure 4.16 illustrates an FTIR spectrum in the range 4000-400 cm^{-1} for a nitride deposited at 750 °C. The Si-N stretching and breathing modes are identified at 850 and 475 cm^{-1}, respectively. The presence of the peak associated with Si-H stretching mode at 2180 cm^{-1} is readily detected. A small peak at 3355 cm^{-1} and a broad peak at 1475 cm^{-1} were also observed and identified as N-H stretching mode and N-H_2 scissors, respectively.

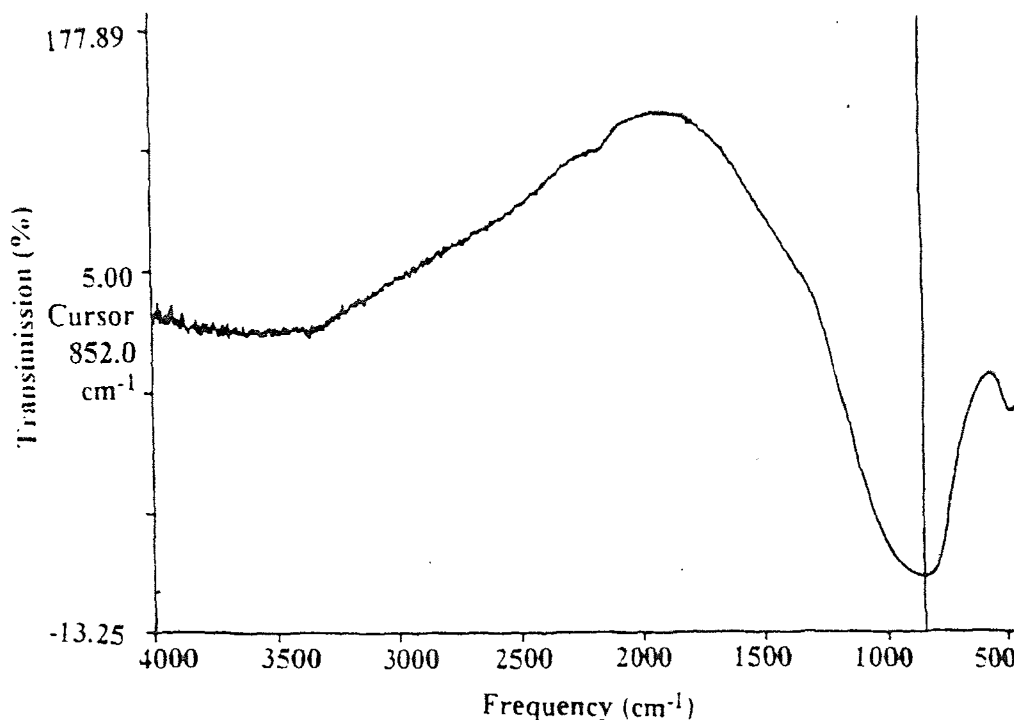

Figure 4.16 FTIR spectrum for a silicon nitride film on silicon deposited at a temperature of 900 °C, pressure of 0.5 Torr, TDMAS flowrate of 10 sccm, and NH_3 flowrate of 100 sccm.

A physical model of Si_3N_4 suggests the following interpretations for the FTIR spectrum of Si_3N_4 thin film. The 850 cm^{-1} band arises from Si-N-Si vibrations in which the nitrogens move in opposite directions to their Si neighbors and parallel to Si-Si lines although these modes are not generally localized on just one group of Si-N-Si atoms. The 475-cm^{-1} band is associated with bond breathing vibrations of nitrogen perpendicular to the Si-N-Si planes but these modes extended spatially throughout the whole network. The breathing vibrations are characterized by much lower frequencies than the stretching modes which involve larger force constants [56]. The presence of N-H bonding (about 1475 cm^{-1}), Si-H

(2180 cm^{-1}) and N-H (3355 cm^{-1}) indicates a number of hydrogen atoms bond to Si or N in the film. The absorption band at 2180 cm^{-1} is assigned to the stretching mode of $Si-H_3$ bonding, and the absorption band at 3355 cm^{-1} is assigned to $N-H_2$ in the Si-H-Si group.

Hydrogen plays an important role in the electrical performance of Si_3N_4 films. The integrated absorption of the N-H and Si-H bands are correlated with the atomic concentration of hydrogen. The position of the Si-N stretching and breathing modes are sensitive to Si-H content: their absorption peaks being shifted to relatively higher wave numbers indicates an increasing number of hydrogen atoms bonded to a specific Si atom, especially when the Si atoms are incorporated with the N atoms, which electronegativity is greater than that of Si atoms [57]. The absorption peak of Si-N stretching bond as a function of deposition temperature is shown in Figure 4.17. It can be seen that this peak is shifted to higher wave numbers as temperature increases from 650 °C to 850 °C, then shifted to lower wave number with further increasing temperature. This phenomenon can be explained by the effects of two contrary tendencies: one is that the entropy of reactants become larger and hydrogens more easily absorb on the film surface to form Si-H bonds with increasing temperature; another is that Si-H bond tends to decompose at higher temperature.

A shoulder or a small peak at 1100 cm^{-1} corresponding to Si-O stretching mode can be observed at 650 °C, 700 °C and 900 °C at which the concentration of oxygen can not be negligible.

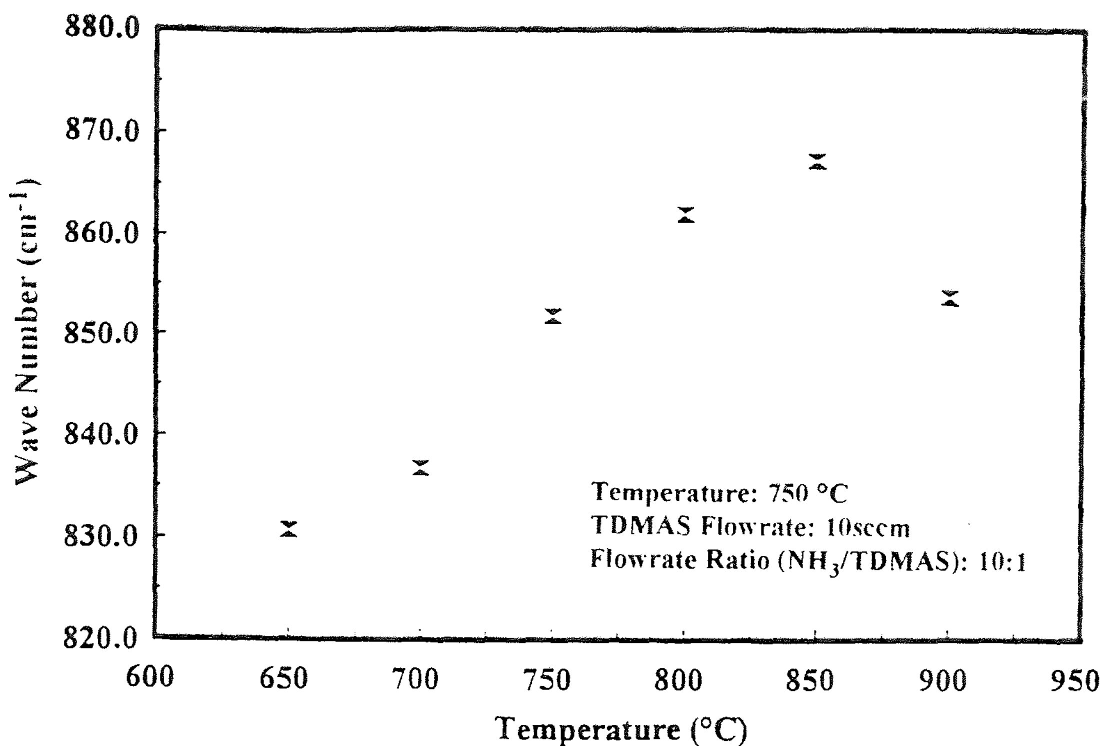

Figure 4.17 Variation of Si-N absorption peak in FTIR spectra for silicon nitride films as a function of deposition temperature.

4.5.2.1 Pressure Dependent Study of Si_3N_4 Thin Films

As shown in Figure 4.18, the positions of Si-N stretching mode are shifted to higher wave numbers when the deposition pressure increases from 0.15 Torr to 0.60 Torr. This observation suggests the Si-H containing molecules are more likely to be incorporated with increasing pressure. For the LPCVD Si_3N_4 films synthesized from NH_3+TDMAS precursor system, the concentration of N-H bonds has little pressure dependence, whereas there are considerably more hydrogen content at higher pressure.

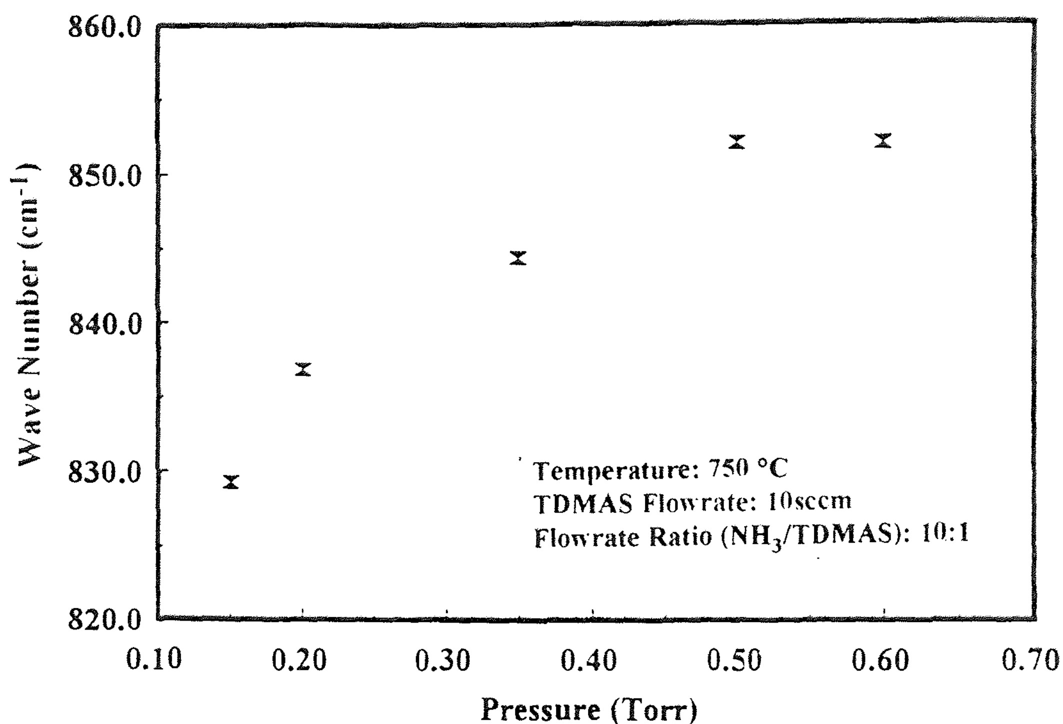

Figure 4.18 Variation of Si-N absorption peak in FTIR spectra for silicon nitride films as a function of deposition pressure.

4.5.2.3 NH_3/TDMAS Flowrate Ratio Study of Si_3N_4 Thin Films

The position of Si-N stretching mode as a function of NH_3/TDMAS flowrate ratio is plotted in the Figure 4.19. It can be seen that this position moves to higher wave number when NH_3/TDMAS flowrate ratio increases from 1 to 10 which results from the increment of density of the thin films, thus the concentration of Si-H molecules becomes high. When NH_3 is absent in the reaction, the broad absorption peak at 859.6 cm^{-1} owing to the combination of Si-N and Si-C absorption peak, relatively larger N-H peak due apparently to a change in the stoichiometry of the films.

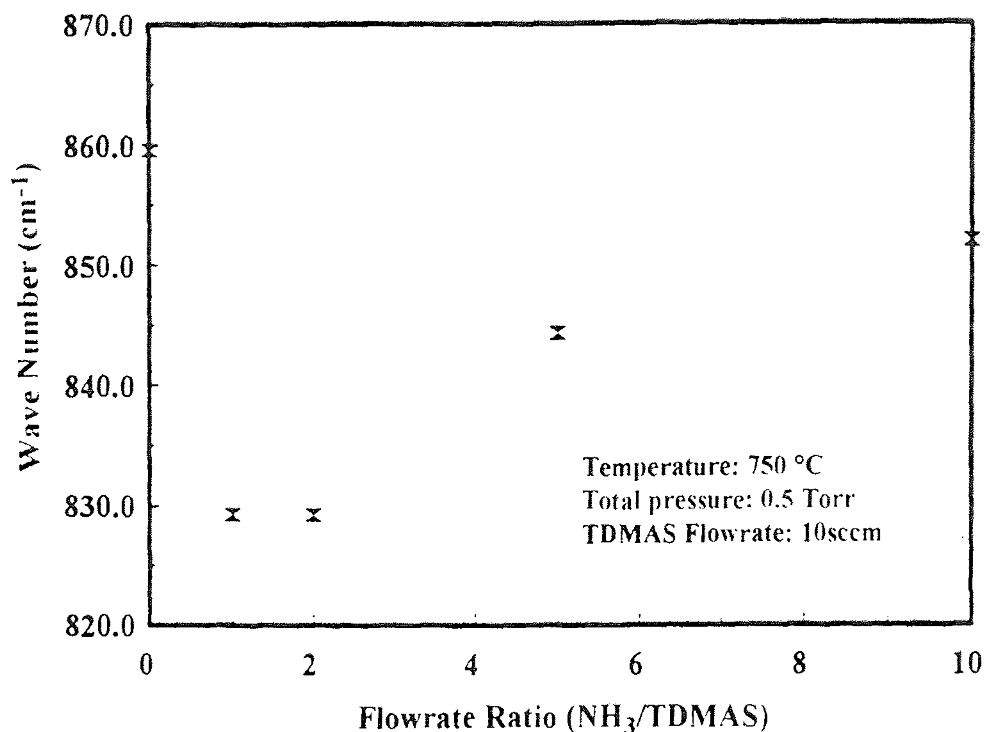

Figure 4.19 Variation of wave number corresponding to Si-N absorption peak in FTIR spectra for silicon nitride films as a function of NH_3/TDMAS flowrate ratio.

Another phenomenon which can be observed in the FTIR spectrum of NH_3/TDMAS flowrate ratio series is that two small at 1820 cm^{-1} and 2005 cm^{-1} begin to be seen as NH_3/TDMAS flowrate ratio decreases to 1. The latter peaks may be assigned to Si≡N mode which is practically at same range as that of Si-H.

4.5.3 UV-visible Analysis

From the UV spectroscopy of the thin films much information can be obtained such as the effect of impurities on the optical property and the index of absorption at certain wavelength.

4.5.3.1 The Temperature Dependent Study of Si_3N_4 Thin Films

The transmission spectrum of the film deposited at 800 °C, 0.5 Torr and 10.1 NH_3/TDMAS flowrate ratio is shown in Figure 4.20. The excellent transmission of Si_3N_4 film in the visible region of the spectrum is terminated at short wavelengths with the onset of the ultraviolet absorption edge.

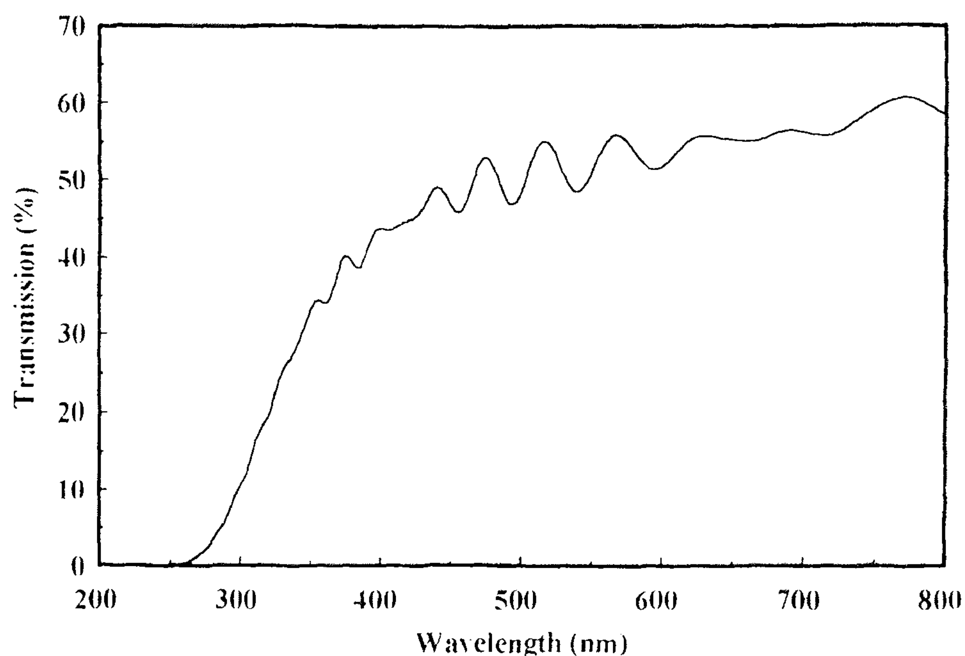

Figure 4.20 UV spectrum for a silicon nitride film on silicon deposited at a temperature of 800 °C, pressure of 0.5 Torr, TDMAS flowrate of 10 sccm, and NH_3 flowrate of 100 sccm.

This absorption edge results from the excitation of valence band electrons in the Si-N network to unoccupied higher energy states such as exciton or conduction band levels. The intensity of the absorption is determined by the density of occupied states in the valence band and of the unoccupied states in the

conduction band which are within energy E_g of each other, as well as by the transition probability of the initial to final state transition.

Multiple peaks near the UV absorption edge in the spectrum indicate the complexity of the processes. The exciton level is associated with bound electron-hole pairs which are created by photons of energy greater than the gap E_g. Since an electron and hole have an attractive Coulomb interaction for each other, it is possible for stable bound states of the two particles to be formed. The photon energy required to create such a pair state will be less then the energy gap E_g. It is difficult to produce excitons in sufficient concentration to observe directly transitions among exciton levels but it is quite common to observe transitions from the valence band edge to exciton levels. Exciton transitions generally occur at energies less than the band gap so that the lowest energy electron transitions are frequently to exciton levels [56].

Absorption resulting from the presence of impurities plays an important role in the temperature series. As the deposition temperature increases from 650 °C to 850 °C, the ultraviolet edge of the films is shifted to longer wavelengths manifesting weakening of the bond, meanwhile, the number of the peaks in UV spectra becomes larger. Higher carbon concentration and lower oxygen content are responsible for the shift of ultraviolet edge and change of peak numbers. Furthermore increasing the temperature to 900 °C, low wavelength absorption edge and small numbers of peak result from low carbon and relatively high oxygen content.

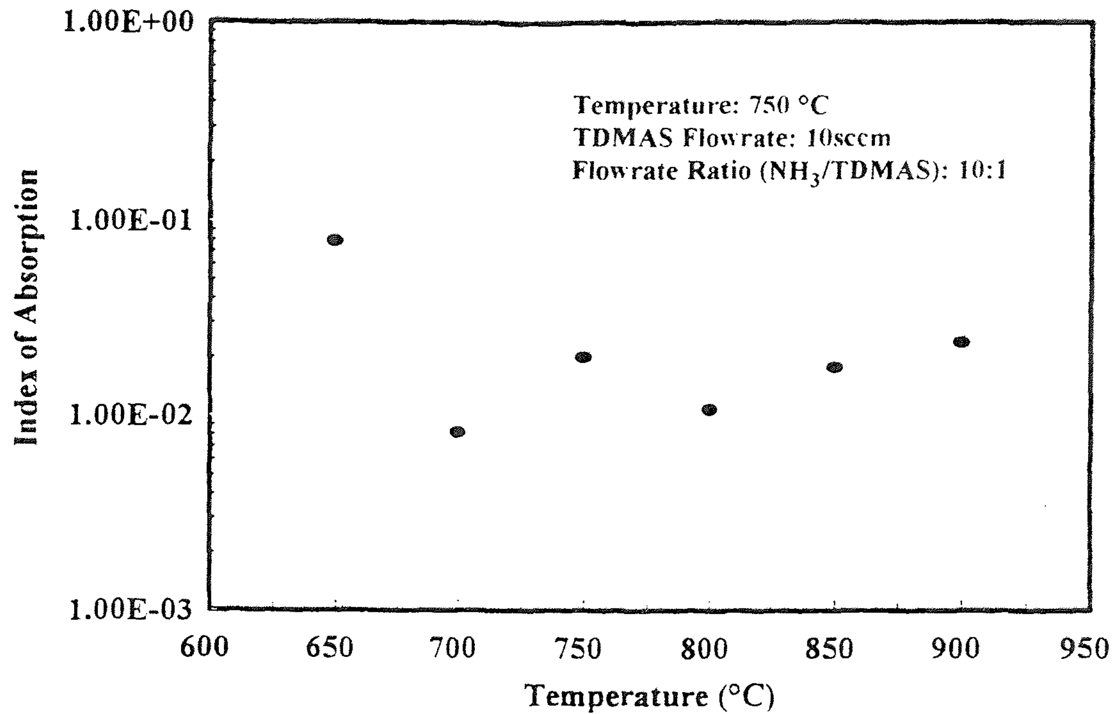

Figure 4.21 Variation of index of absorption of silicon nitride films as a function of deposition temperature.

As shown in Equation 4.4, both the index of absorption and the refractive index are necessary to describe the optical properties of a film. The absorption index k is a function of wavelength λ and is most directly related to the absorption coefficient α,

$$\alpha = 4\pi k/\lambda \qquad (4.6)$$

When a beam of light crosses a thin layer, the intensity of the light decreases as a result of reflection and absorption phenomena which take place in the layer. When the sum of total fraction of the incident light absorbed in the thin

film and the summation of the light transmitted is approximately equal to unit, the fraction of light transmitted (T) can be related with the absorption coefficient β and film thickness x:

$$T = I/I_0 = \exp(-\alpha x) \tag{4.7}$$

where I_0 is the initial density, I is the transmitted intensity [10].

Figure 4.21 shows the index of absorption versus deposition temperature at 633 nm. It is difficult to extract information from that dependency indicating complexity of the processes. Absorption in the visible is typically a composite of the tails of the electronic and vibrational edges of the film plus the contributions from impurities.

4.5.3.2 Pressure Dependent Study of Si_3N_4 Thin Films

No significant shift of the absorption edge is observed in the UV spectra of the films in pressure series. The change of the index of absorption at 633 nm as deposition pressure is investigated shown in Figure 4.22. With increasing pressure from 0.15 Torr to 0.60 Torr, the index of absorption decreases at low pressure region, then it increases as higher pressure obtaining the minimum at 0.2 Torr.

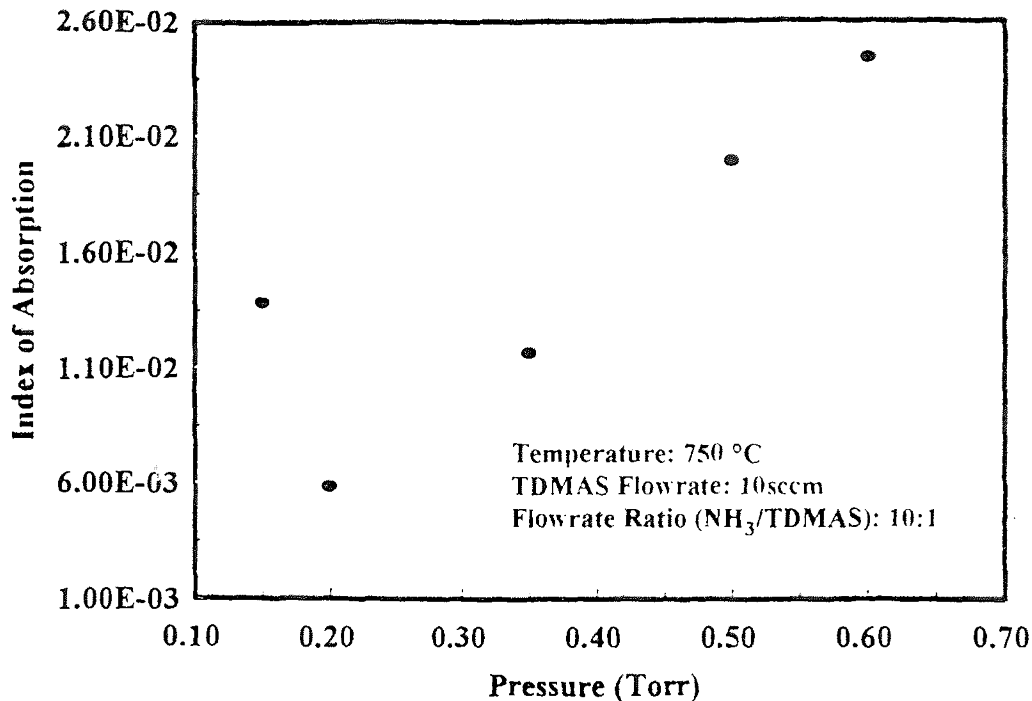

Figure 4.22 Variation of index of absorption of silicon nitride films as a function of deposition pressure.

4.5.3.3 NH_3/TDMAS Flowrate Ratio Study of Si_3N_4 Thin Films

As NH_3/TDMAS flowrate ratio decreases from 10 to 0, absorption edge shifts to long wavelength which corresponds to low energy due to carbide formation. The dependency of the index of absorption of the thin films on NH_3/TDMAS flowrate ratio shown in Figure 4.23 indicates that the index of absorption increases with decreasing this ratio owing to higher carbon content.

4.6 Stress Study

Over the years, many investigators have sought universal explanations for the origin of he constrained shrinkage that is responsible for the intrinsic stress.

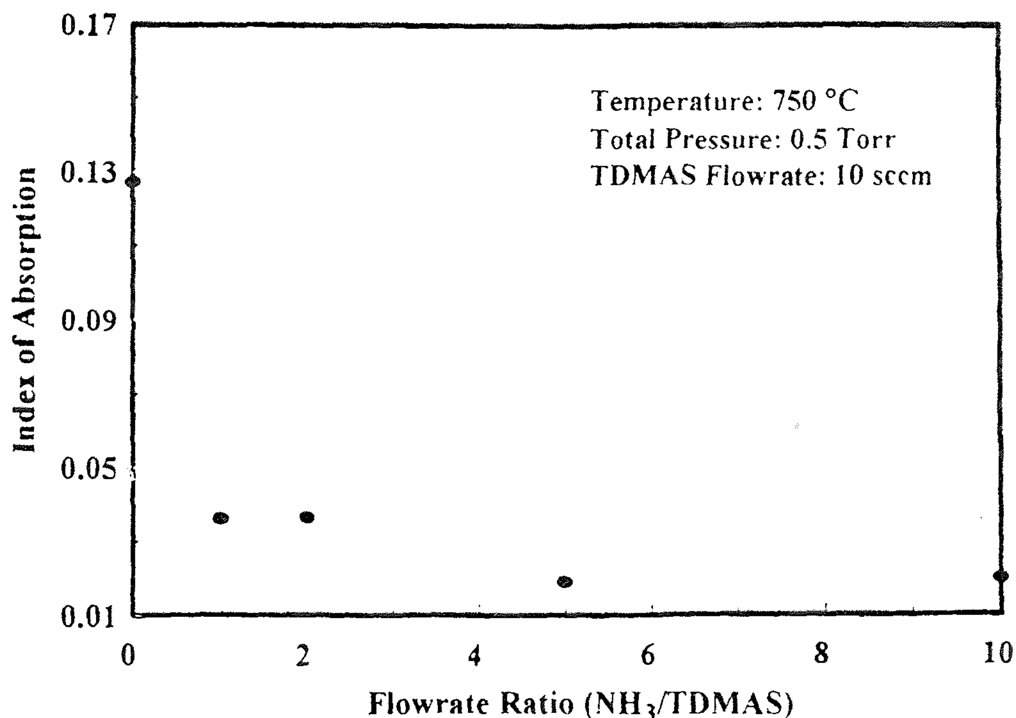

Figure 4.23 Variation of index of absorption of silicon nitride films as a function of NH_3/TDMAS flowrate ratio.

Recently, the factors conductive to internal stress generation in Si_3N_4 films are summarized as the following categories:

1. Difference in the expansion coefficients of the film and substrate
2. Stress relaxation due to viscoelasticity of Si_3N_4 film
3. Microscopic voids

The stress values of all the one side deposited stress wafer show that all the LPCVD silicon nitride films from NH_3/TDMAS precursor system are compressive which strengthens the films. The Si_3N_4 thin films was prepared at elevated temperatures, the system must contract a fixed amount. However, the coefficient of linear expansion of silicon substrate is larger than that of thin film, thus the

substrate shank more than the film, but a compromise was struck; the substrate was not allowed to contract fully and, therefore, placed in tension, and the film hindered from shrinking, was consequently force into compression.

4.6.1 Temperature Dependent Study of Si_3N_4 Thin Films

As the deposition temperature increases, The internal stress resulting from the differences in the expansion coefficients of the films and substrate becomes larger owing to larger shrinkage mismatch. On the other hand, the Si_3N_4 can be modeled as a viscoelastic solid whose overall mechanical response reflects that of a series combination of an elastic spring and a viscous dashpot which does not extent on initial application of the load, but requires a finite time for strain to be imposed on it (shown in Figure 4.24) [10]. Under loading, the spring instantaneously deforms elastically, whereas the dashpot strains in a time-dependent viscous fashion. If ε_1 and ε_2 represent the strains in the spring and dashpot, respectively, then the total strain is

$$\varepsilon_T = \varepsilon_1 + \varepsilon_2 \qquad (4.8)$$

Detail deduction shows the initial compressive stress σ_x acting on both the spring and dashpot relaxes by decaying exponentially with time,

$$\sigma_x = \sigma_0 e^{-Et/\eta} \qquad (4.9)$$

Since η is thermally activated, nitride grown at lower temperatures generally

Figure 4.24 Spring-dashpot model for stress relaxation.

possesses larger intrinsic stress. The two contrary tendencies as higher temperature compete each other. Besides the two principles, the density of the films has a large effect on the film stress, higher film density brings about lower film stress.

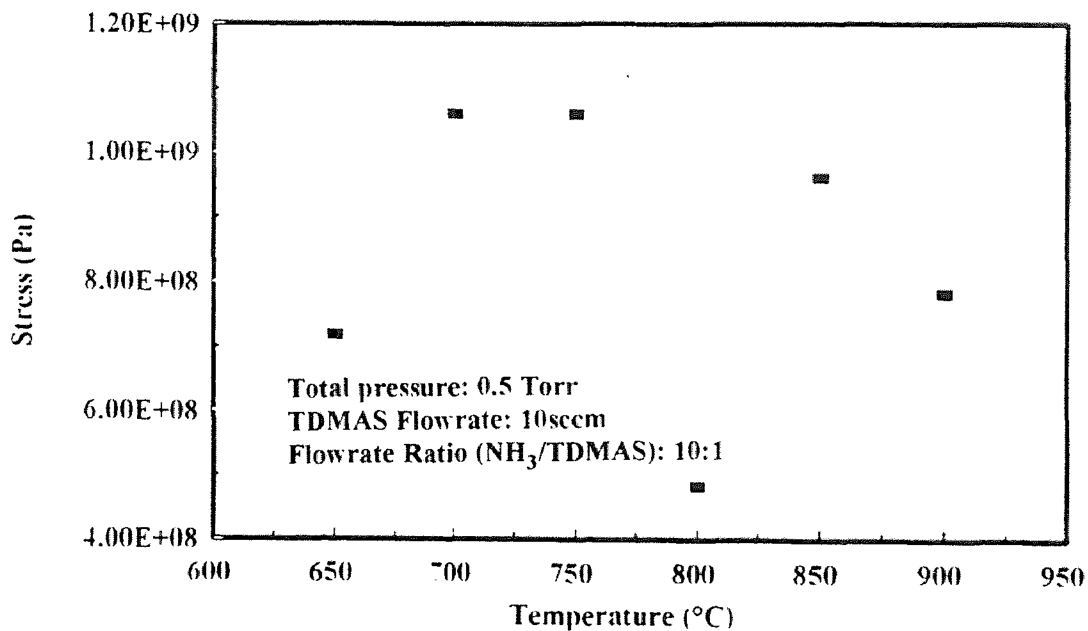

Figure 4.25 Variation of stress in silicon nitride films as a function of deposition temperature.

It can be seen from Figure 4.25 that the difference between expansion coefficients of the film and that of substrate is the principal reason determining internal stress in the temperature range of 650 °C to 700 °C. At higher temperature range viscoelastic behavior of the films becomes noticeable, this causes stress decreasing as further increasing temperature from 700 °C to 900 °C.

However, the stress in the thin films increases with film thickness, and great stress in the thin films would lead to presence of microcraks. The relationship between the density of microcracks and the stress release indicates that higher density of microcracks, more stress release. Stress in the films synthesized at 800 °C drops down to the lowest value because of high microcracks density.

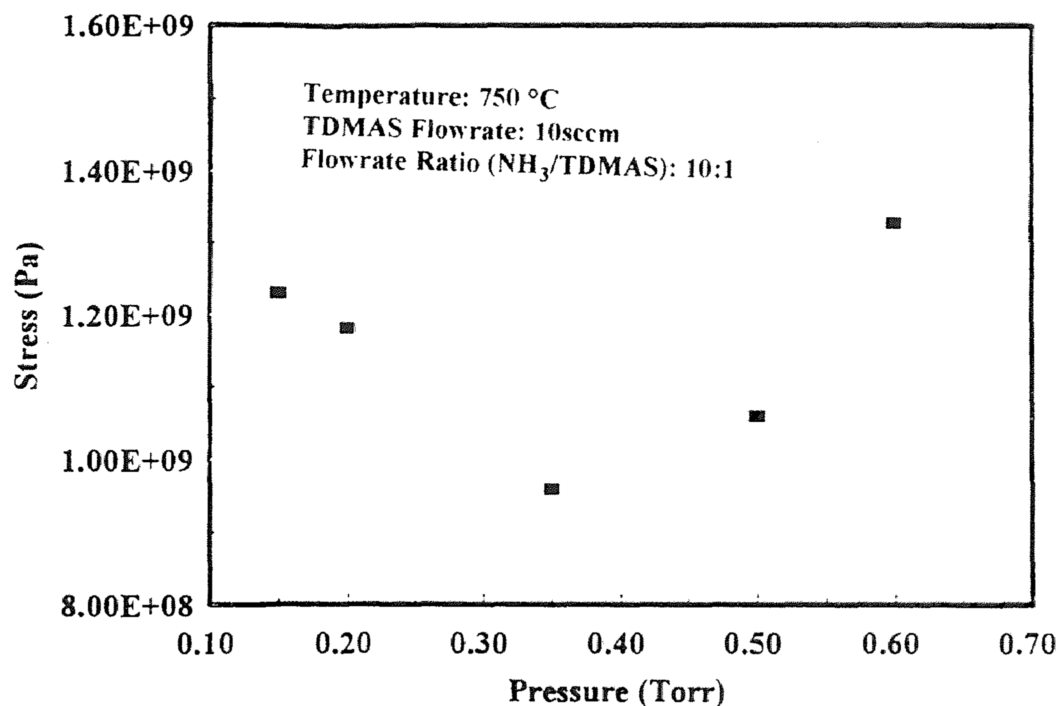

Figure 4.26 Variation of stress in silicon nitride films as a function of deposition pressure.

4.6.2 Pressure Dependent Study of Si_3N_4 Thin Films

Figure 4.26 shows that the relationship between film stress and deposition pressure is opposite to the dependency of the film density on pressure which indicates that density is dominant factor influencing film stress.

4.6.3 NH_3/TDMAS Flowrate Ratio Study of Si_3N_4 Thin Films

Low stress of 1.72×10^8 Pa in Si-C-N film is observed from Figure 4.27 due to large density of microcracks. The film stress decreases as higher NH_3/TDMAS flowrate ratio which thanks to the appearance of the microcracks in the films deposited at 5 and 10 NH_3/TDMAS flowrate ratio.

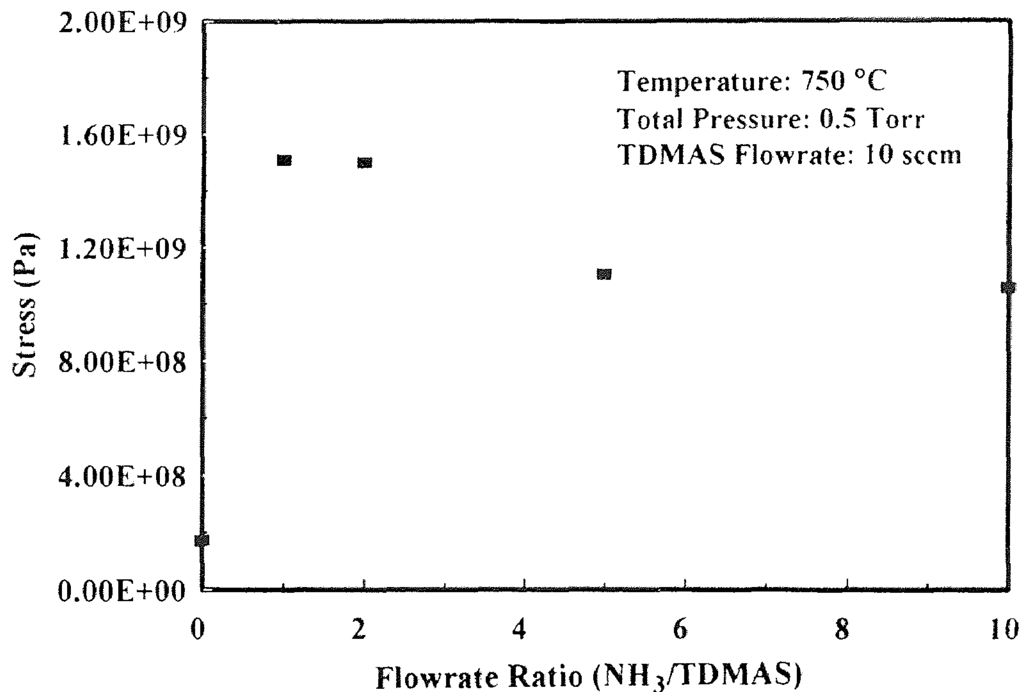

Figure 4.27 Variation of stress in silicon nitride films as a function of NH_3/TDMAS flowrate ratio.

CHAPTER 5

CONCLUSIONS

Amorphous high quality stoichiometric Si_3N_4 films were synthesized on silicon and quartz wafers by low pressure chemical vapor deposition from TDMAS/NH_3 precursor system in the temperature range of 650 - 900 °C, pressure range of 0.15 - 0.60 Torr, NH_3/TDMAS flowrate ratio range of 1 - 10. The feasibility of using TDMAS in LPCVD silicon nitride films is demonstrated through the kinetics studies and film characterization studies. The temperature dependent behavior of deposition rate is found to follow an Arrhenius behavior in the temperature range of 650 °C to 800 °C with an activation energy of 41 ± 3 kcal/mole. The pressure dependent and NH_3/TDMAS flowrate ratio dependent behavior of deposition rates are found to follow an unimolecular surface reaction mode. The X-ray diffraction patterns indicate the amorphous nature of as-deposited silicon nitride films. The density of the thin films obtains the maximums at 800 °C in temperature dependent study and at 0.35 Torr in pressure dependent study. It can be seen that the density increases with higher NH_3/TDMAS flowrate ratio. The refractive index of the films is about 1.9 at low temperatures (650 °C and 700 °C) due to oxidation of porous films. However, it reaches 2.1 and above at higher temperatures (800 °C and 850 °C) which results from high carbon content in the thin films. We can obtain favorable refractive index values at 750 °C and 900 °C. All of these is

corroborated by film compositional analyses from RBS and XPS. There is no fluctuation of the refractive index in the pressure dependent study. But this value increases to the range of 2.359 to 2.395 as NH_3 is absent in the precursor system. FTIR spectra reveal the expected presence of the Si-N vibrational mode at 850 cm^{-1} and Si-N breathing mode at 475 cm^{-1}. The presence of the peaks associated Si-H stretching mode at 2180 cm^{-1}, N-H stretching mode at 3355 cm^{-1} and N-H_2 scissors at 1475 cm^{-1} indicates a number of hydrogen atoms bond to Si or N in the films which effects the position of Si-N stretching bond. This value increases with higher temperature from 650 °C to 850 °C, then it decreases; and the wave number corresponding to Si-N absorption peak increases with increasing pressure and NH_3/TDMAS flowrate ratio. UV-visible spectra show the absorption edge of Si_3N_4 in UV region which position is influenced by the deposition temperature, pressure and NH_3/TDMAS flowrate ratio. All the films are compressive. Stress in the films is mainly determined by difference in the expansion coefficients of the film and substrate, stress relaxation due to viscoelasticity of Si_3N_4 film as well as microscopic voids, it change with deposition temperature, pressure and NH_3/TDMAS flowrate ratio.

Furthermore, through the film growth kinetics studies and film characterization study, an optimum film synthesis condition is found to be under the temperature of 750 °C and NH_3/TDMAS flowrate ratio of 10:1.

REFERENCES

1. Kern, W. *Chemical Vapor Deposition*. Microelectronic Materials and Processes, Kluwer Academic, New Jersey (1986): 203 - 246.

2. Morosanu, C. E. "The Preparation, Characterization and Applications of Silicon Nitride Thin Films." *Thin Solid Film*, 65 (1980): 171-208.

3. G. Wahl. *Chemical Vapor Deposition*. The Electrochemical Society, New Jersey (1984), p. 60.

4. C. Bernard. *Chemical Vapor Deposition*. The Electrochemical Society, New Jersey (1981), p. 3.

5. B. Nolang. *Proc. 5th European Conference on CVD*. Uppsala, Sweden (1985), p. 107.

6. Hammond, M. "Introduction to Chemical Vapor Deposition." *Solid State,Technol.* 63 (Dec. 1979): 61.

7. J. P. Dismukes. *Semiconductor Silicon 1973*. ECS Softbound Symposium Series, New York, 1973.

8. R. Takahashi, N. Sugawara, Y. Nakazawa, and Y. Koga. *Proc. Conf. Chem. Vapor Deposition, Second International Conference, Electrochem. Soc.*, New York, 1972, p. 695-711.

9. E. Tanikawa, O. Takayama, and K. Maeda. *Proc. Conf. Chem. Vapor Deposition, Fourth International Conference, Electrochem. Soc.*, 1974.

10. Milton Ohring. *The Materials Science of Thin Films*. Academic Press, California 1992.

11. S. W. Benson. *Thermochemical Kinetics*. John Wiley & Sons, New York (1976).

12. K. J. Laidler. *Chemical Kinetics*. 2nd Edition, McGraw Hill, New York (1965).

REFERENCES
(Continued)

13. B.Nolang. *Proc. 5th European Conference on CVD*. Sweden (1985), p. 107.

14. Laidler, K. J. *Chemical Kinetics*. Harper & Row, New York (1987).

15. W. Kern and V. S. Ban. *Thin Film Processes*. Academic Press, New York (1978), Chapt. 3.

16. J. M. Blocher, Jr., *Deposition Technologies for Films and Coatings: Developments and Applications*. Noyes, New Jersey (1982).

17. G. R. Srinivasan. *Chemical Vapor Deposition*. The Electrochemical Society, New Jersey (1984), p. 387.

18. J. R. Hollahan and R. S. Rosler. *Thin Film Processes*. Academic Press, New York (1978), p. 335.

19. S. M. Ojha. *Physics of Thin Film*. Vol. 12, Academic Press, New York (1982), p. 237.

20. J. A. Thornton. *Deposition Technologies for Films and Coatings: Developments and Applications*. Noyes, New Jersey (1982).

21. T. D. Bonifield. *Deposition Technologies for Films and Coatings: Developments and Applications*. Noyes, New Jersey (1982).

22. H. Y. Kumagai. *Chemical Vapor Deposition*. The Electrochemical Society, New Jersey (1984), p. 189.

23. Y. Catherine. *Proc. 5th Symp. on Plasma Processing, The Electrochemical Society,* New Jersey (1985), Vol. 85-1, p. 317.

24. T. Sugano. *Applications of Plasma Processes to VLSI Technology*. John Wiley & Sons, New York (1985).

REFERENCES
(Continued)

25. H. M. Kim, S.-S. Tai, S. L. Groves and K. K. Schuegraf. *Chemical Vapor Deposition*. The Electrochemical Society, New Jersey (1981), p. 258.

26. S. D. Allen, A. B. Trigubo, and Y.-C. Liu. *Chemical Vapor Deposition*. The Electrochemical Society, New Jersey (1981), p. 267.

27. D. J. Ehrlich and J. Y. Tsao. *VLSI Electronics: Microstructrue Science*. Vol. 7, Academic Press, New York (1983), Chapt. 3.

28. Stering, H. F., and R. C. G. Swann. "Chemical Vapor Deposition Promoted by r.f. Discharge." *Solid State Electronics*, 8 (1965): 653 - 654.

29. Doo, V. Y., D. R. Nichols and G. A. Silvey. "Preparation and Properties of Pyrolytic Silicon Nitride." *J. Electrochem. Soc.*, 113 (1966): 1279 - 1281.

30. Kenneth, E. B., P. Glein, and R. L. Yeakley. "Some Properties of Vapor Deposited Silicon Nitride Films Using the SiH_4 - NH_3 - H_2 System." *J. Electrochem. Soc.*, 114 (1967): 733 - 737.

31. Satoshi Yoshioka and Shigetoshi Takayanagi. "Deposition of Silicon Nitride Films by the Silane-Hydrazine Process." *J. Electrochem. Soc.*, 114 (1967): 962 - 965.

32. T. L. Chu, C. H. Lee and G. A. Gruber. "The Preparation and Properties of Amorphous Silicon Nitride Films." *J. Electrochem. Soc.*, 114 (1967): 717 - 722.

33. Grieco, M. J., F. L. Worthing and B. Schwartz. "Silicon Nitride Thin Films from $SiCl_4$ Plus NH_3: Preparation and Properties." *J. Electrochem. Soc.*, 115 (1968): 525 - 531.

34. Wohlheiter, V. D. and R. A. Whitner. "A High Production System for the Deposition of Silicon Nitride." *J. Electrochem. Soc.*, 119 (1972): 945 - 948.

REFERENCES
(Continued)

35. Tanikawa, E., T. Okabe and K. Maeda. *Doped Oxide Films by Chemical Vapor Deposition.* The Electrochemical Soc. New Jersey (1973), p. 261.

36. Rosler, R. S. "Low Pressure CVD Production Processes for Poly, Nitride, and Oxide." *Solid State Technol.*, (1977): 63 - 70.

37. Pan, P and W. Berry. "The Composition and Physical Properties of LPCVD Silicon Nitride Deposited with Different NH_3/SiH_2Cl_2 Gas Ratios." *J. Electrochem. Soc.*, 132 (1985): 3001 - 3005.

38. Roenigk, K. F. and K. F. Jensen. "Low Pressure CVD of Silicon Nitride." *J. Electrochem. Soc.*, 134 (1987): 1777 - 1785.

39. J. A. Gregory, Douglas J. Young, R. W. Mountain and C. L. Doherty, Jr.,"Characterization of Low Pressure Chemically Vapor Deposited Silicon Nitride Using Experimental Design." *Thin Solid Films*, 206 (1991): 11 - 17.

40. Zhang, S. L., J. T. Wang, W. Kaplan and M. Ostling. "Silicon Nitride Films Deposited from SiH_2Cl_2 - NH_3 by Low Pressure Chemical Vapor Deposition: Kinetics, Thermodynamics, Composition and Structure." *Thin Solid Film*, 213 (1992): 182 - 191.

41. Ji-Tao Wang, Shi-Li Zhang, Yong-Fa Wang, Ke-Yun Zhang and Sheng-Qi Xie. *Extended Abstracts of Electrochem. Soc. Meeting, Hawaii,* Volume 93-1, May 16 - 21, 1993.

42. E. Scheid, L. K. Kouassi, R. Henda, J. Samitier and J. R. Morante. "Silicon Nitride Elaborated by Low Pressure Chemical Vapor Deposition from Si_2H_6 and NH_3 at Low Temperature." *Materials Science and Engineering*, B17 (1993): 185 - 189.

43. Even P. G. T. van de Ven. "Plasma Deposition of Silicon Dioxide and Silicon Nitride Films." *Solid State Technology*, 12 (1981): 167 - 171.

REFERENCES
(Continued)

44. Kazuhisa Katoh, Masaru Yasui and Hideo Watanabe. "Plasma - enhanced Deposition of Silicon Nitride from SiH_4-N_2 Mixture." *Japanse Journal of Applied Physics*, Vol. 22, No. 5, May, 1983, p.L321 - L323.

45. C. Blaauw. "Preparation and Characterization of Plasma-Deposited Silicon Nitride." *J. Electrochem. Soc.*, 131 (1984): 1114 - 1118.

46. Olin Hunt. Material Safety Data Sheet. *U. S. Patent*, #4877652 (1989).

47. Claassen, W. A. P., J. Bloem, W. Q. J. N. Valkenburg and C. H. J. Van den brekel. "The Deposition of Silicon from Silane in a Low-pressure Hotwall System." *J. Crystal Growth*, 57 (1982): 259 - 266.

48. Kern, W.and R. S. Rosler. "Advances in Deposition Processes for Passivation Films." *J. Vac. Sci. and Technol.*, 14 (1977): 893.

49. Claasen, W. A. P. et al. "Influnce of Deposition Temperature, Gas Pressure, Gas Phase Composition, and RF Freq. on Composition and Mech. Stress of Plasma SiN Layers." *J. Electrochem. Soc.*, 132 (1985): 893.

50. Bohn, P. W. and R. C. Manz. "A Multiresponse Factorial Study of Reactor Parameters in PECVD Growth of Amorphous Silicon Nitride." *J. Electrochem. Soc.*, 132 (1985): 1981.

51. Soller, B. R., C. R. Snider and R. F. Shuman. "A Flexible Multilayer Resist System Using Low Temperature Plasma-deposited Silicon Nitride." *J. Electrochem. Soc.*, 131 (1984): 868 - 872.

52. Suzuki, K., J. Matsui and T. Torikai. "SiN Membrance Masks for X-ray Lithography." *J. Vac. Sci. Tech.*, 20 (1982): 191 - 194.

53. Michael L. Hitchman and Klavs F. Jensen. *Chemical Vapor Deposition*. Academic Press, New York (1982).

54. Hugh O. Pierson. *Handbook of Chemical Vapor Deposition*. Noyes Publications, New Jersey (1982).

REFERENCES
(Continued)

55. Claassen, W. A. P., J. Bloem, W. Q. J. N. Valkenburg and C. H. J. Van den brekel. "The Deposition of Silicon from Dilane in a Low-pressure Hot-wall System." *J. Crystal Growth*. 57 (1982): 259-266.

56. George H. Sigel, Jr., *Optical Absorption of Glasses*. Academic Press, New York (1977).

57 G. N. Parsons, J. H. Souk, and J. Batey. "Low Hydrogen Content Stoichiometric Silicon Nitride Films Deposited by Plasma-enhanced Chemical Vapor Deposition." *J. Appl. Phys*. 70 (3), 1 August 1991.